RPN 96

DNA 2730-F
November 1971

MEGAVOLT-MEGAMPERE ELECTRON GUN STUDY

FINAL REPORT

This work was supported by the Defense Nuclear Agency
under NWER subtask LA013-01

By
H. Jory, F. Friedlander,
D. King, C. Kuglin

Defense Nuclear Agency
Washington, D. C. 20305

Varian Associates
611 Hansen Way
Palo Alto, California 94303

Contract No. DASA01-69-C-0092
DNA Project No. XAXL
Task and Subtask A013, Work Unit 01

TABLE OF CONTENTS

TABLE OF CONTENTS (Cont.)

LIST OF ILLUSTRATIONS

LIST OF ILLUSTRATIONS (Cont.)

LIST OF ILLUSTRATIONS (Cont.)

LIST OF ILLUSTRATIONS (Cont.)

LIST OF ILLUSTRATIONS (Cont.)

I. INTRODUCTION

The major part of the work reported here is concerned with the numerical analysis of electron flow in high current megavolt diodes. The analysis was performed using a digital computer code developed by Varian Associates over the past seven years. Previous related studies were performed under contract DASA-01-68-C-0025.[1] In the previous studies, considerable attention was given to various electron emission mechanisms and to the proper model to be used for the cathode in the digital calculations. Calculations of the electron flow in a needle and plane diode were made using the various models, and the results of the calculations were compared to measured results. It was concluded that in the relatively high impedance megavolt diodes the cathode behaves essentially space-charge limited, and that there is little, if any, ion neutralization of space charge in the flow. Presumably, the source of electrons is a plasma which remains very near the cathode surface, and which is formed by field emission heating of the surface during the early part of the pulse.

One objective of the previous studies was to determine whether or not a 10 MV, 3 MA beam could be generated with a single diode structure. The studies and calculations indicated that it was not feasible to obtain such a beam in a single diode without undesirable severe pinching of the beam near the anode. To keep the inward convergence of the beam at the anode to a reasonable value, it was estimated that a number (in the range of 4 to 10) of diode modules would have to be employed with each diode isolated from the self-magnetic field of the others.

One of the purposes of the work reported here was to further verify the models used in the diode calculations. To accomplish this a number of diodes were analyzed for which measured results were available. The numerical calculations will be compared with the experimental results for several such diodes.

Another purpose of this program was to perform numerical flow calculations for diodes. For these calculations it was assumed that four modules would be used, and that the total desired current would be 1.6 MA over an area of $1m^2$ with a diode voltage of 15 MV. Calculated electron flows will be presented for a number of diode geometries in the range to satisfy this requirement. The calculations give some indications of how changes in the geometry affect the character of the beam.

This final report also includes some theoretical work related to megavolt diodes, and a section dealing with a novel approach for megavolt beam generation in which a cavity resonator is used as an energy storage element.

II. THEORETICAL ANALYSIS RELATED TO MEGAVOLT DIODES

A. RELATIVISTIC SPACE CHARGE FLOW

This section contains a brief review of the equations describing steady state relativistic space charge flow in vacuum, and serves to establish notation.

The electric field $\vec{E}$ and magnetic field $\vec{B}$ obey Maxwell's equations.

$$\vec{\nabla} \cdot \vec{E} = \rho/\epsilon_o \tag{1}$$

$$\vec{\nabla} \times \vec{E} = 0 \tag{2}$$

$$\vec{\nabla} \cdot \vec{B} = 0 \tag{3}$$

$$\vec{\nabla} \times \vec{B} = -\mu_o \vec{j} \tag{4}$$

In equations (1) and (4), ρ and $\vec{j}$ are the charge density and the current density. The constants ϵ_o and μ_o are the dielectric constant of free space and the magnetic permeability. The electric scalar potential V is defined as

$$\vec{E} = -\vec{\nabla} V \tag{5}$$

Using (1) and (5), Poisson's equation is obtained:

$$\nabla^2 V = -\rho/\epsilon_o \tag{6}$$

For laminar flow, a velocity field $\vec{v}$ can be defined so that

$$\vec{j} = -\rho\vec{v} \tag{7}$$

The equation of continuity requires that

$$\vec{\nabla} \cdot \vec{j} = 0 \tag{8}$$

In cylindrical coordinates, the relativistic equations of motion are given by:

$$\frac{d}{dt}(\dot{r}\gamma) - r\dot{\theta}^2\gamma = -\eta(E_r + v_\theta B_z - v_z B_\theta) \tag{9}$$

$$\frac{d}{dt}(r^2\dot{\theta}\gamma) = -\eta r(E_\theta + v_z B_r - v_r B_z) \tag{10}$$

$$\frac{d}{dt}(\dot{z}\gamma) = -\eta(E_z + v_r B_\theta - v_\theta B_r) \tag{11}$$

where $\eta = |e|/m_o$ is the magnitude of the charge to mass ratio for an electron at rest. The relativistic mass ratio γ is defined as:

$$\gamma = \frac{m}{m_o} = \left(1 - \frac{v^2}{c^2}\right)^{-1/2} \tag{12}$$

where v is the magnitude of the electronic velocity and c is the velocity of light in vacuum. Thus, $v^2 = v_z^2 + v_r^2 + v_\theta^2$, with $v_z = \dot{z}$, $v_r = \dot{r}$, and $v_\theta = r\dot{\theta}$.

The kinetic energy is given by

$$|e|\,V = c^2(m - m_o) \tag{13}$$

where it is assumed that $v = 0$ at $V = 0$. Defining a normalized potential

$$U = \frac{\eta V}{c^2} = \frac{V}{V_n} \tag{14}$$

(12) and (13) give

$$\gamma = 1 + U \tag{15}$$

and

$$\left(\frac{v}{c}\right)^2 = \frac{U^2 + 2U}{(1 + U)^2} \tag{16}$$

In the case of cylindrical symmetry, none of the vector or scalar fields defined above are functions of θ. In addition, $E_\theta = 0$. The θ-directed magnetic field, B_θ, will always refer to the self-magnetic field of the beam.

This can easily be obtained by applying the integral form of Ampere's law (equivalent to equation (4))

$$\oint \vec{B} \cdot \vec{d\lambda} = -\mu_o I \tag{17}$$

along a closed circular path of radius r in a plane of constant z:

$$B_\theta(r, z) = \frac{-\mu_o}{2\pi} \frac{I(r, z)}{r} = \frac{-\mu_o}{r} \int_o^r j_z(t, z)\, t\, dt, \tag{18}$$

where I is the current enclosed by the path of radius r.

In addition to the equations describing the electromagnetic field and the particle dynamics, a boundary condition must be established at the cathode in order to specify the initial current density. In what follows, space charge limited flow will always be assumed so that

$$\vec{E} = 0 \tag{19}$$

at the cathode surface.

B. PLANAR FLOW IN A CONFINING AXIAL MAGNETIC FIELD

1. Equations of Motion and Current Density

To obtain planar flow in high current diodes, a uniform dc axial magnetic field over the entire diode region was considered. It was anticipated that the external field would tend to offset the effects of the self-magnetic field and thus prevent beam collapse.

Although the following theoretical analysis of the planar gun is based upon some fairly restrictive assumptions, several useful results can be obtained.

For the analysis of the planar gun, it will be assumed that B_z is sufficiently large so that to first order, the gun resembles a plane parallel diode with $V = V(z)$. Thus, $E_\theta = E_r = 0$, $B_r = 0$, and B_θ is assumed independent of z. Equations (9) through (11) become:

$$\frac{d}{dt}(\dot{r}\gamma) - r\dot{\theta}^2\gamma = -\eta(v_\theta B_z - v_z B_\theta) \tag{20}$$

$$\frac{d}{dt}(r^2\dot{\theta}\gamma) = \eta r v_r B_z \tag{21}$$

$$\frac{d}{dt}(\dot{z}\gamma) = -\eta\,(E_z + v_r B_\theta) \tag{22}$$

Poisson's equation becomes

$$\frac{d^2V}{dz^2} = -\rho/\epsilon_o \tag{23}$$

The condition of nearly parallel flow requires that the radial acceleration, given by the RHS of (20), is negligible. Assuming that this is equal to zero:

$$\frac{v_\theta}{v_z} = \frac{B_\theta}{B_z} \equiv \tau \tag{24}$$

The velocity can then be approximated by:

$$v \approx \sqrt{v_z^2 + v_\theta^2} = v_z\,(1 + \tau^2)^{1/2} \tag{25}$$

Using (16) and (25),

$$v_z = c\left[\frac{U^2 + 2U}{(1 + \tau^2)\,(1 + U)^2}\right]^{1/2} \tag{26}$$

Combining (14), (23), and (26) with the relation $j_z = -\rho v_z$,

$$\frac{d^2U}{dz^2} = \frac{j_z\,(1 + \tau^2)^{1/2}}{V_n c\,\epsilon_o}\;\frac{(1 + U)}{\sqrt{U^2 + 2U}} \tag{27}$$

The equation of continuity (8) requires that

$$\frac{1}{r}\,\frac{\partial(r\,j_r)}{\partial r} + \frac{1}{r}\,\frac{\partial j_\theta}{\partial \theta} + \frac{\partial j_z}{\partial z} = 0 \tag{28}$$

Because of cylindrical symmetry, $\partial j_\theta / \partial \theta = 0$. Also, since $j_r \approx 0$, $\partial j_z / \partial z = 0$ so that j_z is a constant of the motion.

Equation (27), in the limit of $\tau = 0$, is identical to that obtained by Acton[2] for a plane parallel diode neglecting self-magnetic field effects. When these effects cannot be ignored, Acton's solution can only be physically realized by using an infinite, externally applied axial field.

Since both j_z and τ are independent of z:

$$j_z(\tau) = \frac{j_z(0)}{(1 + \tau^2)^{1/2}} \tag{29}$$

where $j_z(0)$ refers to Acton's solution for the current density. Equation (29) is, in fact, a complicated integral equation for j_z since

$$\tau = B_\theta / B_z = -\frac{\mu_o I}{2\pi r B_z} \tag{30}$$

and

$$I = \int \vec{j} \cdot d\vec{S} \tag{31}$$

Even though the current density becomes quite complicated, the flow described above has a simple interpretation near the cathode. Initially, the trajectories are not emitted normal to the cathode surface, but make an angle ($\theta = \tan^{-1} \tau$) to the cathode in the θ-z plane. On the axis the condition $\theta = 0$ holds, whereas at the beam edge the maximum angle θ_m is determined from (30):

$$\theta_m = -\tan^{-1}\left(\frac{\mu_o I_t}{2\pi r_e B_z}\right) , \tag{32}$$

where I_t is the total current and r_e is the radius of the beam edge.

2. Deviation from Planar Flow

The approximate solution (24) can be used in conjunction with the integral of (21) (Busch's Theorem) to yield an expression for the radial deviation in terms of the applied field B_z.

The integral of (21) can be written as:

$$v_\theta = \frac{\eta B_z r}{2\gamma} \left[1 - \left(\frac{r_o}{r} \right)^2 \right] \tag{33}$$

where r_o is the initial radius of the trajectory. Defining the fractional radial deviation of the beam edge; i.e., a radial pinching factor, as

$$\alpha = \left(\frac{r_o - r}{r_o} \right) \quad , \tag{34}$$

equation (33), to first order in α, can be written as

$$v_\theta \approx - \frac{\eta B_z r_o \alpha}{\gamma} \tag{35}$$

Using (24) and (35),

$$B_z = \left(\frac{-B_\theta \gamma v_z}{\eta r_o \alpha} \right)^{1/2} \quad , \tag{36}$$

or

$$B_z = \left(\frac{\mu_o I \gamma v_z}{2\pi \eta r_o^2 \alpha} \right)^{1/2} \tag{37}$$

equation (37) gives the amount of B_z field required to restrict the radial pinching of the beam to an amount given by α. The equation neglects space charge forces. Hence it will overestimate the required B_z.

3. The Axial Self-Magnetic Field

When the rotational velocity becomes sufficiently large, the induced axial self-magnetic field B_z^s must be considered. In the case of no radial motion and j_θ independent of z, the application of (17) over a rectangular path in the R-Z plane gives:

$$B_z^s(r) = -\mu_o \int_r^{r_e} j_\theta(t)\, dt \tag{38}$$

From (7) and (24),

$$j_\theta = j_z \frac{B_\theta}{B_z} \tag{39}$$

Since B_θ is constant along a trajectory ($\alpha << 1$), and j_z is independent of z, j_θ is independent of z as assumed above. Using (24), (38), and (39),

$$B_z^s(r) = -\mu_o \int_r^{r_e} \tau(t)\, j_z(t)\, dt \tag{40}$$

The axial self-magnetic field thus vanishes at the beam edge and reaches a maximum on the axis. Since $\tau < 0$, B_z^s adds to the applied external field. A comparison between (18) and (40) shows that

$$B_z^s(0) / B_\theta(r_e) \approx \tau(r_e), \tag{41}$$

so that the induced axial field is a higher order effect than the induced θ field.

C. SELF-INDUCED MAGNETRON EFFECTS

Computer studies of high current electron guns show that the electron flow can be divided into essentially two regions. The front portion of the cathode, where emitted electrons reach the anode, behaves somewhat like a magnetron operating above cutoff, whereas the back portion exhibits cutoff magnetron behavior. The

changing character of the flow along the cathode is caused by the variation of the self-magnetic field, which is equal to zero on the axis and reaches a maximum at the beam edge.

The cutoff portion of the cathode consists of a space-charge sheath of variable thickness. This is a difficult portion of the flow to model with the computer, since a substantial portion of the sheath is often less than one mesh distance thick; this thickness can give rise to large errors in the numerical procedures and tends to create unstable flow conditions. In addition, since a portion of the flow returns to the cathode in this region, the usual procedures for computing the emission from $\vec{E} = 0$ are no longer valid. Indeed, the current density $\vec{j}$ is a function of the self-magnetic field B_θ over the entire cathode.

1. The Conducting Region

The following analysis attempts to study the flow near the cathode only, by setting up a local coordinate system at each point on the cathode and assuming that the self-magnetic field B_θ is constant over the region to be studied. The local coordinate perpendicular to the cathode is denoted by y, and the coordinate parallel to the cathode is x. The potential is assumed to be a function of y only. Implicit in this assumption is that the local radius of curvature of the cathode is much greater than that of the trajectories in this region. Thus, each portion of the cathode, to a first approximation, is assumed to behave as a portion of an infinite linear magnetron with applied field B_θ. The "anode" in this case is a potential surface located at a distance y.

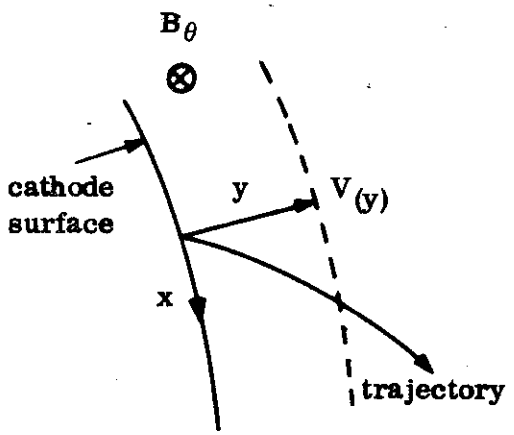

In the local coordinate system, the flow equations near the cathode are given by:

$$\frac{d}{dt}(\dot{y}\gamma) = -\eta\,(E_y - \dot{x}\,B_\theta) \tag{42}$$

$$\frac{d}{dt}(\dot{x}\gamma) = -\eta\,B_\theta\,\dot{y} \tag{43}$$

Equation (43) can be integrated to give:

$$\dot{x} = -\frac{\eta\,B_\theta\,y}{\gamma} \tag{44}$$

Since $v^2 = \dot{x}^2 + \dot{y}^2$, (16) gives

$$\dot{y}^2 = c^2\left[\frac{U^2 + 2U}{(1 + U)^2}\right] - \dot{x}^2 \tag{45}$$

Using (15), (44), and (45),

$$\dot{y}^2 = (1 + U)^{-2}\left[c^2\,(U^2 + 2U) - (\eta\,B_\theta\,y)^2\right]$$

$$= v^2\,(1 - f) \tag{46}$$

where the cutoff factor f is defined as

$$f = \frac{\eta\,(B_\theta\,y)^2}{2\,V\,(1 + U/2)} \tag{47}$$

In equation (47), f, V, and U are all functions of y. When $f = 1$, $\dot{y} = 0$ so that motion in the y direction has stopped. A comparison of the expressions for $\dot{y}$ and $\dot{x}$ shows that

$$\frac{dx}{dy} = \left(\frac{f}{1 - f}\right)^{1/2} \tag{48}$$

For this geometry, Poisson's equation becomes:

$$\frac{d^2V}{dy^2} = V_n\,\frac{d^2U}{dy^2} = -\rho/\epsilon_o \tag{49}$$

The equation of continuity becomes

$$\frac{\partial j_x}{\partial x} + \frac{\partial j_y}{\partial y} = 0 \tag{50}$$

Since V = V(y) implies that j_x is not a function of x, j_y is a constant of the motion.

Combining (46), (49), with $j_y = \rho v_y$,

$$\frac{d^2U}{dy^2} = \frac{j_y (1 + U)}{\epsilon_o V_n \sqrt{c^2 (U^2 + 2U) - (\eta y B_\theta)^2}} \tag{51}$$

Unfortunately, (51) cannot be solved analytically, so it is not possible to find j_y. This could be done numerically, however, and would be an interesting problem for future study. Instead, it was decided to use the non-relativistic form of (51) in order to solve for j_y, and then make certain assumptions about the relativistic corrections. This is probably a reasonable approach since in the region of interest near the cathode, the voltages are usually less than 1 MV. Our solution is similar to that given by Slater[3]. The cathode current density can be obtained from the following set of equations:

$$j_y (f') = j_y (0) \left[\frac{9}{4} \frac{f' (1 - f')}{\nu} \right] \tag{52}$$

$$p = \nu I_k^2 (\nu) \tag{53}$$

$$I_k (\nu) = \left[\frac{(2k + 1)\pi}{2\nu^{3/2}} - \frac{\sqrt{1 - \nu}}{\nu} - \frac{1}{\nu^{3/2}} \tan^{-1} \sqrt{\frac{1 - \nu}{\nu}} \right] \tag{54}$$

$$(k = 0, \pm 1, \pm 2, \ldots .)$$

$$f' = p/(1 + p) \tag{55}$$

In the above equations, f' is the non-relativistic form of f in (47):

$$f' = \frac{\eta}{2} \frac{(B_\theta y)^2}{V} \tag{56}$$

The parameters p and ν are dummy variables to simplify the writing of the equations.

The first branch $0 \leq f' \leq 1$ is generated by a combination of the solutions for $k = 0$ ($0 \leq \nu \leq 1$) and $k = -1$ ($1 \geq \nu \geq 0$). In the conduction region, this is probably the only solution that is physically realized. The above equations are expressed in parametric form with respect to ν. Given a value for ν, p can be solved for using (53) and (54). Then f' is obtained from (55). Finally, j_y is determined from (52) using f' and the assumed value for ν. In (52), $j_y(0)$ is the current density obtained for $f' = 0$, or no self-magnetic field.

In this manner, the functional relationship

$$j_y (f') = j_y (0)\ F (f') \quad (0 \leq f' \leq 1) \tag{57}$$

can be generated numerically and is displayed in Figure 1. A least squares fit to F, accurate to 1%, gives

$$F (f') = 1.0 - 0.0578\ f' - 0.7423\ f'^2 + 1.4871\ f'^3 - 0.9797\ f'^4 \tag{58}$$

with $F (0) = 1$, $F (1) = 9/4\pi$.

The transition to a relativistic solution is then made by assuming that the functional form of F remains unchanged, letting $f' \rightarrow f$, and interpreting $j_y (0)$ as Acton's relativistic solution for planar diodes neglecting self-magnetic field effects (since $f = 0 \rightarrow B_\theta = 0$).

Thus:

$$j_y (f) = j_y (0)\ F (f) \quad (0 \leq f \leq 1) \tag{59}$$

where f is given by (47).

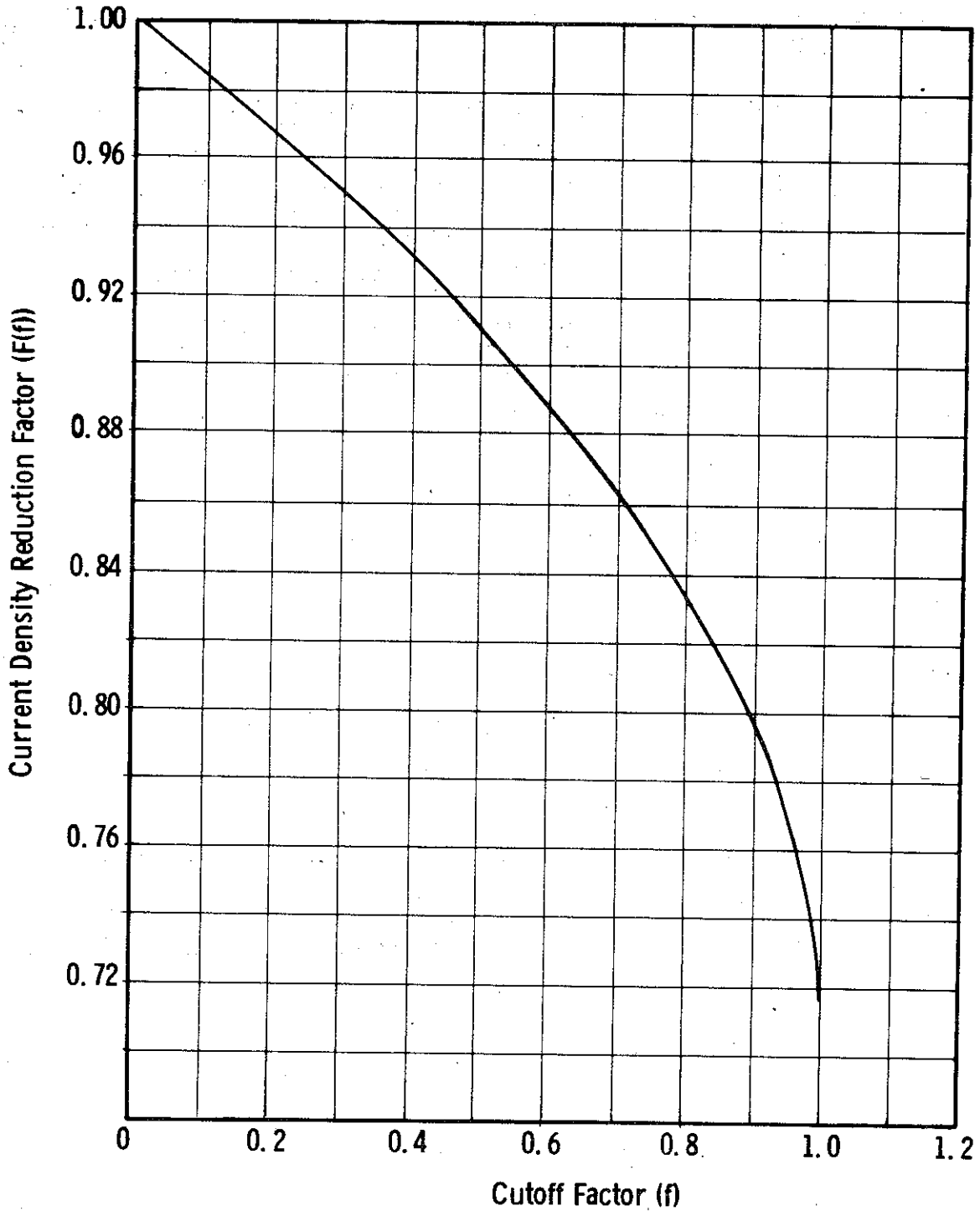

Figure 1. Current Density Reduction Factor Versus Cutoff Parameter for Conduction Region

If $0 \leq f \leq 1$, the position of y is located inside of the beam; if $f > 1$, y is located outside of the beam; at the beam edge, $f = 1$. If y is chosen to be much smaller than the radius of curvature of the cathode, trajectories having $f \geq 1$ will generally return to the cathode, thus forming a space-charge sheath.

If $f > 1$ and the trajectory reaches the anode, presumably the factor of $9/4\pi$ should still be used, although an additional correction is now required since the potential V(y) is being determined outside of the beam. (The limitations inherent in finite difference methods require that V be measured at a distance of at least one mesh diagonal from the cathode. However, the sheath thickness, y_s, is often less than this.) If $f > 1$ and the trajectory returns to the cathode, still another correction is needed to account for the multistream flow pattern. Both additional factors have been estimated and both tend to significantly reduce $\vec{j}$.

At this point, the question naturally arises as to whether it is possible to predict, a priori, the beginning of the cutoff region. If $f \geq 1$, y lies outside of the beam. If y has been chosen to lie sufficiently close to the cathode, it is likely that the trajectory will either return to the cathode or at least never travel beyond y_s. If $f < 1$, this behavior is still possible if $y_s > y$, but y_s does not extend to the real anode. Fortunately, because of equation (48), the transition between the conducting and cutoff regions occurs fairly rapidly as $f \to 1$, so that $f \approx 1$ is a reasonable choice to describe the transition.

2. The Cutoff Region

The self-magnetic field, dependent emission current density required by space-charge limited flow for the conductance region is given by (59). The proper form for the cutoff region is, however, an unsolved problem. Certainly F should be reduced below $9/4\pi$ to account for multistream flow. If equal and opposite streams of electrons are flowing near the cathode, for instance, F should be replaced by F/2.

It is thus reasonable to suppose that as f becomes larger than unity, $j_y(f) \to 0$. Since the least squares fit to F(f) goes smoothly to 0 at f = 1.35, it was decided to calculate cathode emission using the following approximate expression:

$$j_y(f) = j_y(0)\ F(f),\ 0 \le f \le 1.35 \qquad (60)$$

$$= 0 \qquad f > 1.35$$

This model for cathode emission allows the computer to determine the edge of the emitting portion of the cathode. The cutoff region is actually generated by launching trajectories having an associated current density given by (60). The emission ends at that point on the cathode where f > 1.35. Multistream flow which can occur in the conduction region is not taken into account.

Another approach used to describe the cutoff region has been to first use the computer program to ascertain where the cutoff region appears to begin. Then, on subsequent calculations, the space-charge sheath is simulated by using an additional zero-potential electrode on the back portion of the cathode that depresses the potential in much the same manner as the sheath.

The potential at the surface of the sheath is given by setting $f(y_s) = 1$ in (47):

$$V_1(y_s) = V_n \left[\sqrt{1 + \eta \frac{(B_\theta\ y_s)^2}{V_n}} - 1 \right] \qquad (61)$$

The space charge density is obtained from (49):

$$\rho_1(y_s) = \eta \epsilon_o B_\theta^2 \left(1 + \frac{\eta B_\theta^2 y_s^2}{V_n} \right)^{-3/2} \qquad (62)$$

It is then assumed that (61) holds in a region year y_s and that for $y > y_s$, the potential obeys Laplace's equation and has the form

$$V_2(y') = V(y_s) + \frac{(y' - y_s)}{(y - y_s)} \left[V(y) - V(y_s) \right] , \qquad (63)$$

where $y_s \le y' \le y$.

Here $y > y_s$ is some arbitrary distance (near y_s) at which the potential V(y) is determined. The form of (63) has been chosen so that $V_1(y_s) = V_2(y_s) \equiv V(y_s)$.

Setting $dV_1/dy = dV_2/dy$ at y_s, the sheath thickness can be solved for:

$$y_s = y \left[\frac{1 - \sqrt{\gamma^2 - (1 - 1/f)}}{1 - (\gamma^2 - 1)(f - 1)} \right] , \tag{64}$$

where γ and f are evaluated at y and $f > 1$. If the zero potential cathode surface is then extended by an amount y_o in the +y direction such that

$$y_o = \left[\frac{y_s V(y) - y V(y_s)}{V(y) - V(y_s)} \right] , \tag{65}$$

the resultant Laplacian potential will be equal to $V(y_s)$ at y_s. The effective electrode thus establishes the potential at the sheath edge at the value which would have been produced by the actual presence of the sheath.

A limitation to this approach is that it does not account for the possibility of current flow out of the sheath electrode, essentially parallel to the cathode surface. It is, therefore, important to begin the sheath electrode far enough back on the cathode so as to minimize the neglected current flow. A plot of V (y) as given by (61) within the sheath region ($y \leq y_s$) is compared to the actual values obtained from the potential matrix of a flow calculation in Figure 27(a) in a later section of this report. The agreement is quite good.

3. Cathode Curvature Effects

In the case of the toroidal guns investigated, the cathode radius of curvature is often significant in comparison to one mesh diagonal, thus violating the important assumption that V = V (y) over the region of interest. Since storage considerations limit the total number of mesh points that can be used ($\leq 10^4$), this problem could not be solved by decreasing the mesh size.

The effects of curvature were determined by rederiving the initial results of Section II-C-1 for a cathode of circular cross section. A local system of cylindrical coordinates (r, ϕ) is set up with origin located at the center of curvature. The equation of the surface of the cathode (in a plane of constant θ) is thus $r = r_c$ and the anode is represented by $r = r_a$. It is further assumed that $V = V(r)$ and $\vec{j} = \hat{r}\, j(r)$, where $\hat{r}$ is a unit vector in the radial direction. The quantity $\hat{r}\, j(r)$ is a constant of the motion so that

$$j_r = j_c\left(\frac{r_c}{r}\right) \tag{66}$$

Both of the cases $r_c < r_a$ and $r_c > r_a$ were investigated. In the first case, $r \geq r_c$ in (66), in the second case $r \leq r_c$.

Each portion of the cathode is then assumed to be a part of a cylindrical magnetron with applied field B_θ and have a radius equal to the <u>local</u> radius of curvature. In this way, a general result can be obtained for the cutoff factor.

$$f_\kappa = f\left(\frac{1 + y\kappa/2}{1 + y\kappa}\right)^2 \tag{67}$$

where $\kappa = 1/r_c$ is the local curvature of the cathode. The quantity y is a distance which is parallel to the local normal and f is given by (47). Note that $|y\kappa|$ must be < 1 if $\kappa < 0$. The three cases are:

$\kappa < 0$, concave cathode region,

$\kappa = 0$, planar cathode region,

$\kappa > 0$, convex cathode region.

Equation (67) is assumed to hold locally so that κ can vary from point to point on the cathode provided that this variation is not too rapid. Since y will be equal to 1 or 2 mesh diagonals measured from the cathode surface, the assumption of space-charge limited flow guarantees that the equipotential surfaces more or less follow the local outline of the cathode.

If it is now assumed that F is independent of κ, (59) can be generalized to read:

$$j_y(f_\kappa) = j_y(0)\, F(f_\kappa) \qquad (0 \le f_\kappa \le 1) \tag{68}$$

where $j_y(0)$ is now Acton's solution for cylindrical diodes. There is certainly some justification for this. The current-voltage relation for the cylindrical magnetron has been solved in the limit of cutoff conditions.[4] The important result for this discussion is that for $\kappa y < 3$, $F(1) \sim 9/4\pi$ is as obtained in the linear case. Thus, it seems reasonable to assume that the "linear" and "cylindrical" F functions are reasonably close, and that curvature effects are essentially all contained in f_κ. Again, this would be an interesting problem to investigate on a rigorous basis.

III. COMPUTER ANALYSIS OF MEGAVOLT DIODES

A. COMPUTER PROGRAM FOR GUN ANALYSIS

The Varian Electron Gun Analysis Program has been successfully used for over seven years in the design of electron guns. The main purpose of the program has been to simulate the steady-state behavior of thermionic cathode guns used for the production of long cylindrical beams in microwave tubes. The program can handle electrodes having arbitrary potentials and arbitrary shapes in cylindrical geometry. The effects of both beam space charge fields and the induced circumferential self-magnetic field are included in the analysis. In addition, a nonuniform dc magnetic field can also be specified.

1. Program Design

The general design of the program is shown in the flow chart on the following page. The input to the program consists of a mesh size and a set of closed boundaries defined by data points at which potentials are specified. Two types of boundaries are possible: Dirichlet, on which the potential is defined; and Neumann, on which the normal derivative of the potential is zero.

The program overlays the gun region with a rectangular mesh limited to 10^4 cells. The quantities of interest are assumed to vary in a relatively simple fashion between mesh points (stepwise or linear). A number of representative trajectory origins are chosen at the cathode surface. A trial space-charge is then constructed, if desired, and Poisson's equation is solved for that potential which is consistent with the combined effects of the boundary potentials and the space-charge. The solution is obtained by applying successive over-relaxation techniques to the difference equations defined on the mesh. The current density to be associated with each trajectory is then computed, and the trajectories are traced through the gun region using the equations for relativistic space-charge flow together with a

Electron Gun Program Flow Chart

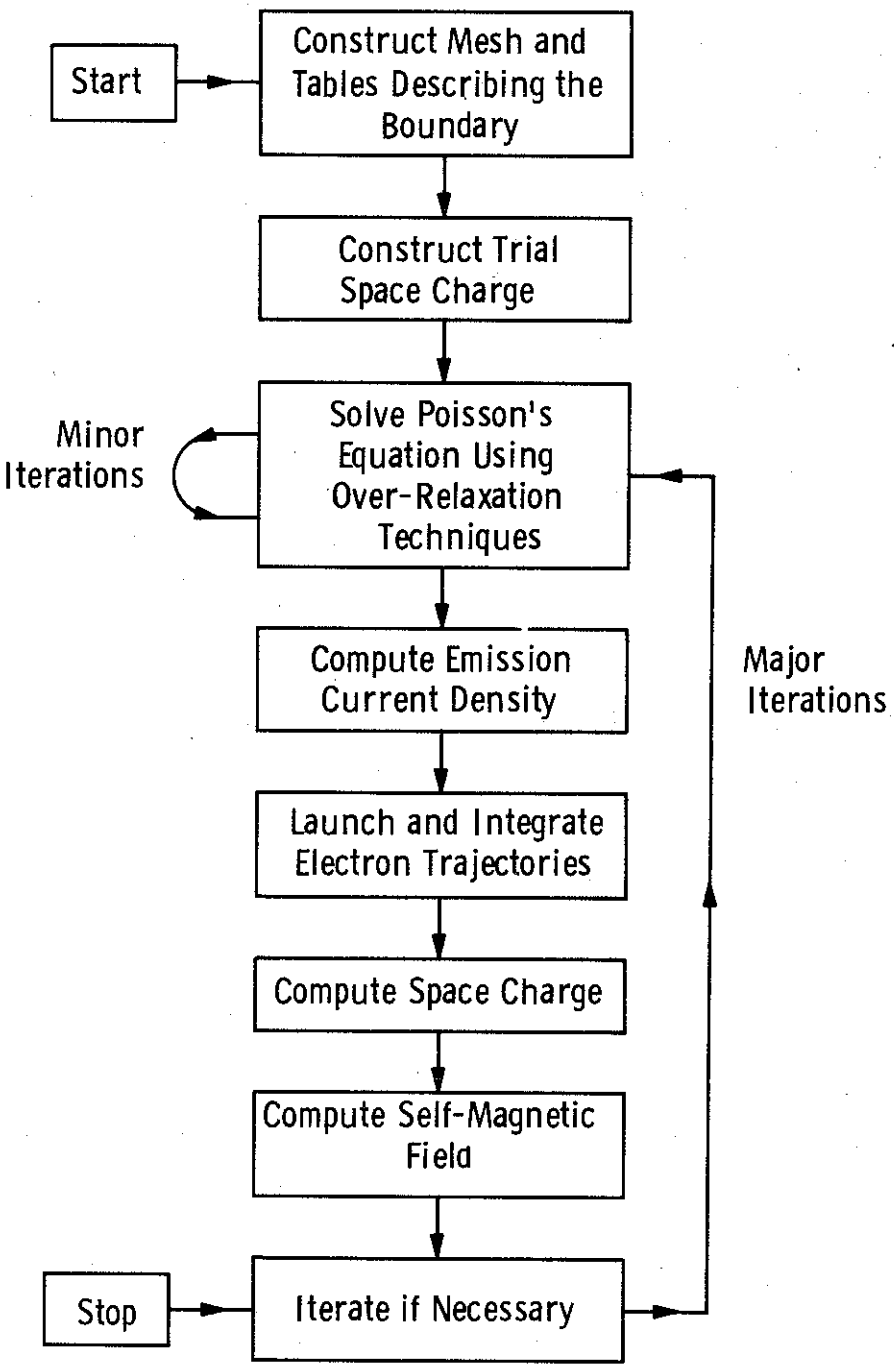

simplified model for the self-magnetic field. A new space-charge is then computed for each mesh cell interior to the beam, using the trajectory coordinates, velocity, and associated current density. Finally, the self-magnetic field is computed at each mesh point.

Next, the program iterates using the new space-charge distribution to resolve Poisson's equation and establish new potentials and electric fields. The current density is again computed and the trajectories retraced, this time using the self-magnetic field matrix based on the previous iteration. The entire process is repeated until either a specified number of iterations have been completed or there is a sufficiently small difference between one iteration and the next.

2. Cathode Emission Model

The proper implementation of the boundary condition $\vec{E} = -\vec{\nabla} V = 0$ at the cathode for space-charge limited flow is one of the major problems of computer gun simulation. The strategy adopted here is to obtain an equation expressing the electric field near the cathode as a function of the field at the cathode, the distance, the magnetic field, and the current density. By setting the field at the cathode to zero, and integrating the resulting differential equation for V, the required current density can be expressed as a function of potential, distance, and magnetic field. Most of the theoretical investigations under this contract, presented in Sections II and III, were related to this important problem.

The program makes use of these results in the following way. At each trajectory origin, the potential and self-magnetic fields are determined at a perpendicular distance y. The theoretical results are then used to find the current density. Since the self-magnetic field at any point is proportional to the total current enclosed, the current density calculation must involve iterative procedures.

In addition to the provision for space-charge limited emission, the program can simulate thermally-limited flow by specifying a maximum allowable

current density. In those cases where the initial conditions of the flow are known (or assumed), an "injected beam option" allows the current and initial velocity to be specified as input.

3. Space-Charge Calculation

Two types of space-charge models are used in the program. The first type, the "laminar model," assumes that the flow is laminar and distributes the space charge between trajectories on the basis of their relative positions and intertrajectory currents at the cathode. The second type, the "line model," associates a fixed amount of current with each trajectory and distributes space-charge only to those mesh cells through which the trajectory passes.

The line model thus assumes no correlation between neighboring trajectories and is the more appropriate method for treating nonlaminar flow. It is also considerably faster than the laminar model. On the other hand, the line model can introduce significant errors into the calculation if the "gaps" in the space-charge are too large.

4. Self-Magnetic Field

There are also two models used to represent the self-magnetic field: a laminar model, and a model based on a "current enclosed matrix," $I(r, z)$ (see Equation (18)) obtained from the previous iteration.

The laminar model assumes that the current contained between a trajectory and the axis remains constant and is given by the initial value at the cathode, I_c. Provided the beam remains laminar, this method is completely rigorous. However, the beam becomes nonlaminar so that outer trajectories begin to cross inner ones, $B_\theta \propto I_c/r$ becomes too large and results in a "self-feeding" force that may result in a spectacular beam collapse. This model is normally used for the first iteration only, and B_θ is usually reduced by some factor to prevent beam collapse.

On subsequent iterations, the self-magnetic field is obtained from the current matrix of the previous iteration scaled to reflect the new total current content of the beam. In the case of convex cathodes, the current flowing through the cathode must be considered in setting up the matrix. Special care is taken to keep track of those trajectories which return to the cathode, so that the current matrix will be based upon the net cathode-anode current. This treatment, of course, is only rigorous in the limit of self-consistency. However, it can handle very nonlaminar beams without difficulty and, in addition, exerts a stabilizing influence on the flow.

5. Averaging Techniques

There are several types of averaging and limiting techniques that can be used in the program to enhance the stability of solutions and to speed self-consistency. No general rule can be readily discerned for their optimal use; this may well change for each new configuration.

It has already been mentioned that a maximum current density, j_{max}, can be specified as input. In addition, the current density associated with each trajectory is usually averaged with the value obtained on the previous iteration.

The total current can also be limited by specifying a maximum and minimum perveance as input. If either of these limits is exceeded on a given iteration, the current is scaled to the nearest limit by applying a constant correction factor to each value of the emission current density. Finally, the space-charge used to solve Poisson's equation can be any predetermined weighted average of the last two space-charge calculations. No attempt was made to average successive current matrices, although this may be a worthwhile approach.

When these various techniques are used, the term "self-consistency" now implies that not only are several consecutive iterations reasonably similar in beam size, current, and current density distribution, but that j_{max} has not been exceeded and the perveance has remained within the required limits.

B. PLANAR DIODES WITH APPLIED AXIAL MAGNETIC FIELD

Previous experience with the computation of flows in megavolt-megampere guns[1] revealed that a major problem was choosing the proper initial guess as to a beam current, beam size, and potential distribution in order to obtain convergence to a self-consistent iterative solution to the problem. In order to provide a gradual transition from a relatively predictable flow to the one being sought, an axial magnetic focusing field was employed in a series of cases with the same electrode geometry and voltage, but with the magnetic field reduced in steps to zero. The initial guess for the flow could be adjusted for each successive case according to the results of the previous case (or cases, using extrapolation). Also, the results with a strong confining field may prove directly useful since it is clearly possible to employ such a field in practice.

Initially, a computer solution was tried using a planar diode with 70 cm cathode-to-anode spacing and an applied axial magnetic field of 3000 gauss. The emitting surface was circular with a radius of 50 cm. Execution of the simulation stopped during the first integration since the cyclotron wavelength became too small a multiple of the integration step. Data for the edge of the beam was printed out indicating an outer beam radius of 49.25 cm, and although the solution was not converged, this value for the radius appears to be reasonable.

Other values of focusing field used with this geometry were (in gauss): 1,000, 500, 250, 125, and 0.

The solution obtained with an axial field of 1,000 gauss converged to within 3% of a self-consistent solution after six iterations. Comparison with ideal planar flow for this case gave the following results for the beam edge at the anode:

$$V_\theta / V_z = 1.74 \times 10^{-2}$$

$$V_r / V_z = 2.33 \times 10^{-2}$$

where V_r, V_θ, and V_z are, respectively, the radial, circumferential, and axial

components of energy in electron-volts. From these criteria, planar flow was essentially achieved in this case.

Figure 2 is a plot showing the computed flow. For this same gun, Figures 3 and 4 show, respectively, plots of current density versus radius at the cathode and at the anode. The sharp peak in current density at the edge of the beam results from arbitrarily limiting the emitting portion of the zero potential planar electrode.

From Equation (34) of the report referenced on the previous page, current for an ideal planar gun with a 70 cm gap and a 50 cm radius is 94.5 kA; the computer analysis gave a current of 137.8 kA. The enhanced cathode emission at the beam edge accounts for the high current in the computer calculations.

Figure 5 shows the flow for the 70 cm gun with an axial magnetic field of 250 gauss. The self-magnetic field in this case produced a substantial constriction or "pinch" of the beam, thereby increasing potential depression in the beam.

As the magnetic focusing field was reduced, the convergence of the solutions became worse. Figure 6 is a plot of beam radius and beam current versus iteration number for the 70 cm gun at 15 MV, with no focusing field. The degree of convergence can be seen from this plot. Indications are that iteration number 6 is a representative solution. Computed electron trajectories and equipotentials for iteration 6 of the 70 cm gun with no focusing field are shown in Figure 7.

For comparison with the gun using a 1000 gauss focusing field, Figures 8 and 9 show the current densities at the cathode and anode versus the radius with no focusing field. The current densities at the inner radii of the cathode are substantially reduced by the increase in potential depression caused by the beam pinch. The current density in the beam at the anode is greatly increased and appears to be more irregular (but this may be due to the coarseness of the numerical solution).

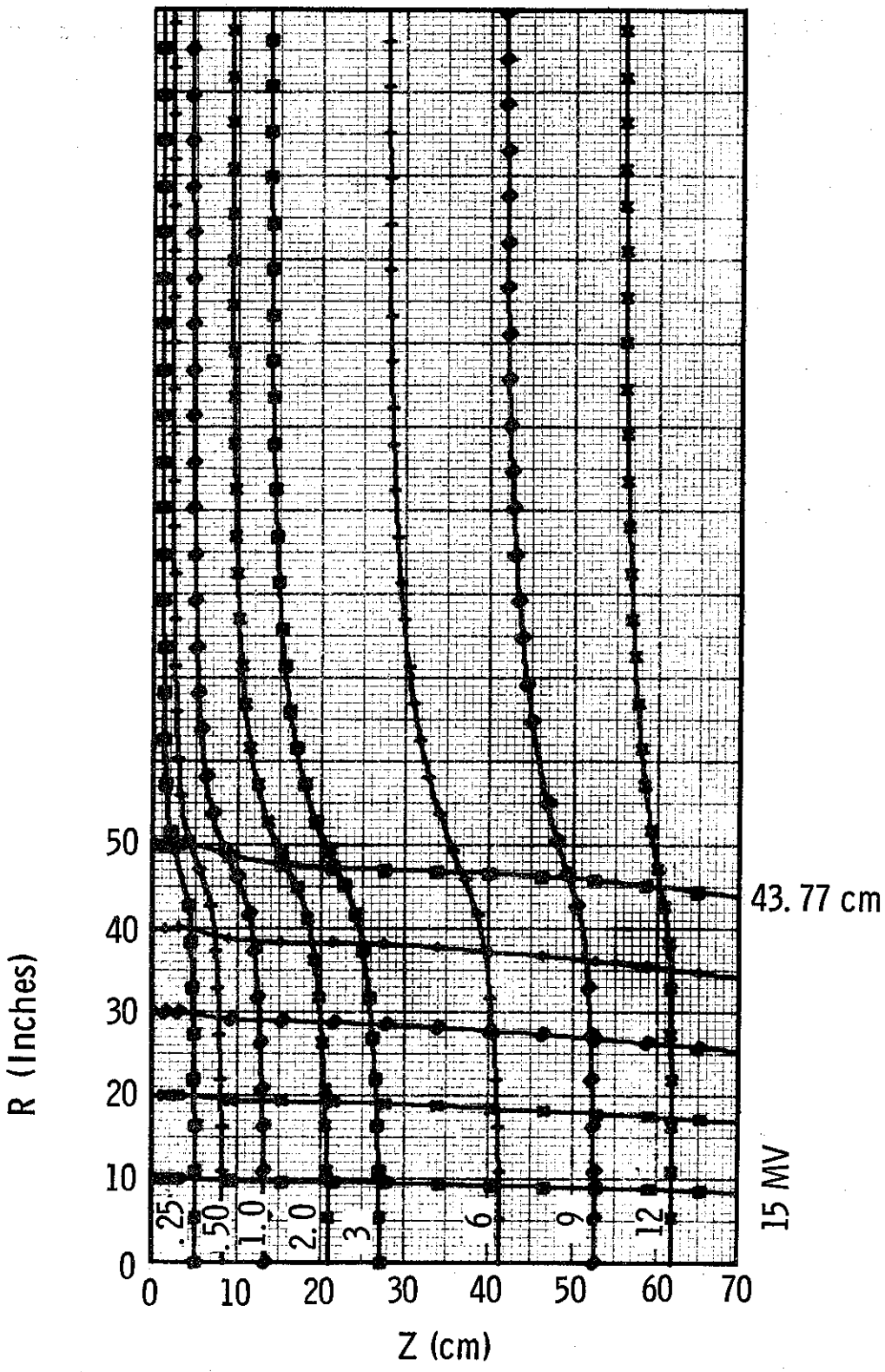

Figure 2. Computed Electron Trajectories and Equipotentials, Planar Gun at 15 MV with a 70 cm Spacing and a 50 cm Cathode Radius and a 1000 Gauss Axial Magnetic Field

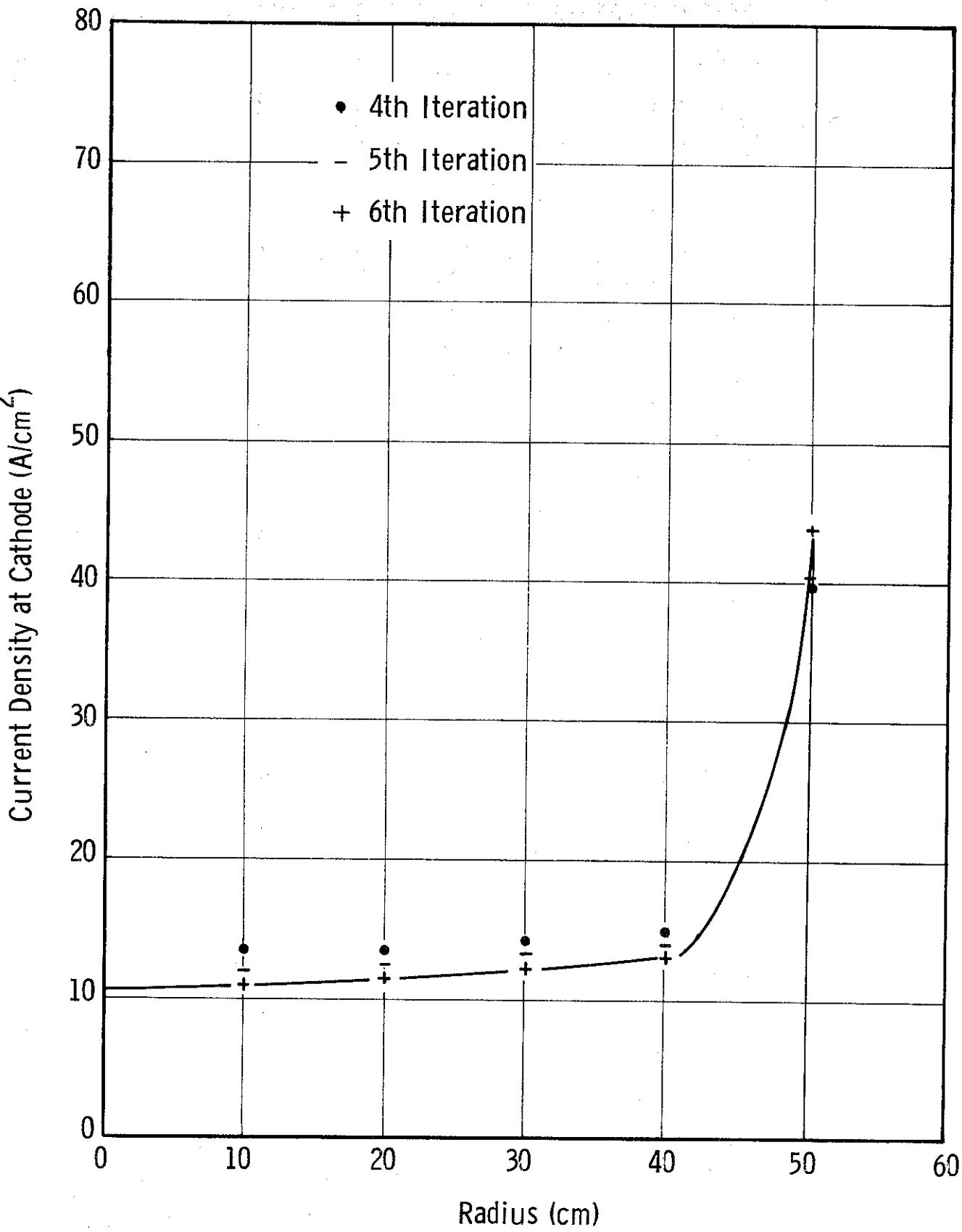

Figure 3. Computed Value of Current Density at Cathode Versus Radius, Planar Gun at 15 MV with a 70 cm Spacing and a 50 cm Cathode Radius and a 1000 Gauss Axial Magnetic Field

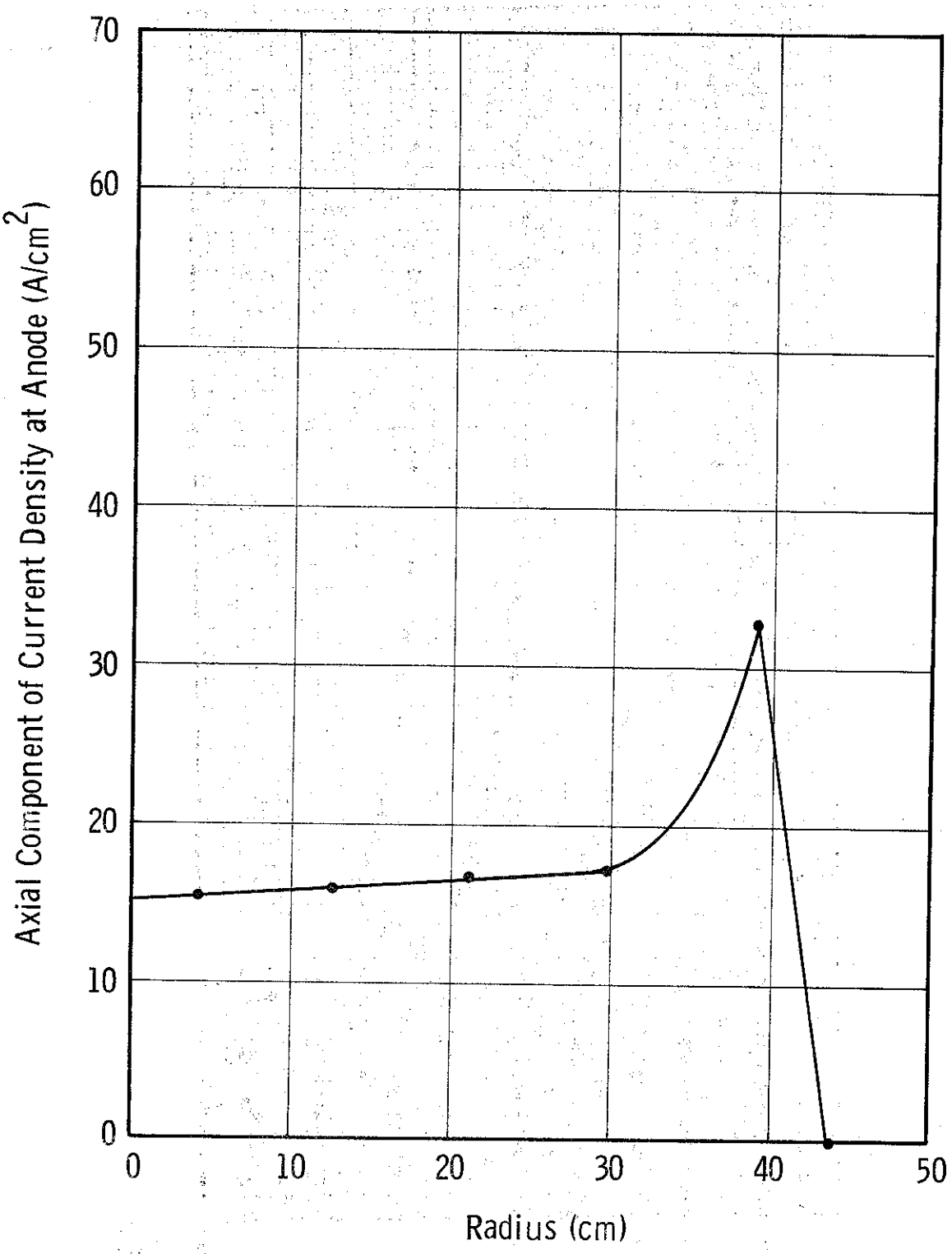

Figure 4. Computed Value of Axial Component of Current Density at Anode Versus Radius, Planar Gun at 15 MV with a 70 cm Spacing and a 50 cm Cathode Radius and a 1000 Gauss Axial Magnetic Field (Iteration 6)

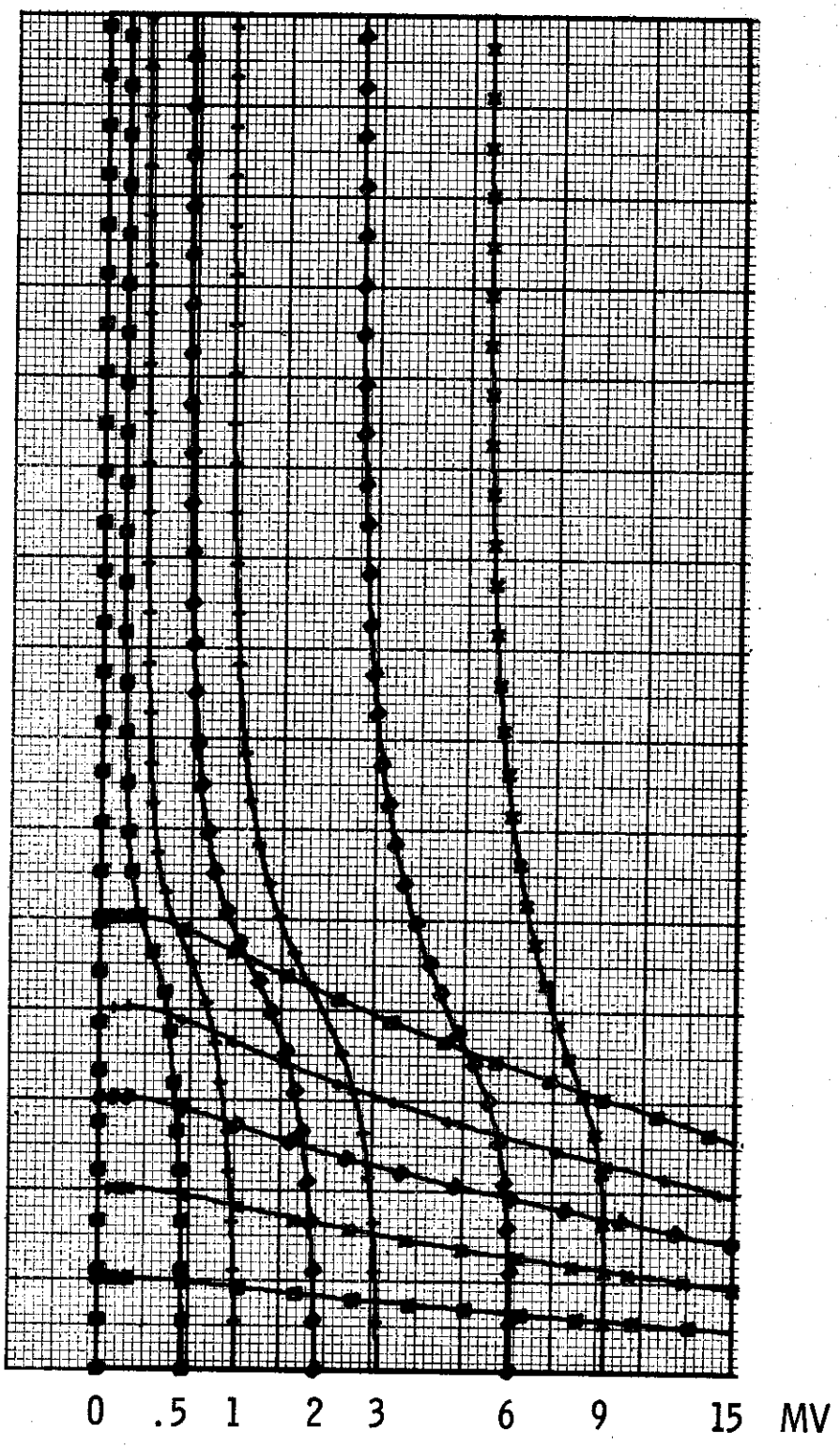

Figure 5. Computed Electron Trajectories and Equipotentials, Planar Gun with a 70 cm Spacing and a 50 cm Cathode Radius and a 250 Gauss Axial Magnetic Field

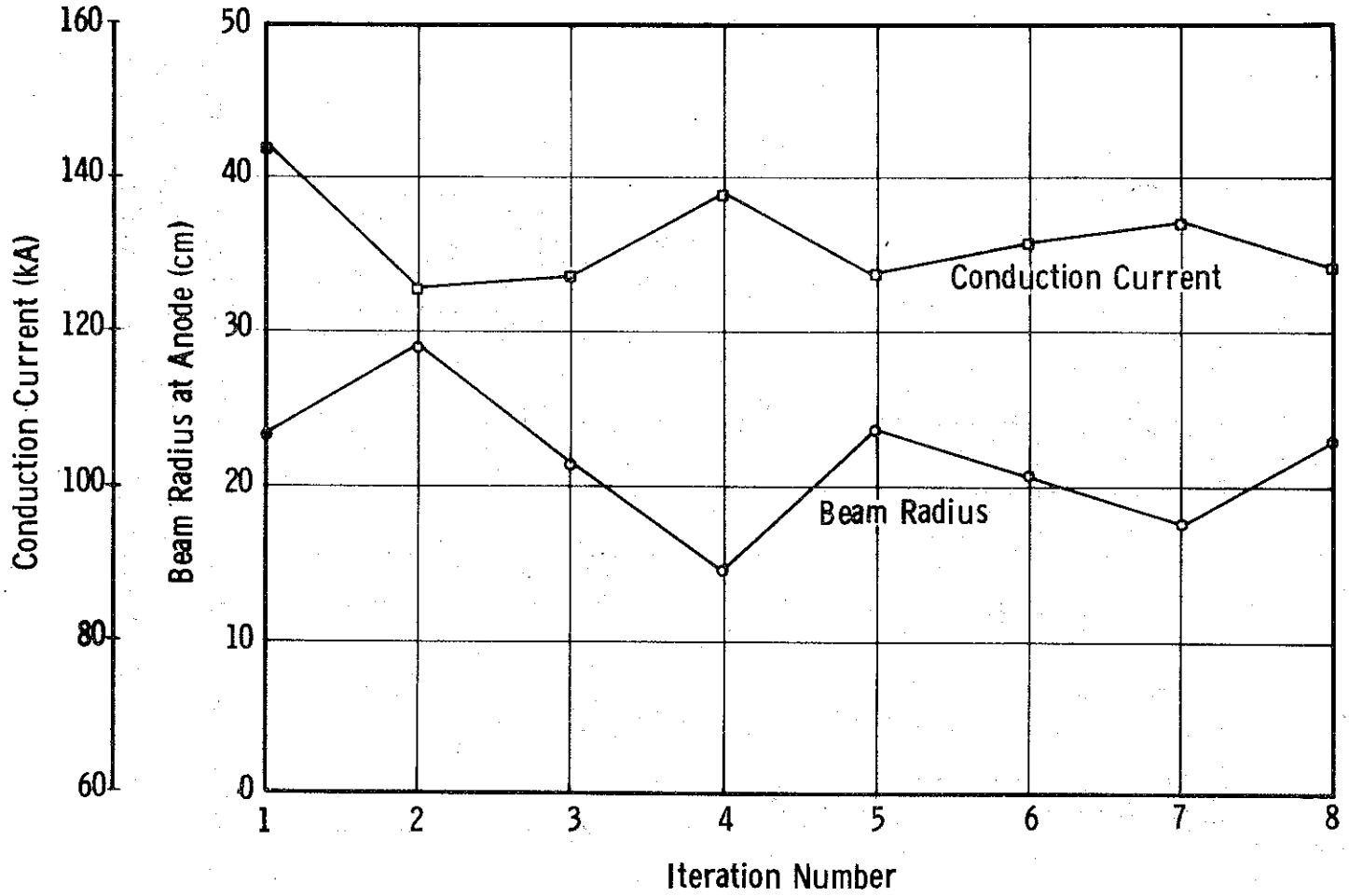

Figure 6. Computed Values of Beam Radius at Anode and of Conduction Current Versus Iteration Number, Planar Gun at 15 MV with a 70 cm Spacing and 50 cm Cathode Radius and with No Axial Magnetic Field

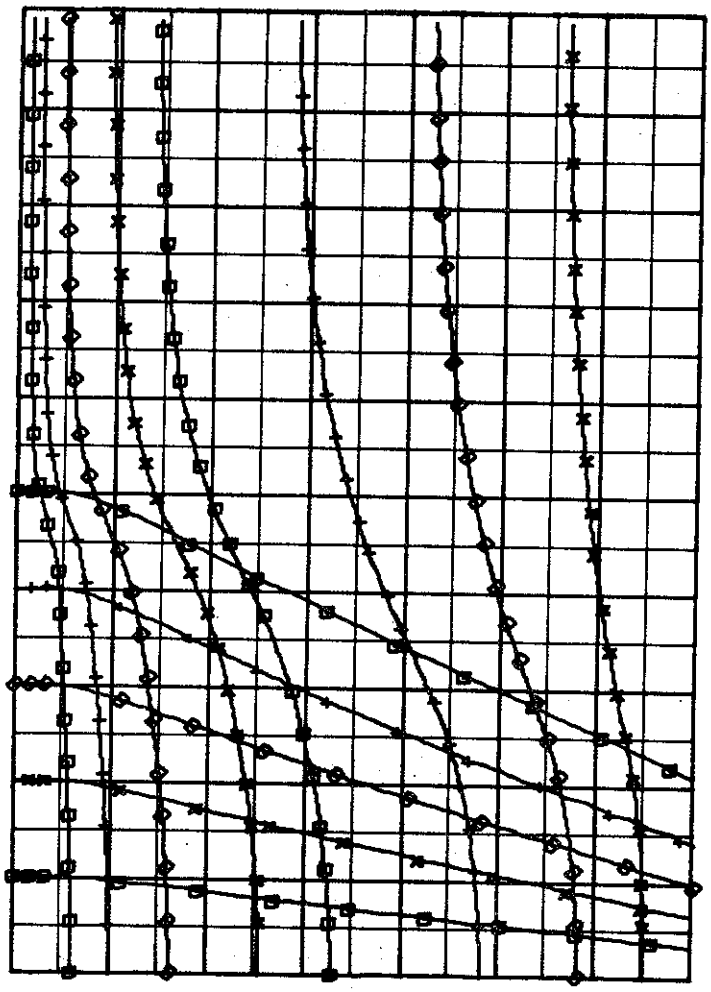

Figure 7. Computed Electron Trajectories and Equipotentials, Planar Gun at 15 MV with a 70 cm Spacing and a 50 cm Cathode Radius and with No Axial Magnetic Field

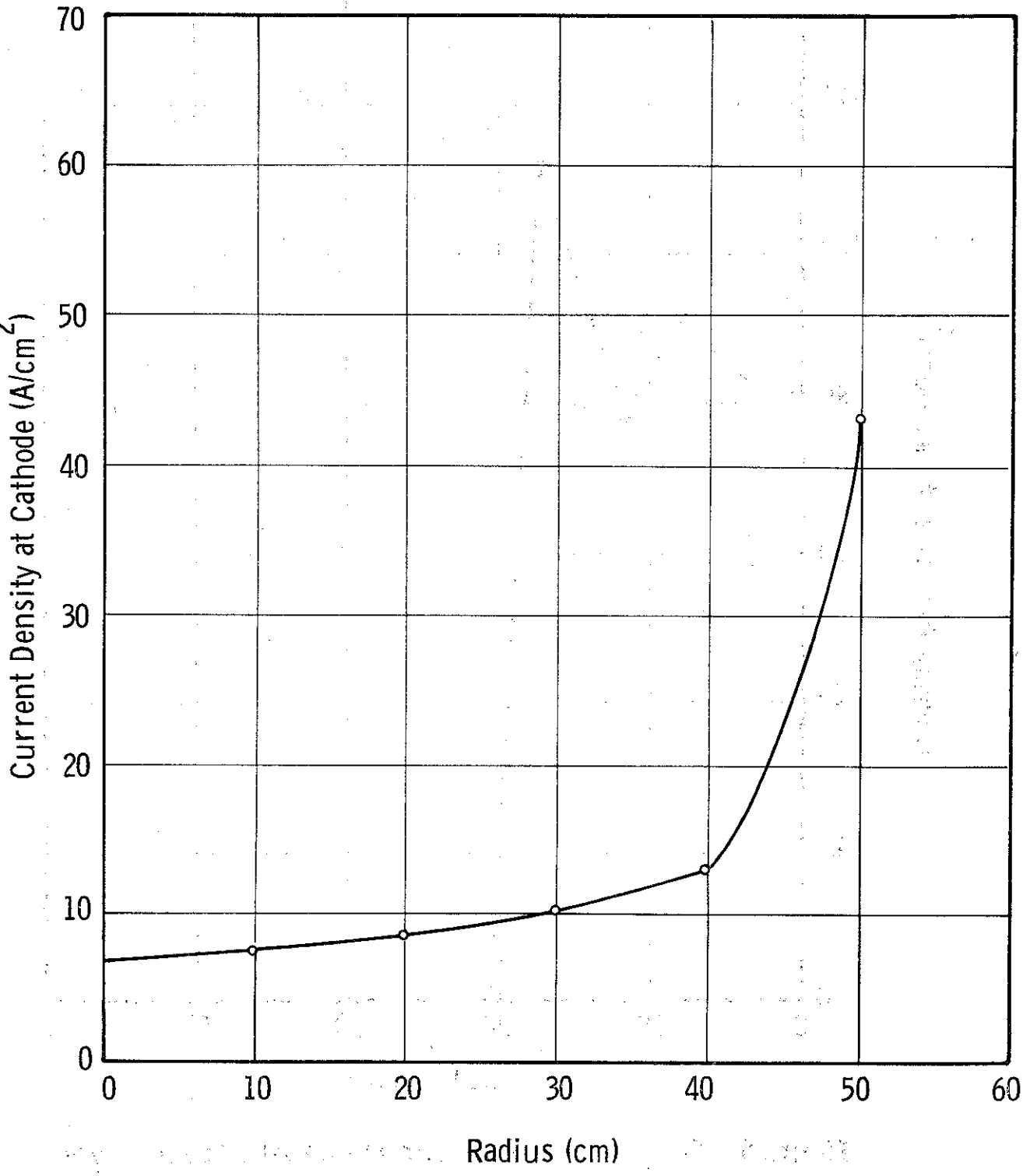

Figure 8. Computed Value of Current Density at Cathode Versus Radius, Planar Gun at 15 MV with a 70 cm Spacing and a 50 cm Cathode Radius and with No Axial Magnetic Field (For Most Representative Iteration, No. 6)

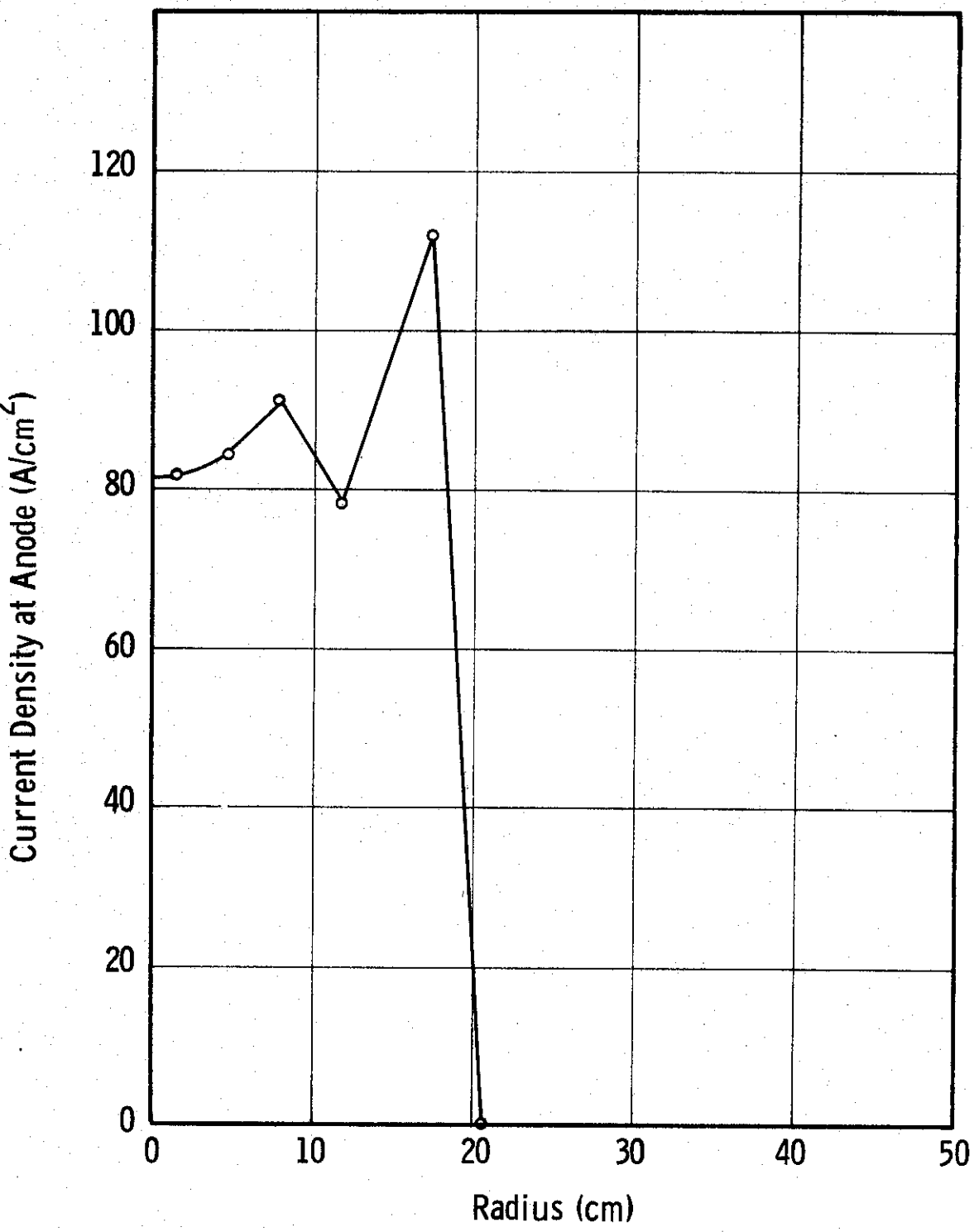

Figure 9. Computed Value of Current Density at Anode Versus Radius, Planar Gun at 15 MV with a 70 cm Spacing and a 50 cm Cathode Radius and with No Axial Magnetic Field (For most Representative Iteration, No. 6)

Figure 10 shows beam current, beam radius, and the ratio of the circumferential self-magnetic field at the anode to the axial focusing field. Each curve is plotted versus the axial magnetic flux density for the planar gun computations with the 70 cm electrode spacing. The curves show the reduction in conduction current which occurs as the beam is allowed to pinch. Note also that the focusing field required to almost eliminate the pinch is about equal to the self-magnetic field which produces it. The field of 800 gauss required for this gun would be readily achievable in practice. The improvements in convergence indicated in Figure 10 for the solution with no axial field over that for 125 gauss is due to a more optimal choice of damping factors used in the numerical solution.

The ratios of radial to axial and tangential to axial velocity at the beam edge at the anode are plotted versus the axial magnetic field strength in Figure 11. The radial velocity monotonically decreases as the focusing field is increased. As the focusing field is raised from zero, the tangential velocity increases from zero to a maximum value (at the flux density for which the curve for anode radius versus flux density has a point of inflection), and then decreases monotonically. Thus, with a sufficiently high axial magnetic field, the flow can be made to be essentially parallel to the axis at the anode. A theoretical treatment for confined flows with high self-magnetic field is discussed in Section II-B.

Calculations were performed for a 15 MV planar diode with the interelectrode spacing reduced to 20 cm. The emitting area was again limited to a radius of 50 cm. Consecutive computer studies were made using axial focusing field values of 10, 5, 2.5, 1.5, and 0 kgauss. The convergence of the solution was excellent at 10 kgauss but deteriorated as the axial field strangth was reduced. Without an axial magnetic field, no meaningful solution could be obtained.

The computed electron trajectories and equipotentials with an axial field of 10 kgauss are shown in Figure 12. Though the conduction current is about 1.28 MA, the flow is nearly parallel to the axis and the field inside the beam nearly independent

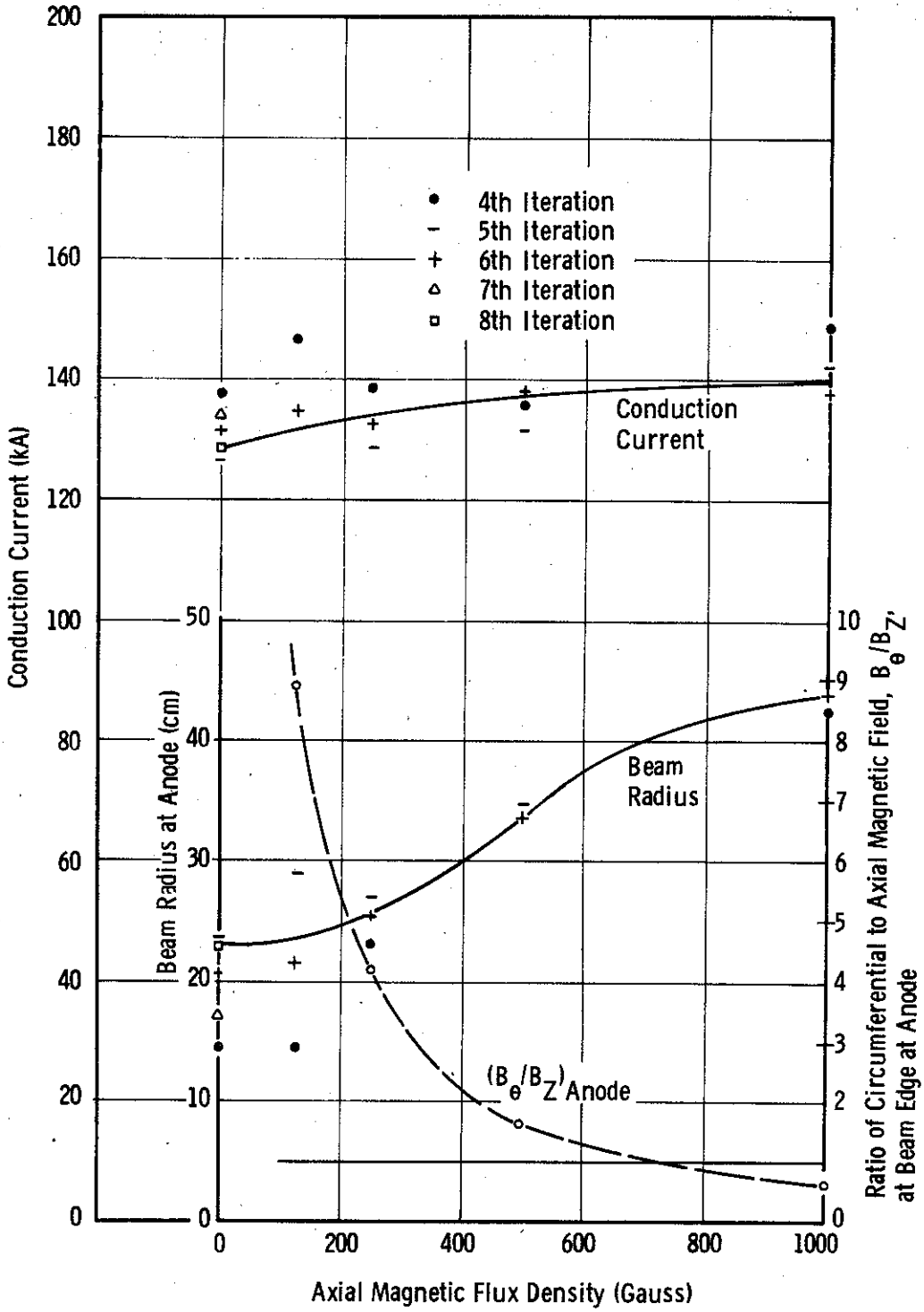

Figure 10. Ratio of Circumferential to Axial Magnetic Field at Beam Edge and Conduction Current and Beam Radius Versus Axial Magnetic Flux Density, Planar Gun at 15 mV with a 70 cm Spacing and 50 cm Cathode Radius

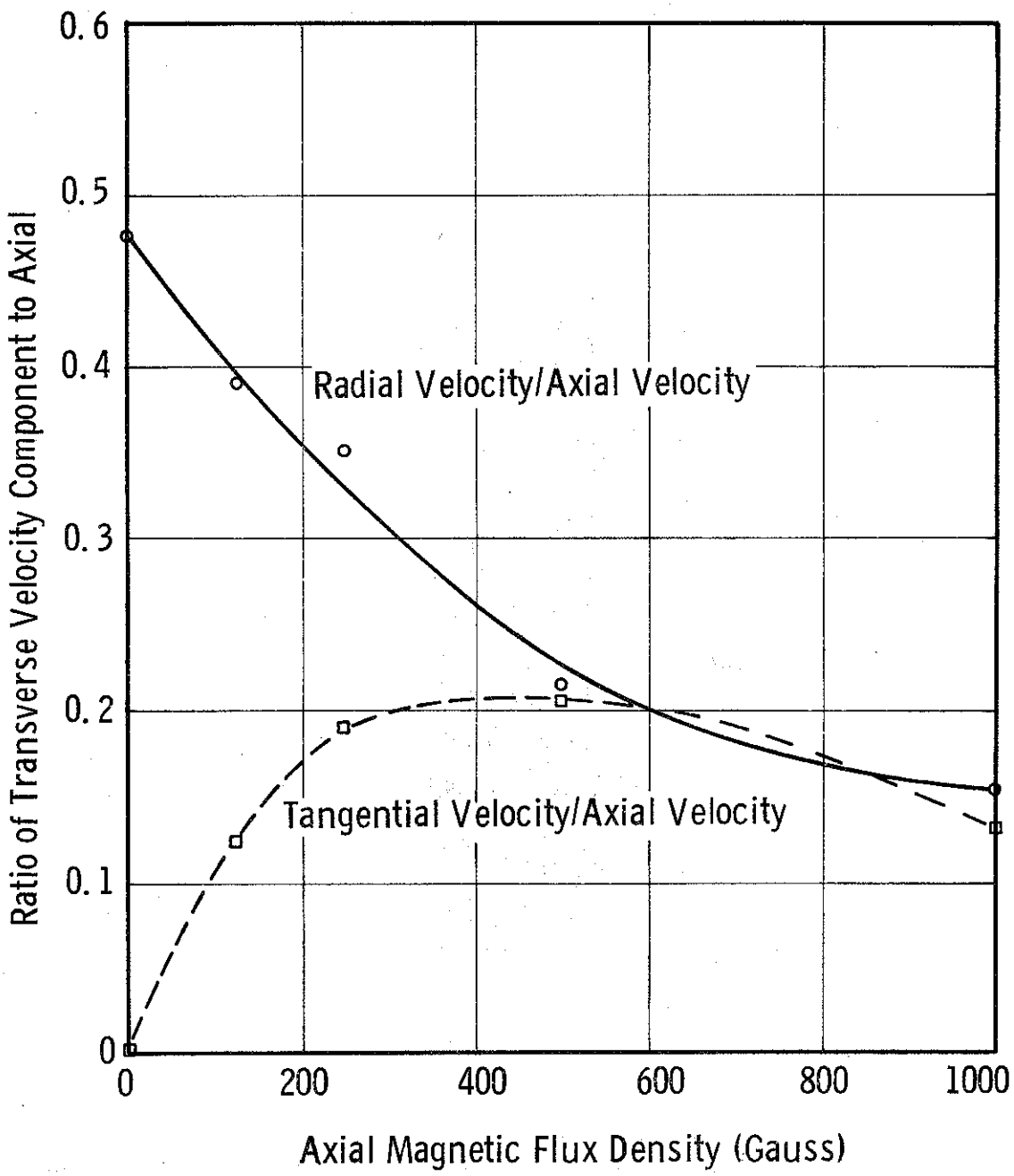

Figure 11. Computed Values of Radial and Tangential Velocity Components Normalized to Axial Velocity at Beam Edge at Anode Versus Axial Magnetic Flux Density, Planar Gun at 15 MV with a 70 cm Spacing and 50 cm Cathode Radius

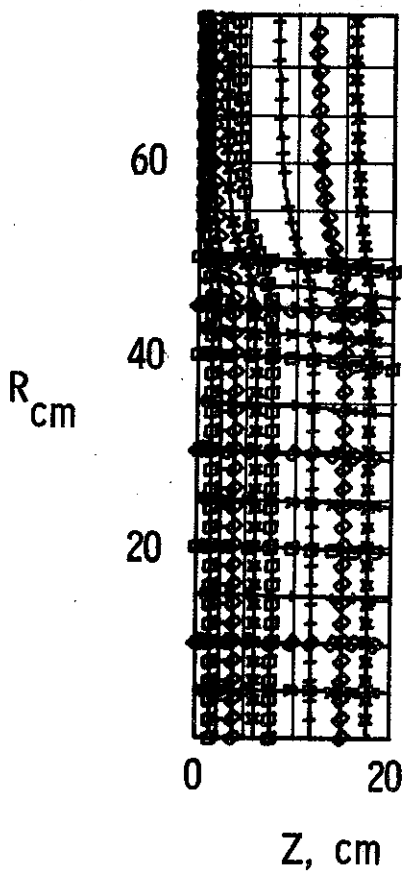

Figure 12. Computed Electron Trajectories and Equipotentials, Planar Gun at 15 MV with a 20 cm Spacing, a 50 cm Cathode Radius, and a 10,000 Gauss Axial Magnetic Field

of radius. As a result, the cathode current density is almost uniform, except for a sharp peak at the edge of the beam due to the arbitrary ending of the emitting area. The computed current density at the anode is plotted in Figure 13, and is similar to the current density profile at the cathode. The electron trajectories and equipotentials computed for an axial field of 5,000 gauss are shown in Figure 14. The onset of beam pinch due to self-magnetic field can be clearly seen.

The convergence of the iterative computation became very poor when the axial field strength was reduced to 1500 gauss. This is evident in the plot of conduction current and beam radius versus iteration number in Figure 15. The electron trajectories and equipotentials for iteration 8 are shown in Figure 16.

The conduction current and beam radius at the anode are plotted versus axial flux density for the planar gun with 20 cm spacing in Figure 17. The ratio of the circumferential self-magnetic field to axial magnetic field is also shown. As compared with the results for a 70 cm spacing (Figure 10), the rate of change of the conduction current with axial field strength is very high for low values of axial magnetic field, and the values of current from different iterations appear to fall into two distinct groups. Comparing the plots of (B_θ / B_z) anode for the 20 cm and 70 cm guns, it appears that additional cases of intermediate values of field between 1,500 gauss and zero might have led to a successful solution of the zero gauss case for the 20 cm gun. Though this would be an expensive effort and the beam would certainly be strongly pinched, it might be useful in establishing whether such a flow has a steady stage solution.

The ratios of the radial to axial and tangential to axial components of velocity calculated at the beam edge in the plane of the anode, are plotted versus axial flux density in Figure 18. Note that as the axial magnetic field was reduced, the radial velocity reached a very high value before the maximum tangential velocity was obtained. This was not the case with the 70 cm spacing (Figure 11). It is also worth noting that with axial fields large enough to prevent pinching, the tangential

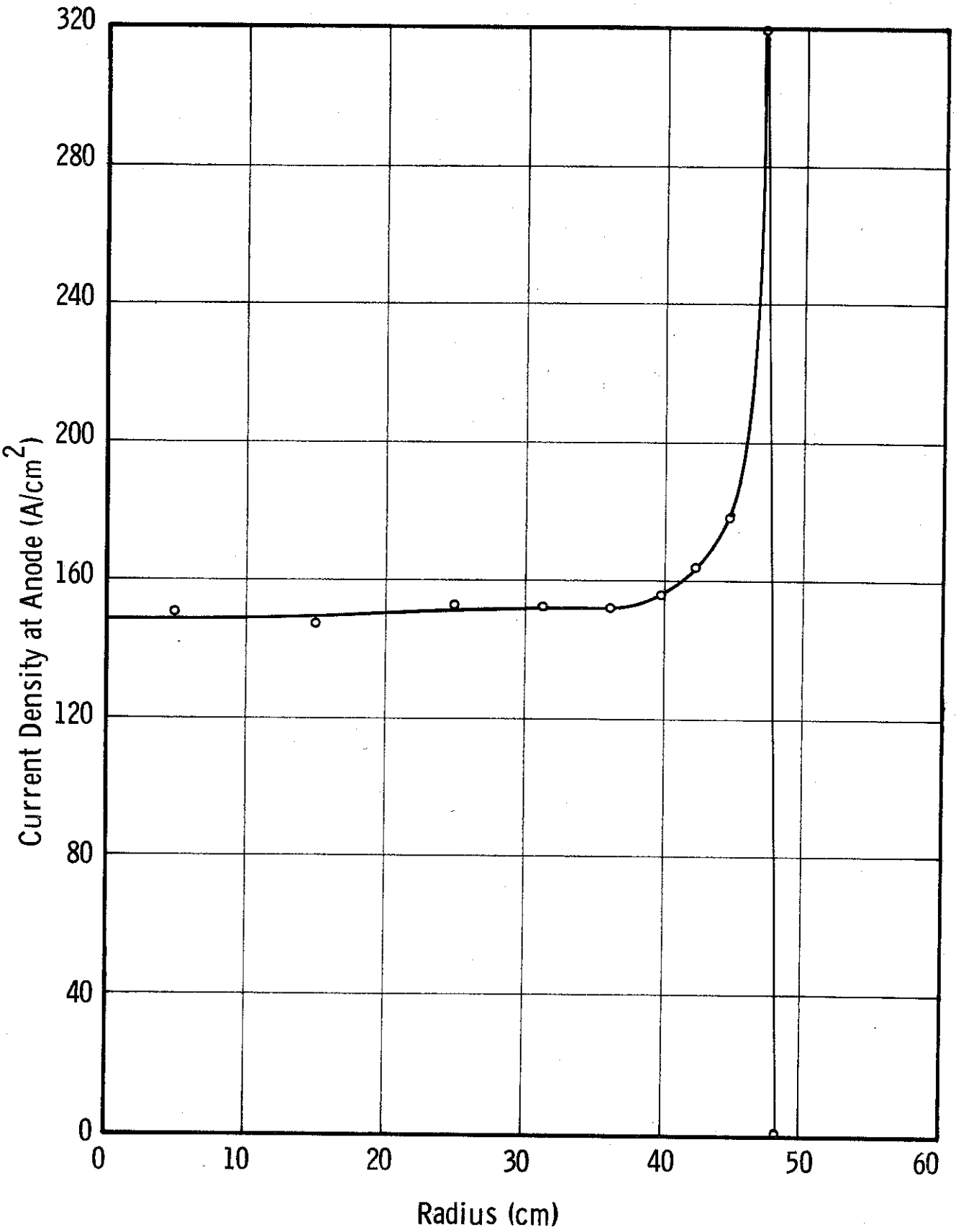

Figure 13. Computed Value of Current Density at Anode Versus Radius, Planar Gun at 15 MV with a 20 cm Spacing and a 50 cm Cathode Radius and with a 10,000 Gauss Axial Magnetic Field

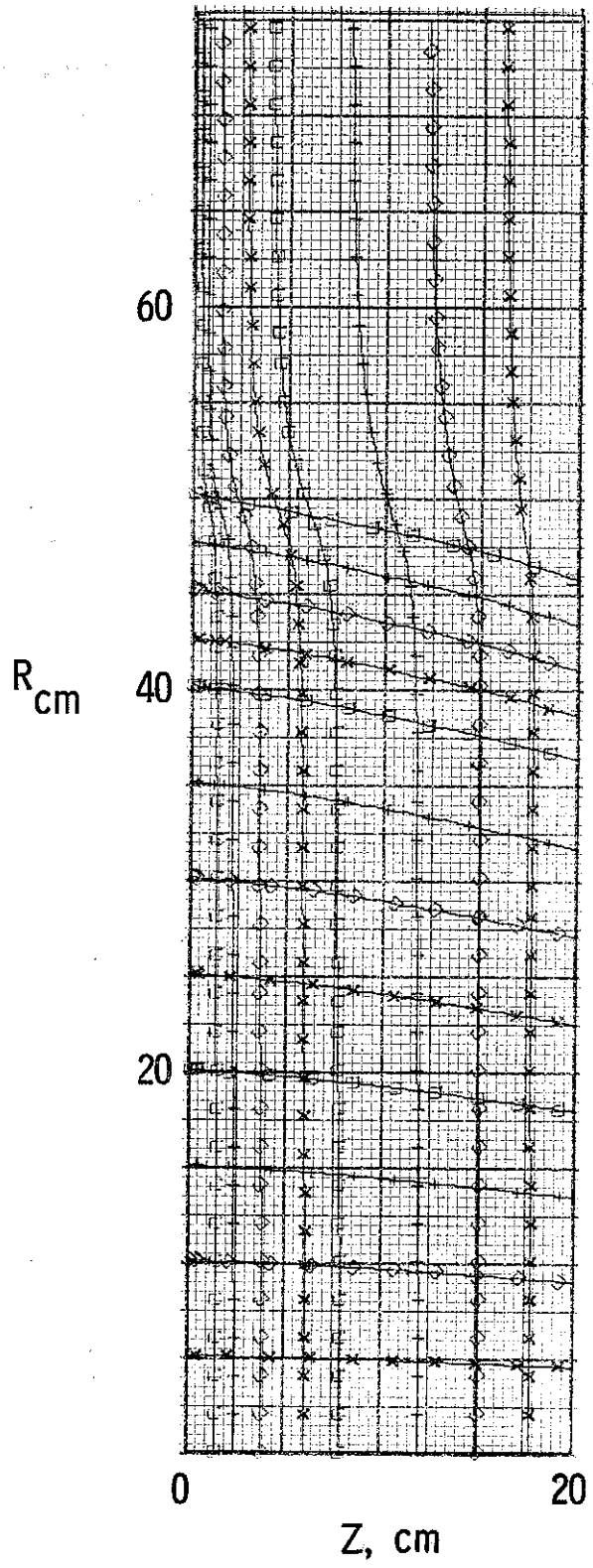

Figure 14. Computed Electron Trajctories and Equipotentials, Planar Gun at 15 MV with a 20 cm Spacing, a 50 cm Cathode Radius, and a 5000 Gauss Axial Magnetic Field

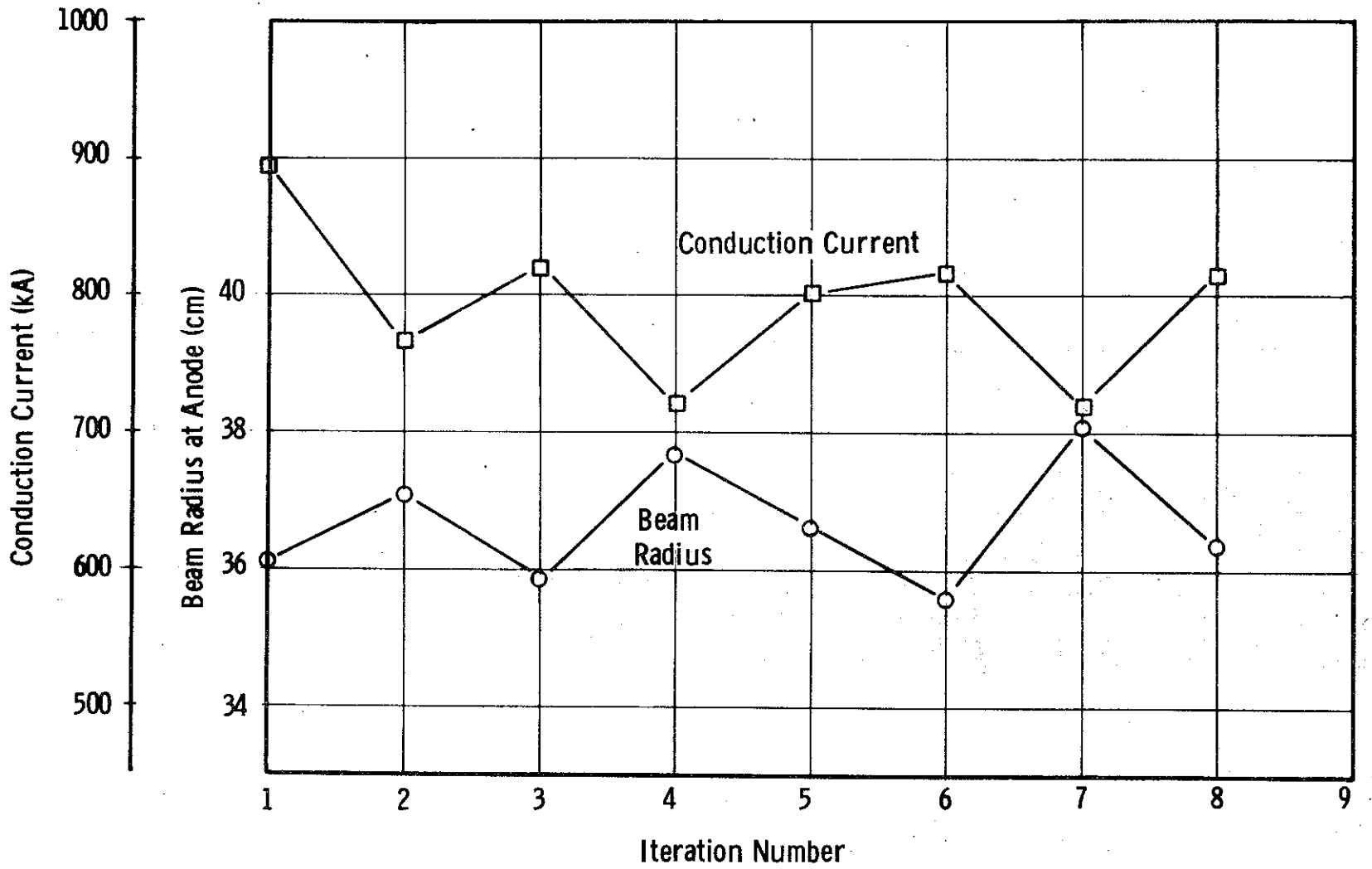

Figure 15. Computed Values of Beam Radius at Anode and of Conduction Current Versus Iteration Number, Planar Gun at 15 MV with 20 cm Spacing and 50 cm Cathode Radius with 1500 Gauss Axial Field

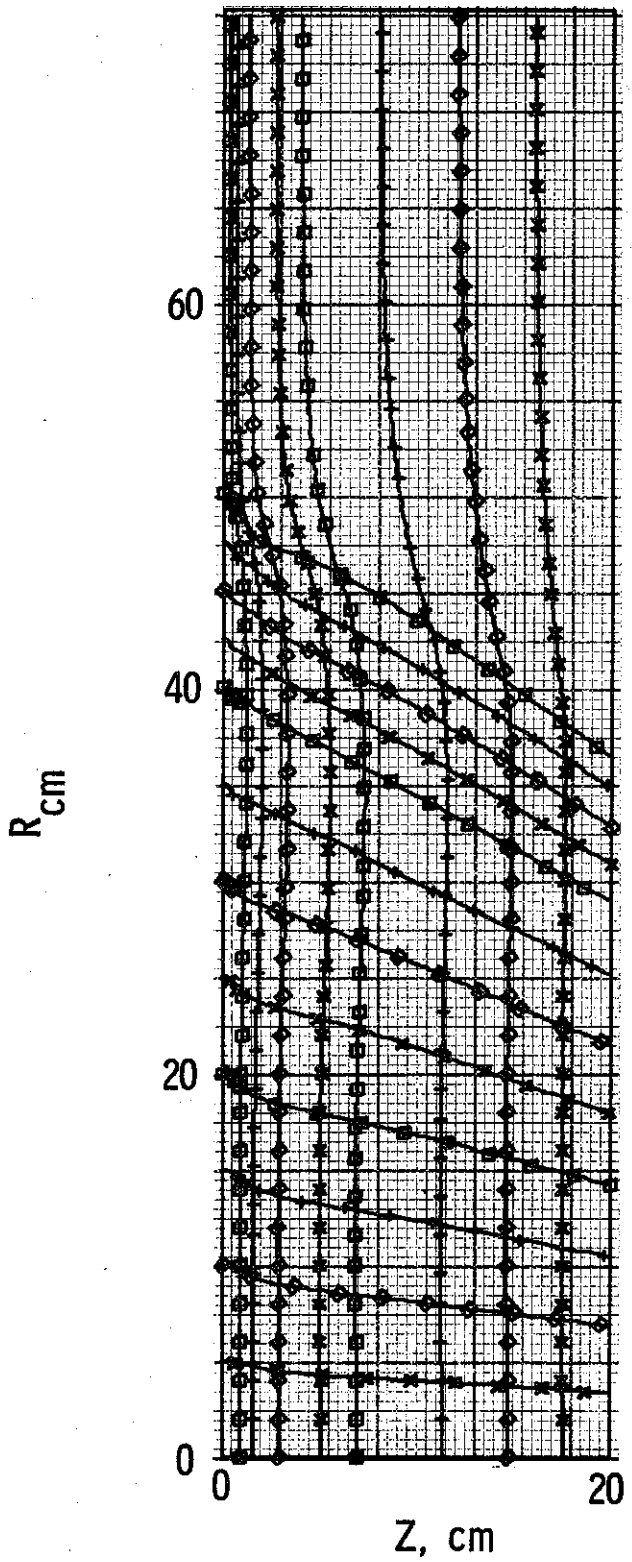

Figure 16. Electron Trajectories and Equipotentials Computed in Iteration 8 for Planar Gun with 20 cm Spacing and an Axial Magnetic Field of 1500 Gauss

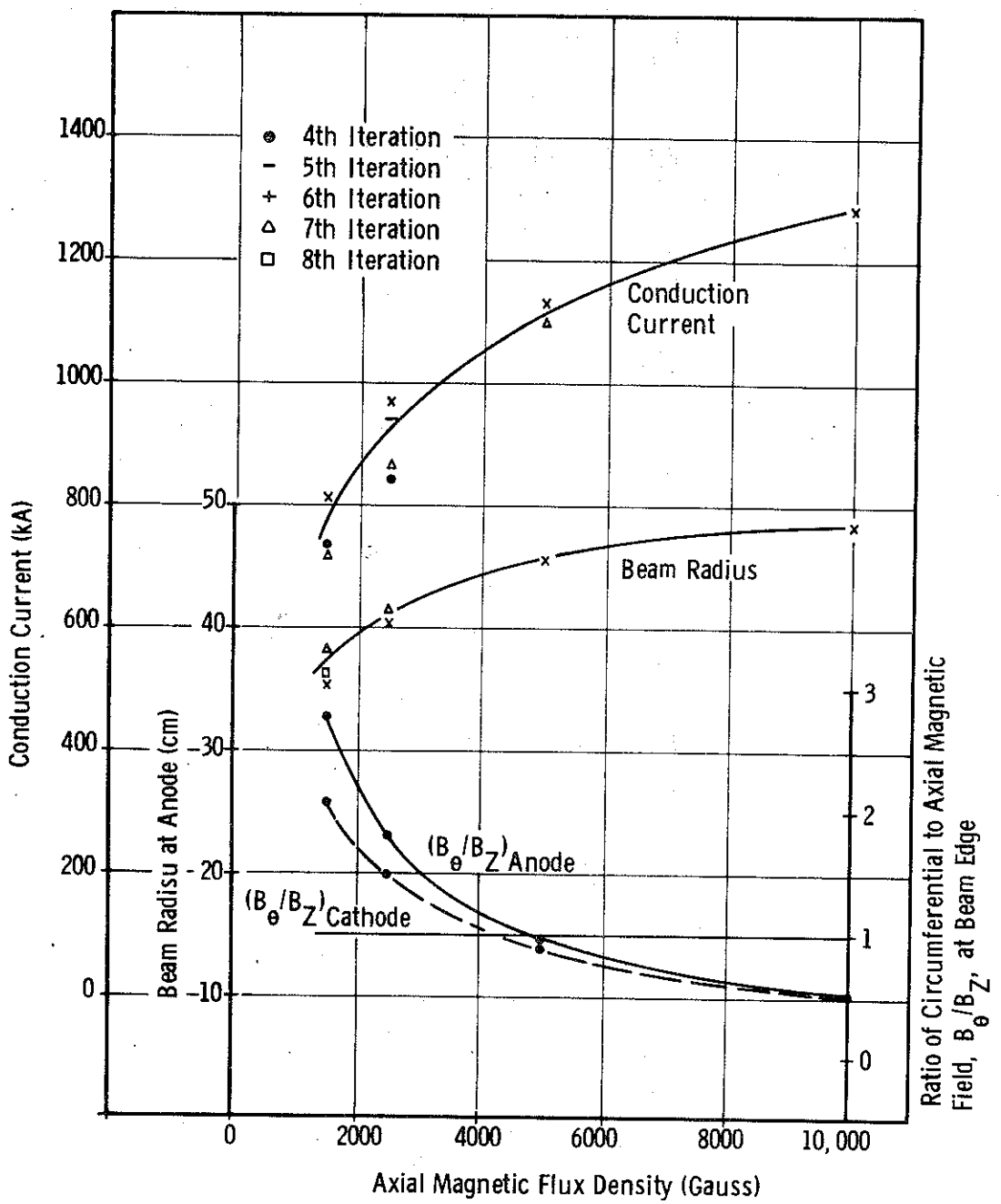

Figure 17. Ratio of Circumferential to Axial Magnetic Field at Beam Edge and Computed Values of Conduction Current and Beam Radius Versus Axial Magnetic Flux Density, Planar Gun at 15 MV with a 20 cm Spacing

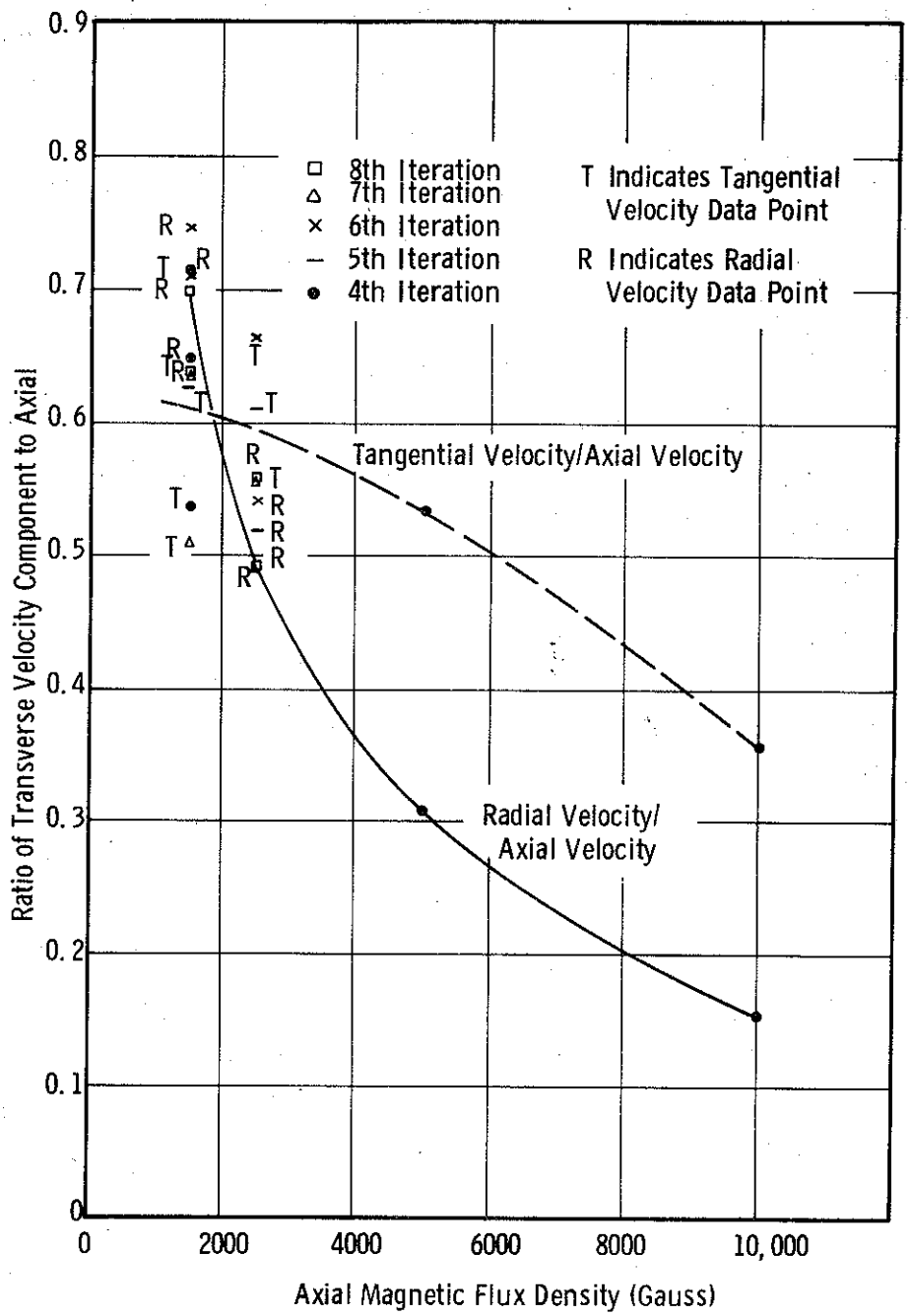

Figure 18. Computed Values of Radial and Tangential Velocity Components Normalized to Axial Velocity at Beam Edge at Anode Versus Axial Magnetic Flux Density, Planar Gun at 15 MV with a 20 cm Spacing

velocity is considerably greater than the radial velocity. For the 70 cm case, in Figure 11, the two transverse velocity components are of comparable magnitude at suitable values of confining field.

C. EXPERIMENTAL DIODES WITH SPHERICAL CATHODES AND PLANAR ANODES

Varian's beam analysis computer program was used to analyze flow in a sphere and plane diode developed by the Physics International Company. Figure 19 is a sketch of the diode. First, computations were made for an anode-to-cathode spacing (A-K) of 4 inches. According to measured results furnished by Physics International, the peak anode current was 60 kA with a peak anode-to-cathode potential of 2.7 MV. A plot of measured radiation intensity at the anode was also supplied; this plot is shown in Figure 20. This figure shows the current density profile at the anode except that the radiation density should be smoother because of time averaging effects and scattering.

Initially, attempts were made to arrive at a self-consistent solution by assuming that a region of the cathode with an arbitrarily defined outer boundary emits electrons in a space-charge limited fashion. High emission at the outermost trajectory prevented the solution from converging with simple space-charge limited flow. When the emission at the outer trajectory was arbitrarily limited, good convergence was achieved. Figure 21 shows a well-converged solution with the emission limit set at 220 A/cm^2. Only the outermost (No. 1) trajectory was emission limited; all other trajectories were space-charge limited. The total current of 63.2 kA was consistent with measured results. Nevertheless, the boundary condition of arbitrarily limited emission seems undesirable. The result of the high edge emission can be seen in the plot of anode current density versus radial position in Figure 22. A sharp peak in the current density profile occurs at the beam edge which is not indicated in the experimental data plotted in Figure 20.

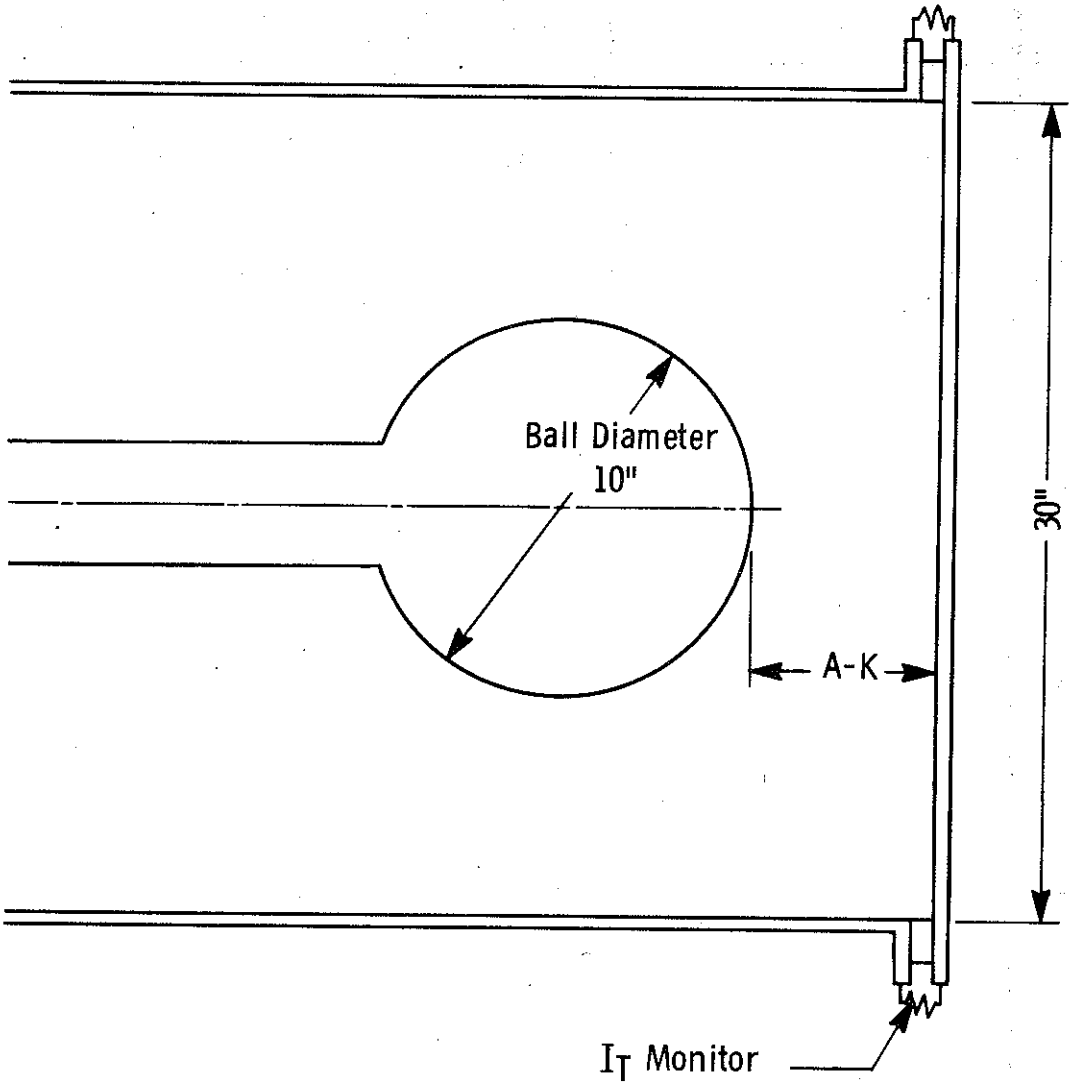

Figure 19. Sketch of Physics International Sphere and Plane Diode

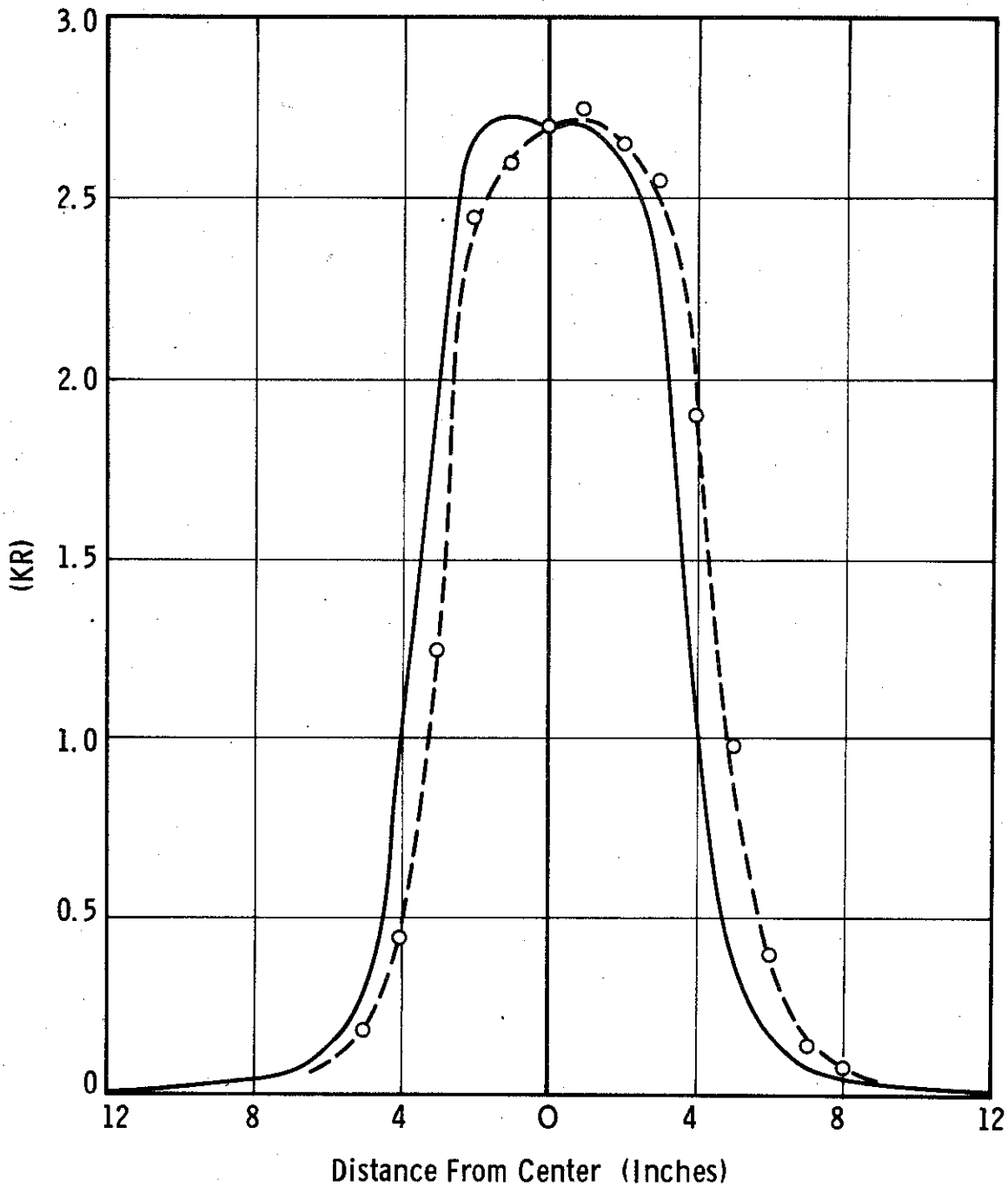

Figure 20. Radiation Intensity Profile at the Anode For the Sphere and Plane Diode, A-K Spacing 4 Inches.

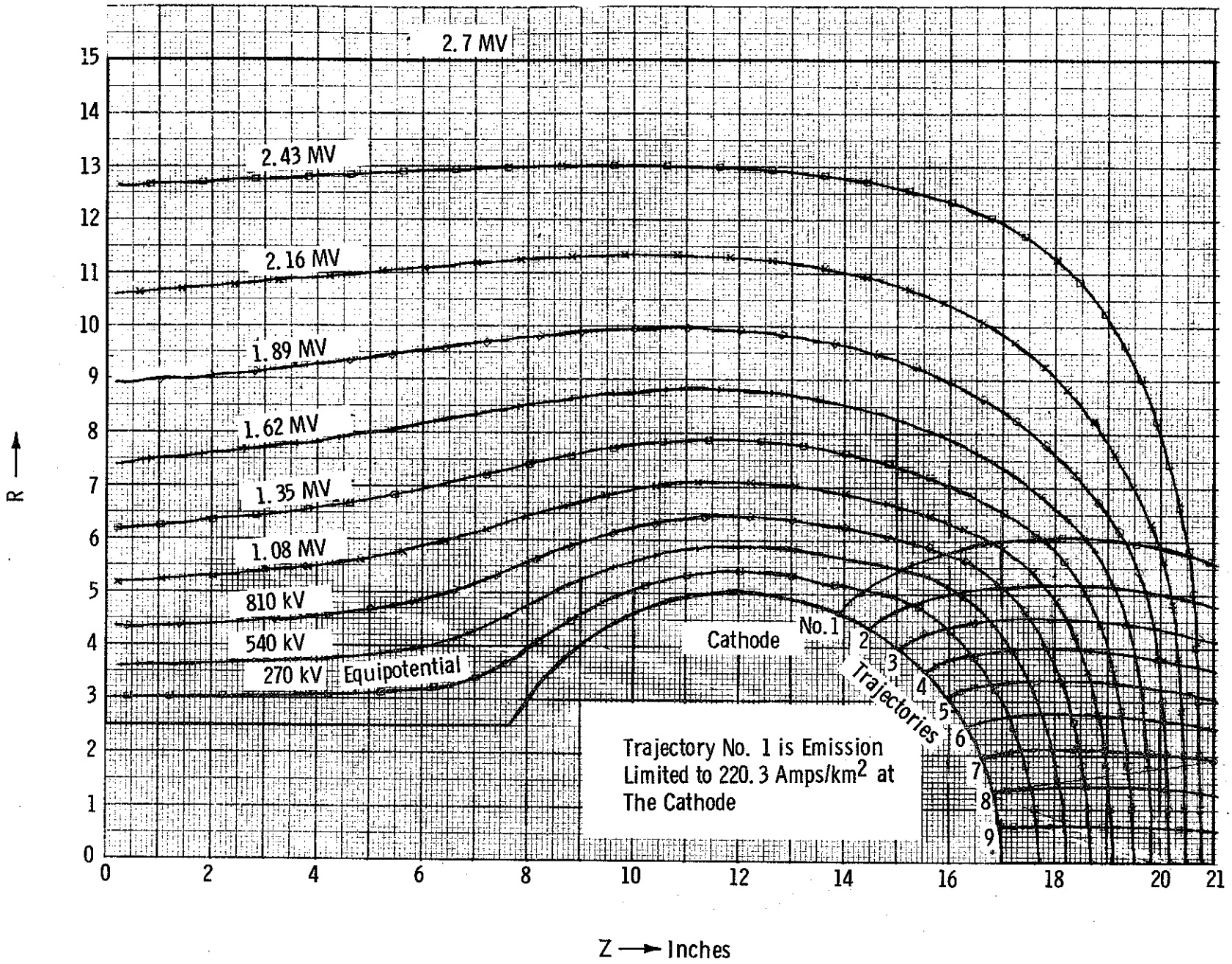

Figure 21. Flow Computed for Sphere and Plane Gun with 4 Inch Spacing

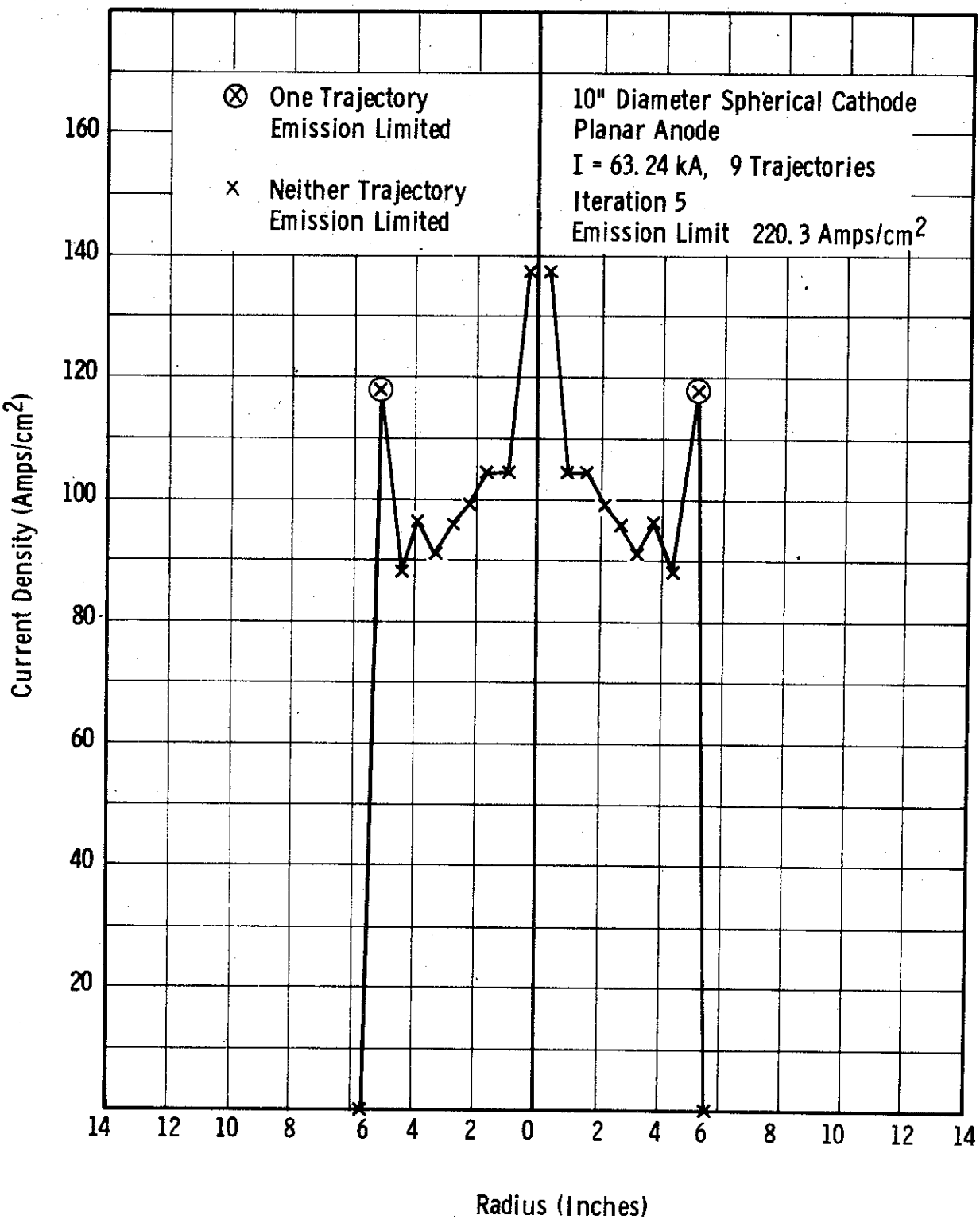

Figure 22. Physics International Gun, Average Current Density Between Trajectories at Anode Versus Average Radius.

The Laplacian (zero space-charge) fields at the cathode are in the range of 10^7 V/m even on the cylindrical portion of the cathode. Therefore, field emission of electrons probably takes place over the cylindrical portion of the cathode as well as the spherical portion. The cylindrical portion of the cathode is similar to a cutoff magnetron where the magnetic field is produced by the main diode current. Therefore, in the sphere and plane gun, a sheath of space-charge probably exists over the back portions of the cathode which depresses the cathode electric field to zero. If this sheath were properly accounted for in the computer analysis, the excessive current in the outermost trajectory would not be present. A theoretical analysis related to the sheath is contained in Section II-C.

Figure 23 shows an initial trial using an electrode to simulate the sheath along the cutoff portion of the cathode. The total sheath thickness was predicted to be 0.935 inch; the distance to the zero-volt equipotential (from the cathode surface) was 0.367 inch. The portion between the cathode and the zero-potential surface is labeled as the sheath on the plot. At its end, the zero potential surface was connected to the cathode in such a way that the electrostatic field would be approximately normal to the emitting part of the cathode surface. Flow for this computation was space-charge limited and the solution was self-consistent. Total current was 66.9 kA. The computed current density profile at the anode is shown in Figure 24. It is evident that the current density at the beam edge is still excessive in comparison with the empirical data for the radiation intensity profile. This is partly due to the excessive current density computed at the cathode at the edge of the beam in this computation.

Figure 25 shows the flow for a more successful computation of the 4 inch spacing gun. For this case, a better choice of the angle of the sheath-electrode-to-cathode transition was used, and the number of computed trajectories was increased from 10 to 30. Only every third trajectory (plus the last one) is shown in the figure. Originally the sheath electrode was terminated, assuming that flow to the cathode surface at the transition was normal. Further study indicated that in this region

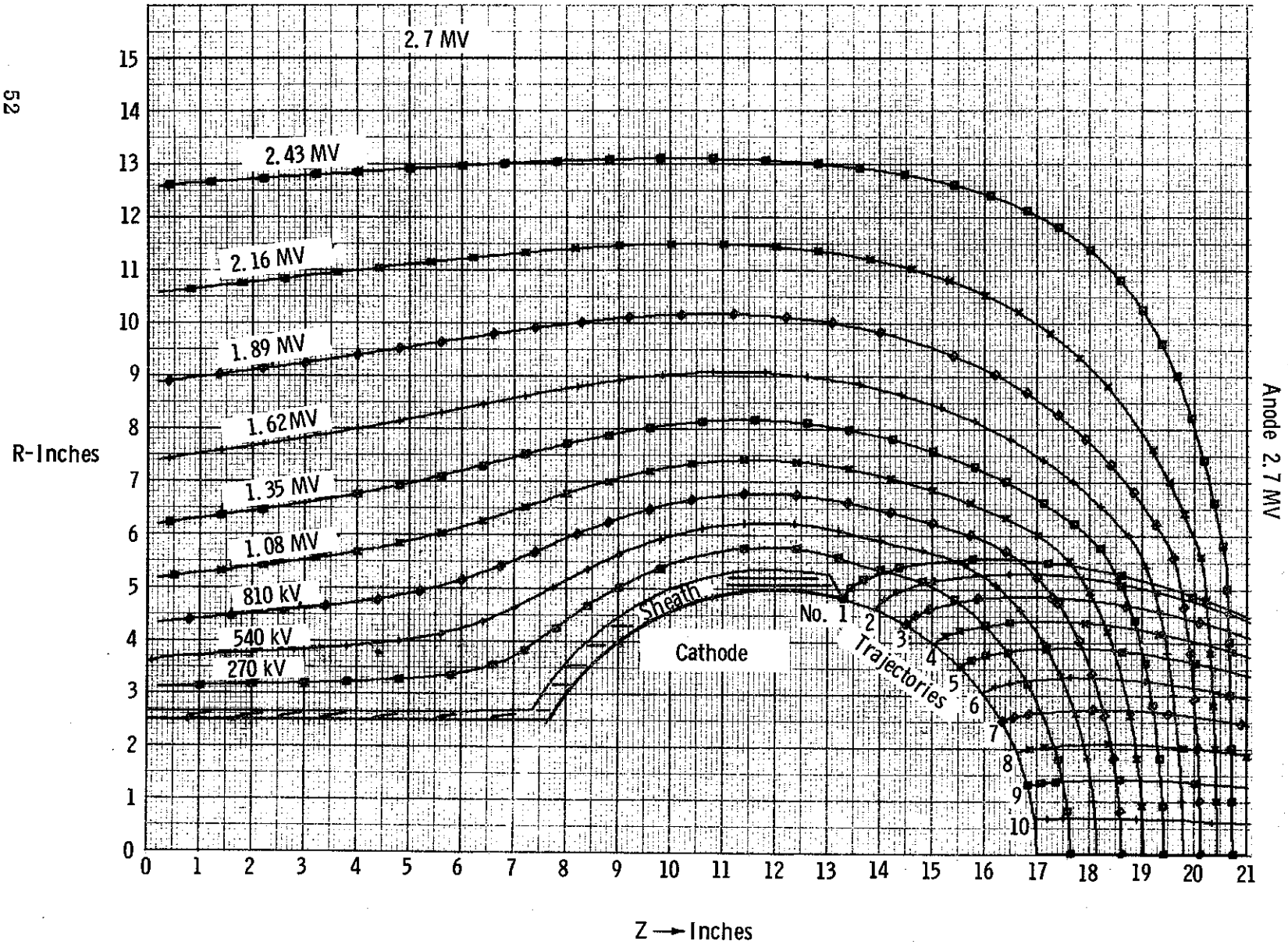

Figure 23. Flow for Sphere-Plane Gun Using "Sheath Electrode", 4" A-K Spacing

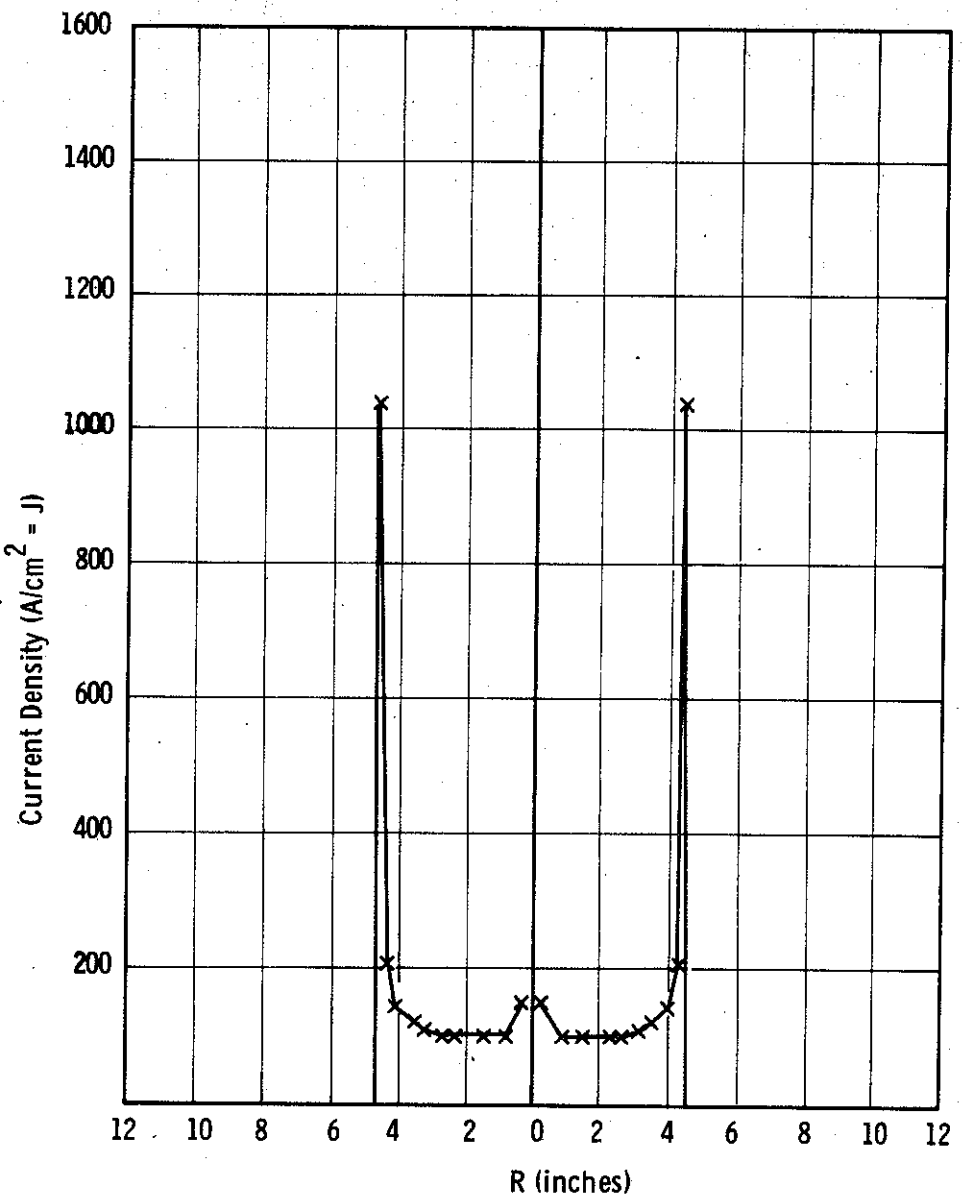

Figure 24. Current Density Versus Radius at Anode, Sphere-Plane Gun Using "Sheath Electrode", 4" A-K Spacing

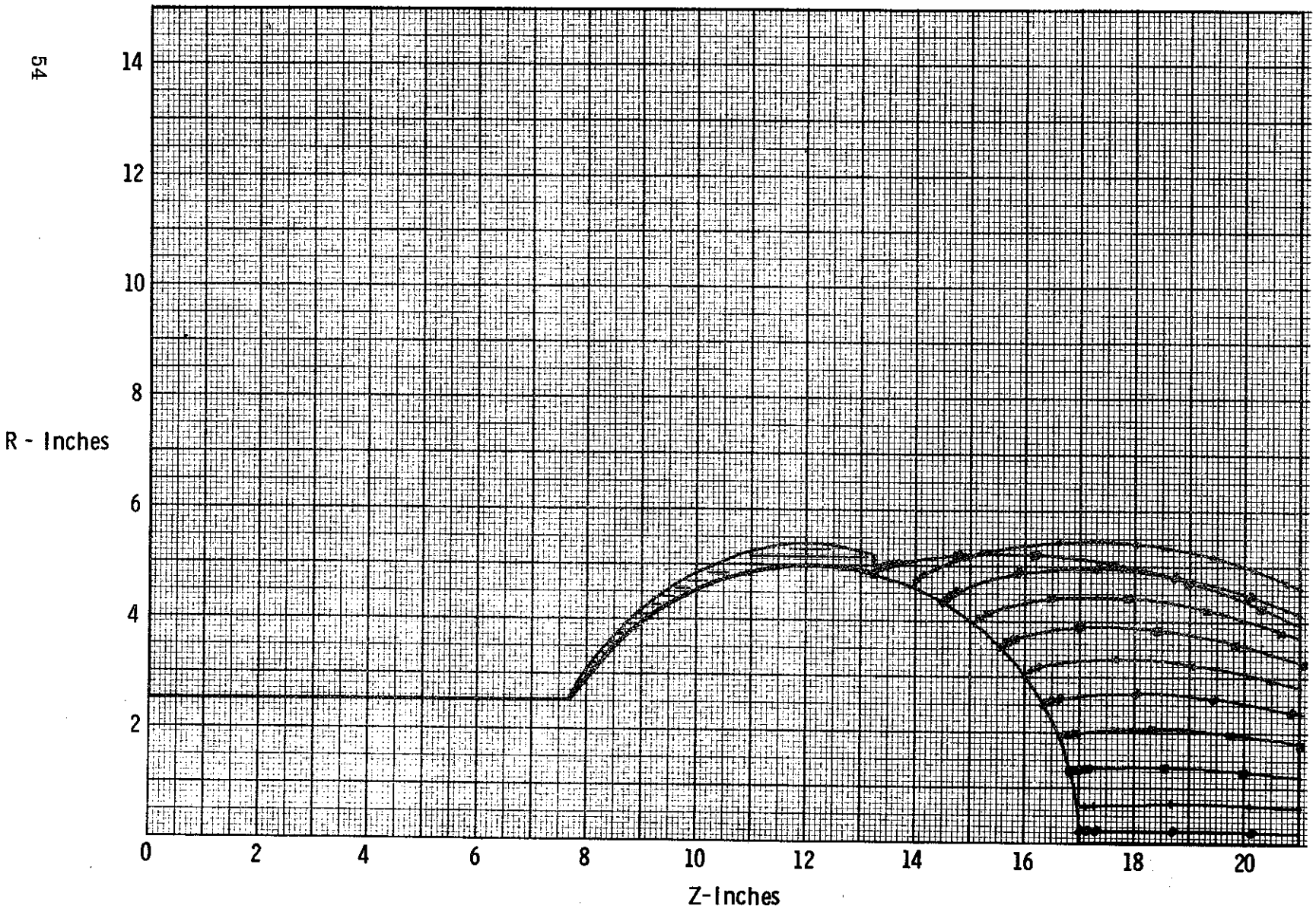

Figure 25. Sphere-Plane Gun With Improved " Sheath Electrode "
4 Inch A-K Spacing

flow goes through an arc before the program computes the emission current density and begins to integrate the trajectory. To compensate, the angle from the sheath termination to the normal was decreased. This reduced the peak in the computed current density at the edge of the emitting area, producing a more reasonable result. For this case, the flow is completely space-charge limited, and the solution for the cathode current density is self-consistent to within 2%. The total beam current had converged to within 0.86%. This case was the first where limits were set for the perveance (and thus the currents) to restrict the values from the wild fluctuations usually present in the first few iterations. In the same number of iterations, a calculation for the same gun (except using 10 trajectaries) has converged to within 2.0% for the beam current. The method of limiting the current in each iteration to a specified range proved to be of increasing importance with higher current diodes; this importance will be shown in the succeeding sections of this report. Total anode current is 62.2 kA which agrees closely with the experimentally measured value of 60 kA. The beam radius of 4.83 inches is also close to the experimentally measured value. Figure 26 is a plot of anode current density versus radial position. The agreement with Figure 20 is not exceptional, but is better than that achieved previously. A discussion of the comparison of computed and experimental data is given at the end of this section. Figure 27 shows flow from a computer solution in which the sheath electrode has been decreased so that the sheath to cathode transition is at a position 120° from the cathode tip. Emission is calculated to an angle of 116° from the tip. In this case, the convergence of the solution was not good, but the result shown in Figure 27 can be considered representative of the actual solution. Total current reaching the anode is 61.9 kA, thus the self-magnetic field is essentially the same in the cutoff or sheath region as in the case shown in Figure 25. The point on the cathode at which emitting electron trajectories actually start to reach the anode closely corresponds to the sheath edge in Figure 25. Thus, the result shown in Figure 27 serves to justify the sheath position shown in Figures 23 and 25. Inaccuracies inherent in finite-difference methods make convergence more difficult if the electron trajectories remain within a distance of one or two mesh cells

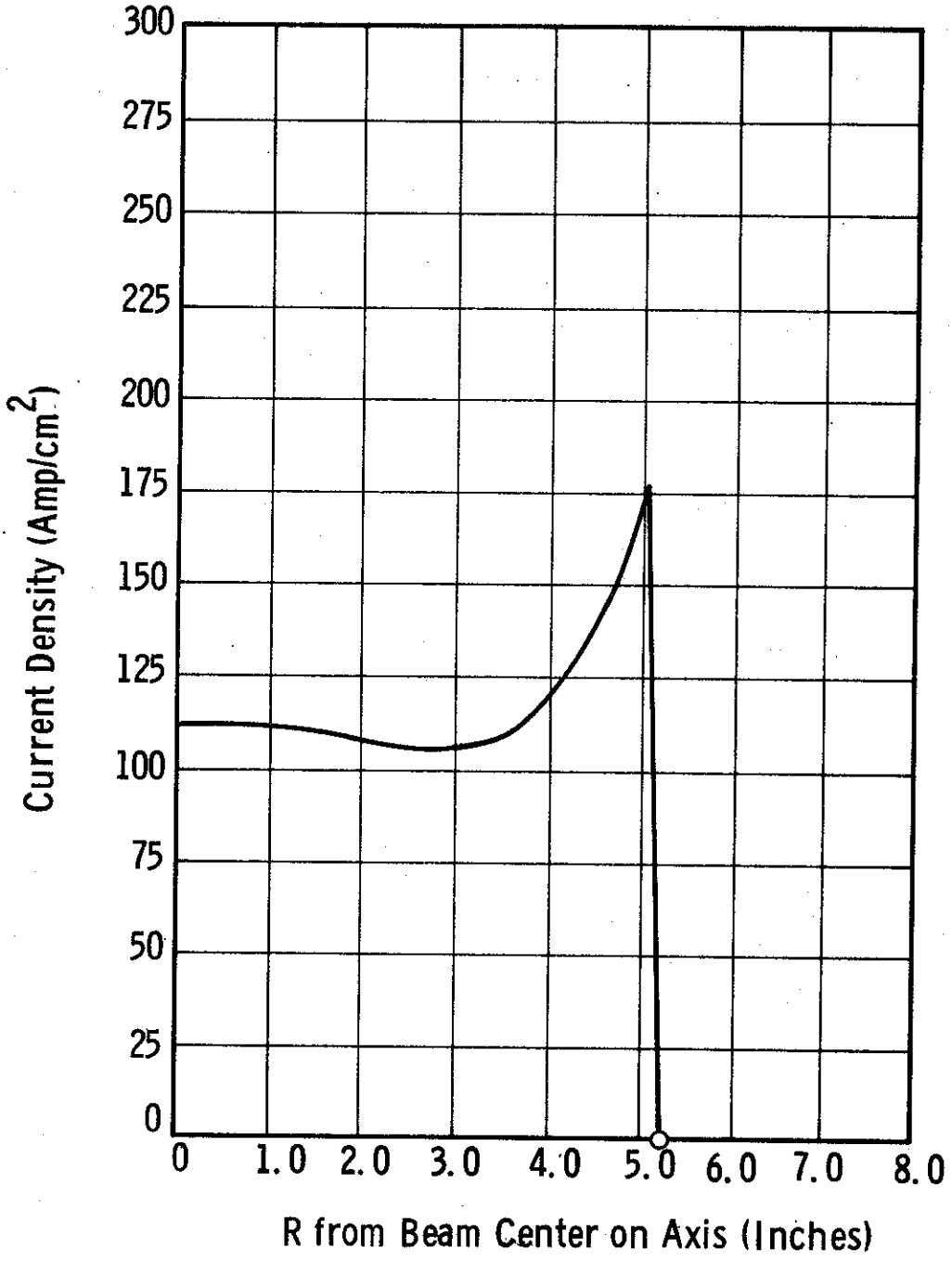

Figure 26. Anode Current Density Profile, Sphere-Plane Gun with Improved "Sheath Electrode" 4" A-K Spacing

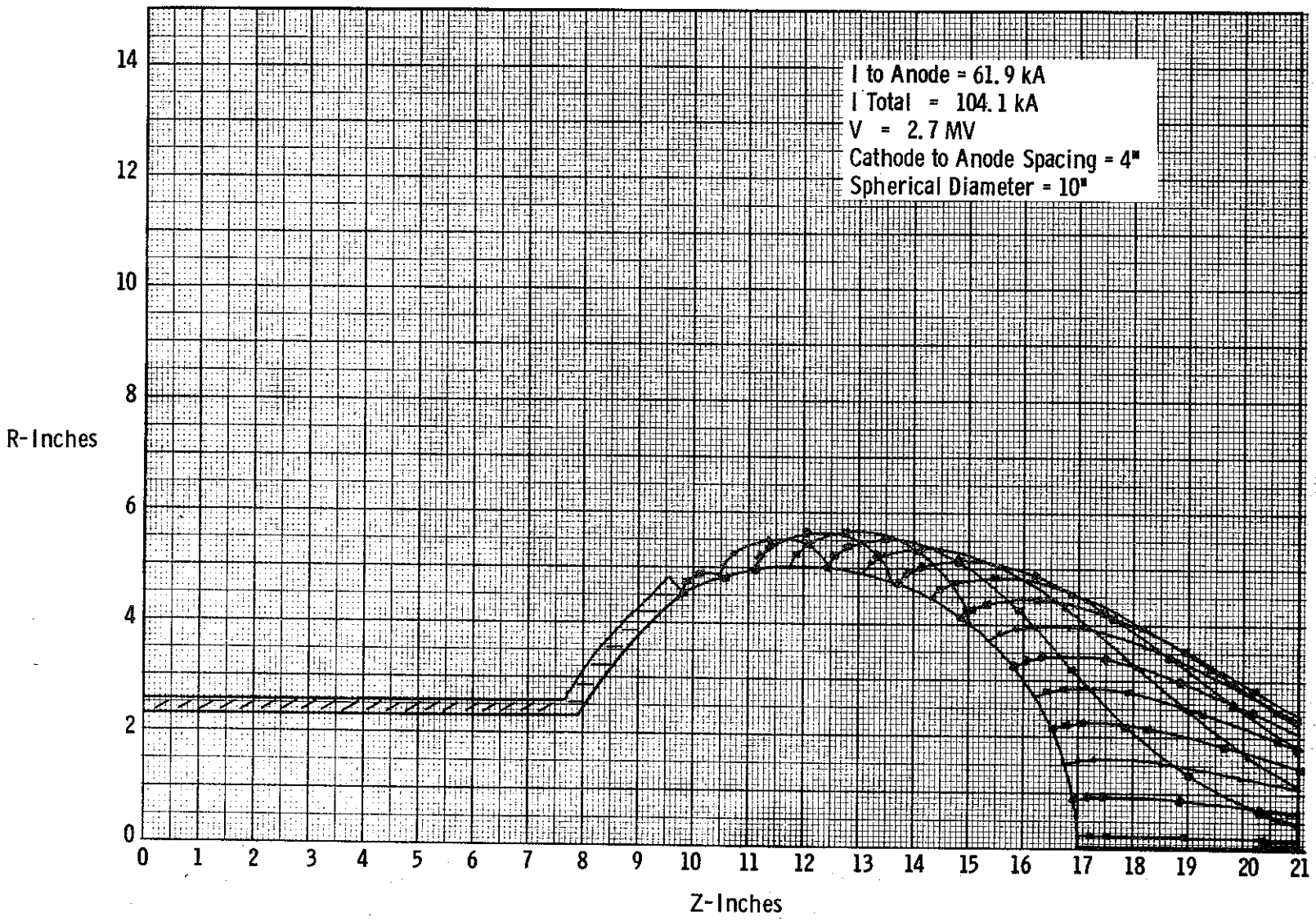

Figure 27. Sphere-Plane Flow with a Portion of the Sheath Computed, 4" A-K Spacing

of the cathode surface. This is one cause of the poor convergence in Figure 27. The use of a zero-potential surface to simulate the presence of these cycloidal trajectories greatly reduces computer time and speeds convergence.

The calculation shown in Figure 27 affords a good opportunity to compare the cutoff magnetron theory in Section II-C with a numerical calculation. At an angular position of 90° on the cathode in Figure 27, all electrons return to the cathode; thus, the conditions of a cutoff sheath prevail. Figure 27(a) shows potential versus distance normal to the cathode for the numerical flow calculation compared to theoretical values obtained from Equation (61). A third curve in the figure shows the potential variation that would have been present if a zero potential sheath electrode had been used at the 90° position instead of allowing the cathode to emit. The observed agreement is fairly good.

Equipotentials computed for the flow shown in Figure 25 are plotted in Figure 28. The portion of flow near the cathode adjacent to the sheath electrode is rapidly pinched away from the normal to the cathode. As a result, the computed space charge potential depression is minimized at this part of the emitting surface, as can be seen by the dip in the 5% equipotential in the figure. This results in a sharp peak in the cathode current density very near the edge of the permitted emitting area. This can be seen in Figure 29, which is a polar plot of the cathode current density drawn in the r-z plane. Zero angle in the figure represents the cylindrical axis of the diode. A similar plot is shown in Figure 30 for the flow of Figure 27, where a portion of the sheath is actually computed. A peak in the cathode current density again occurs near the edge of the allowed emitting area, but this time it lies almost entirely in the cutoff sheath region, where emitted electrons return to the cathode, instead of in the conducting portion of the cathode. This indicates that the peak in current density is due to the assumptions made in the simulation. The peak in the curve in Figure 30 would perhaps be completely eliminated if:

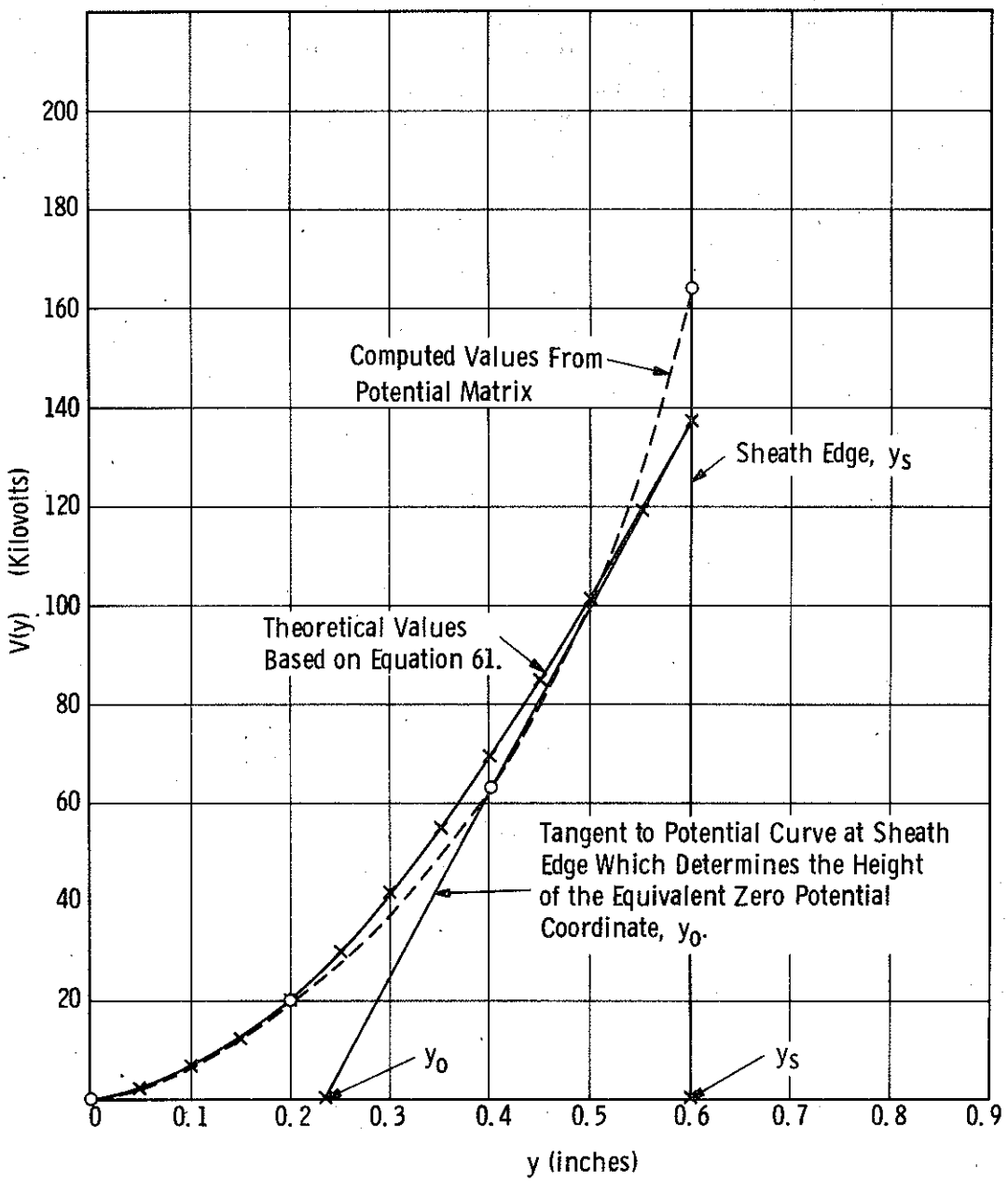

Figure 27(a). Comparison of Theoretical and Computed Potential Variation in the Cutoff Sheath in the Plane Z = 12" of Figure 27.

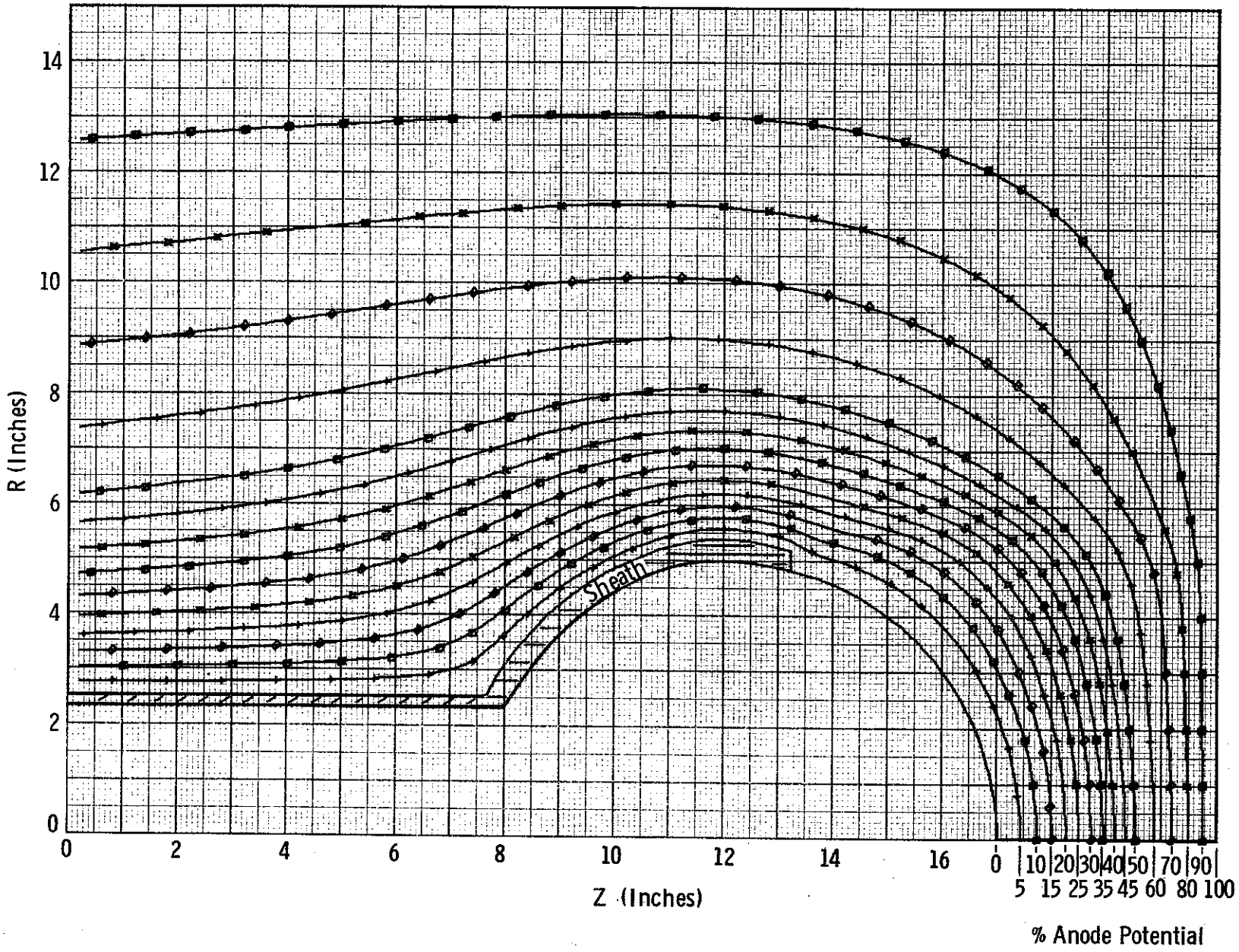

Figure 28. Equipotentials for Sphere-Plane Gun with Improved "Sheath Electrode", 4" A-K Spacing

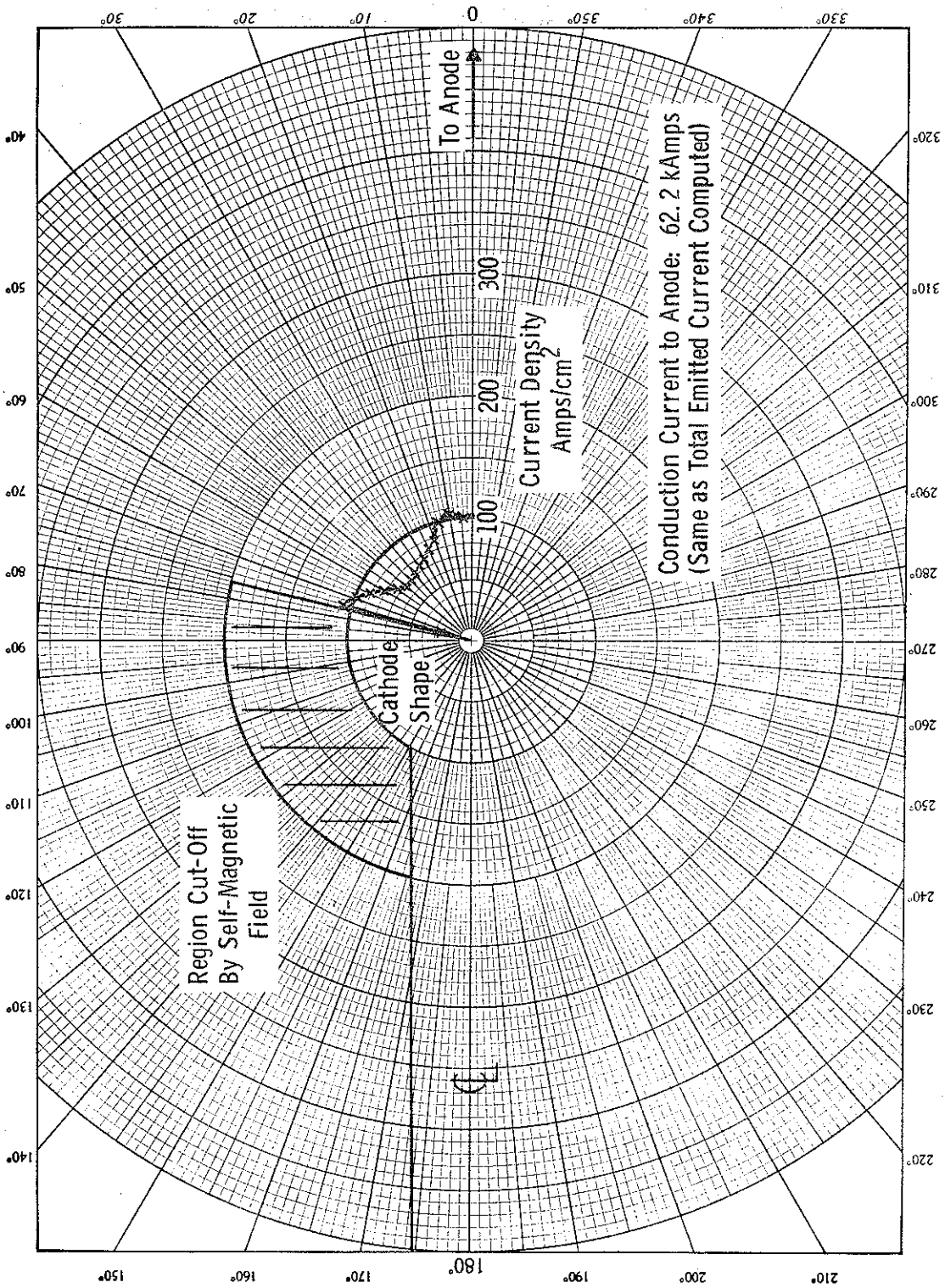

Figure 29. Polar Plot of Current Density at Cathode, Sphere-Plane Gun with Improved "Sheath Electrode", 4" A-K Spacing

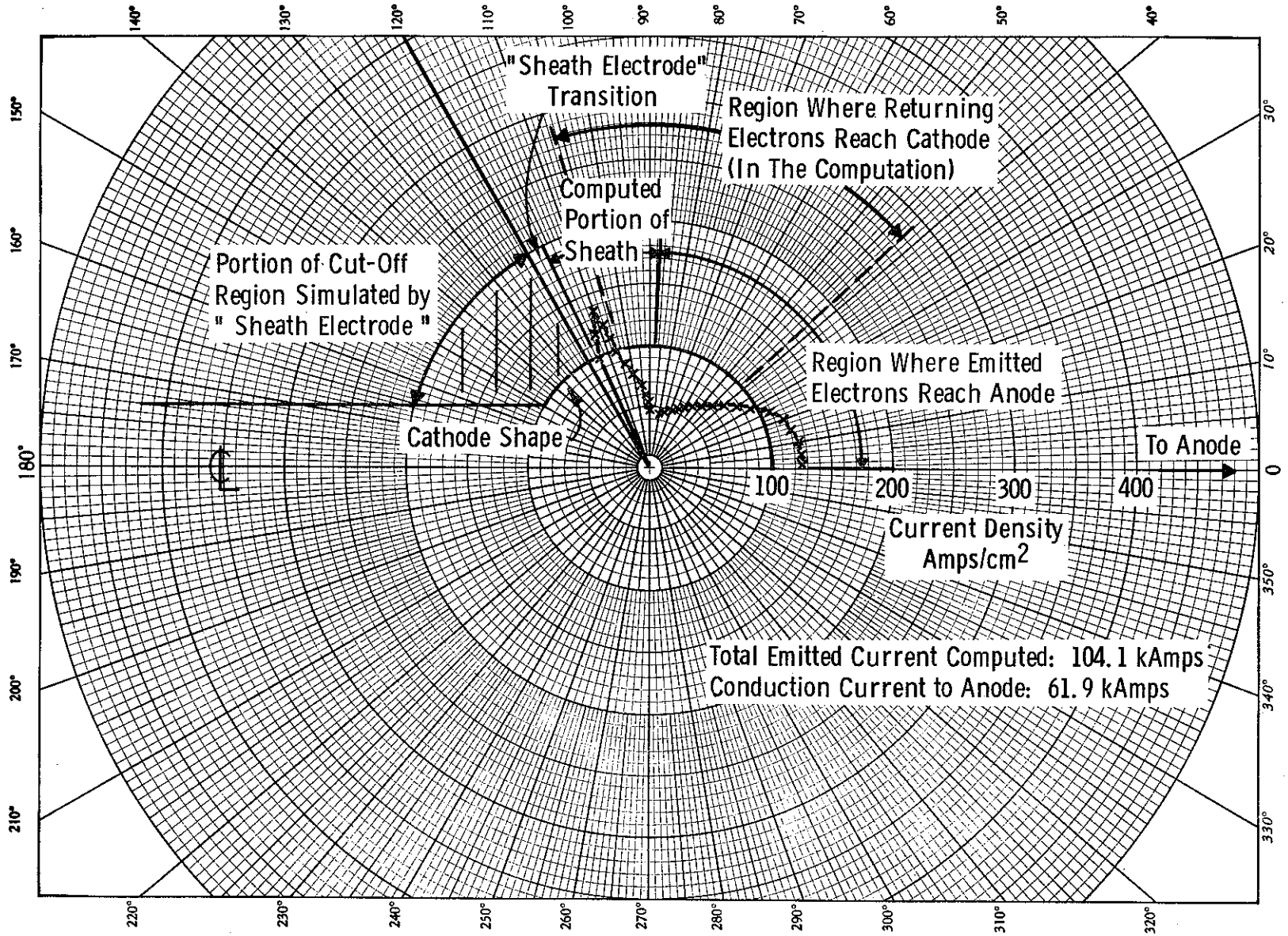

Figure 30. Polar Plot of Current Density at Cathode, Sphere-Plane Gun with a Portion of the Sheath Computed, 4" A-K Spacing

1. All the current emanating from the sheath that passes near or returns to the cathode in the region of the peak was taken into account (notice in Figure 27 that nearly all returning electrons computed for this flow do not begin to reach the cathode until after the peak in current density), and
2. the computed emission current density was properly reduced from the normal conducting region value (presently assumed) by the ratio of the charge density due to outgoing electrons to that due to both the outgoing and incoming electrons.

Thus, the present simulation does not take into account the reduction in emission current density due to the potential depression caused by the returning electrons. The simulation of these flows could obviously be improved in this area.

Flow for the spherical cathode, planar anode gun with 2-inch spacing is shown in Figure 31. Calculated current is 81.8 kA and beam radius is 2.27 inches. Again, a self-consistent solution (within 1%) was achieved using space-charge limited flow. The experimentally measured values for this gun were an anode current of 70 kA and a beam radius of approximately 3 inches, as indicated by the radiation plot in Figure 32. Figures 33 and 34 show, respectively, anode and cathode current density distributions. The cathode current density distribution has much higher values of current density close to the axis than does the gun with 4-inch spacing. In this region, the closely spaced gun acts more like a planar diode.

D. EXPERIMENTAL DIODES WITH TOROIDAL CATHODES AND PLANAR ANODES

These calculations use the cutoff magnetron theory represented by Equation (59) to control the current emitted from the cathode. With this model, the introduction of the sheath-simulating electrode is not necessary. Upper and lower limits for the perveance were used here, as in the previous section, to reduce large changes in total current until the solution approaches self-consistency.

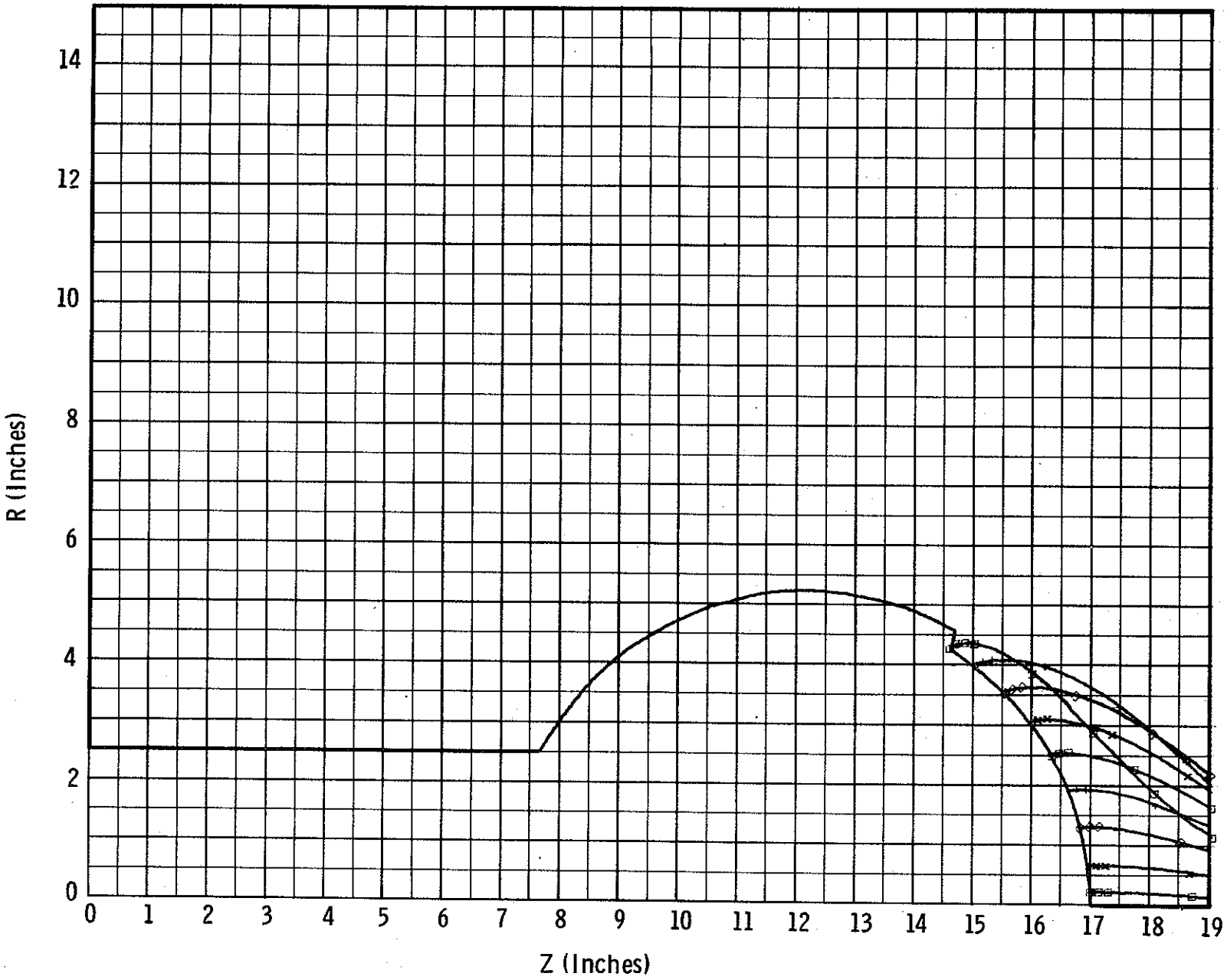

Figure 31. Flow for Sphere-Plane Gun with Improved "Sheath Electrode" and A-K Spacing Reduced to 2"

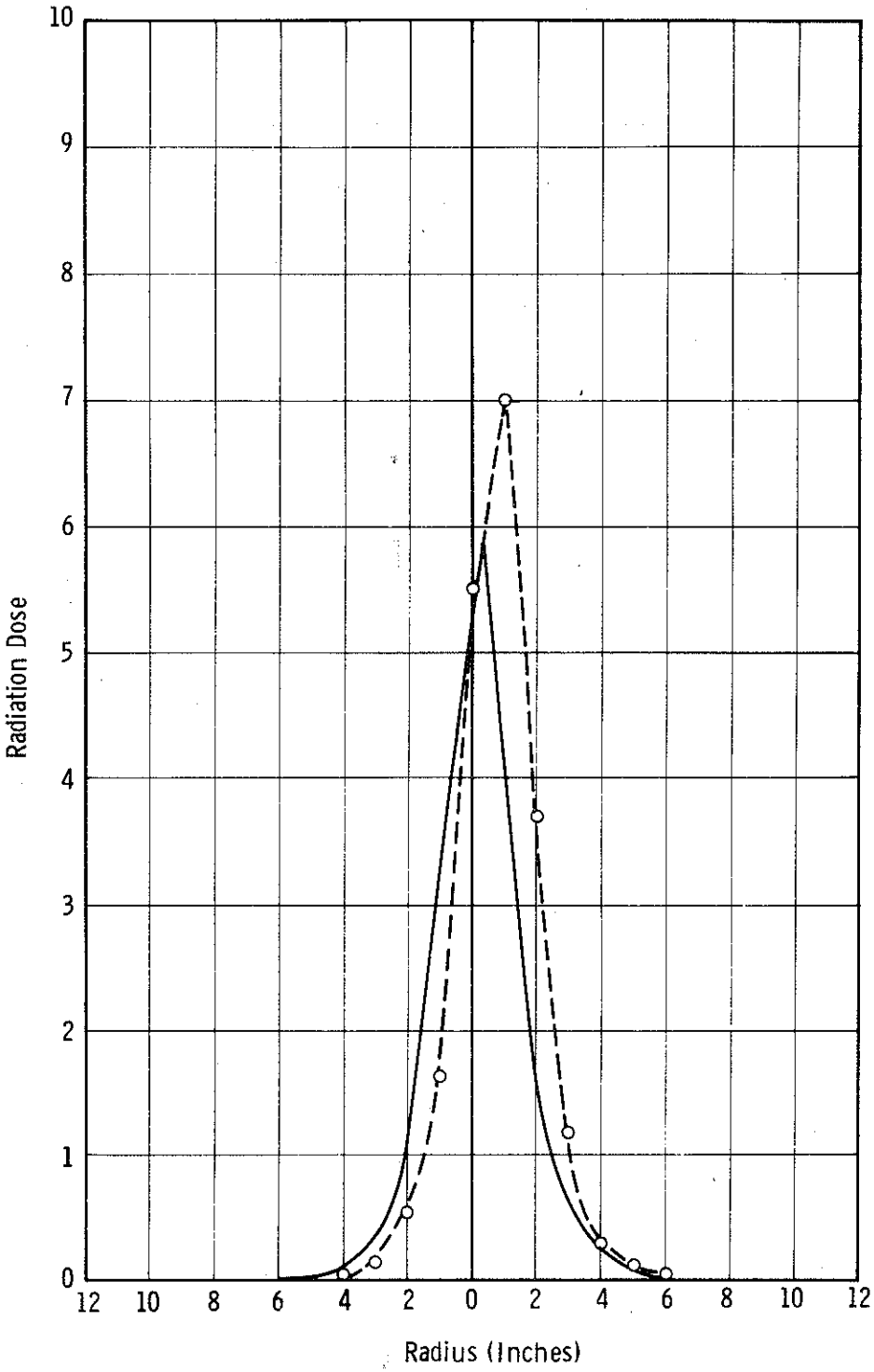

Figure 32. Radiation Intensity Profile at Anode for Sphere-Plane Gun with 2" A - K Spacing

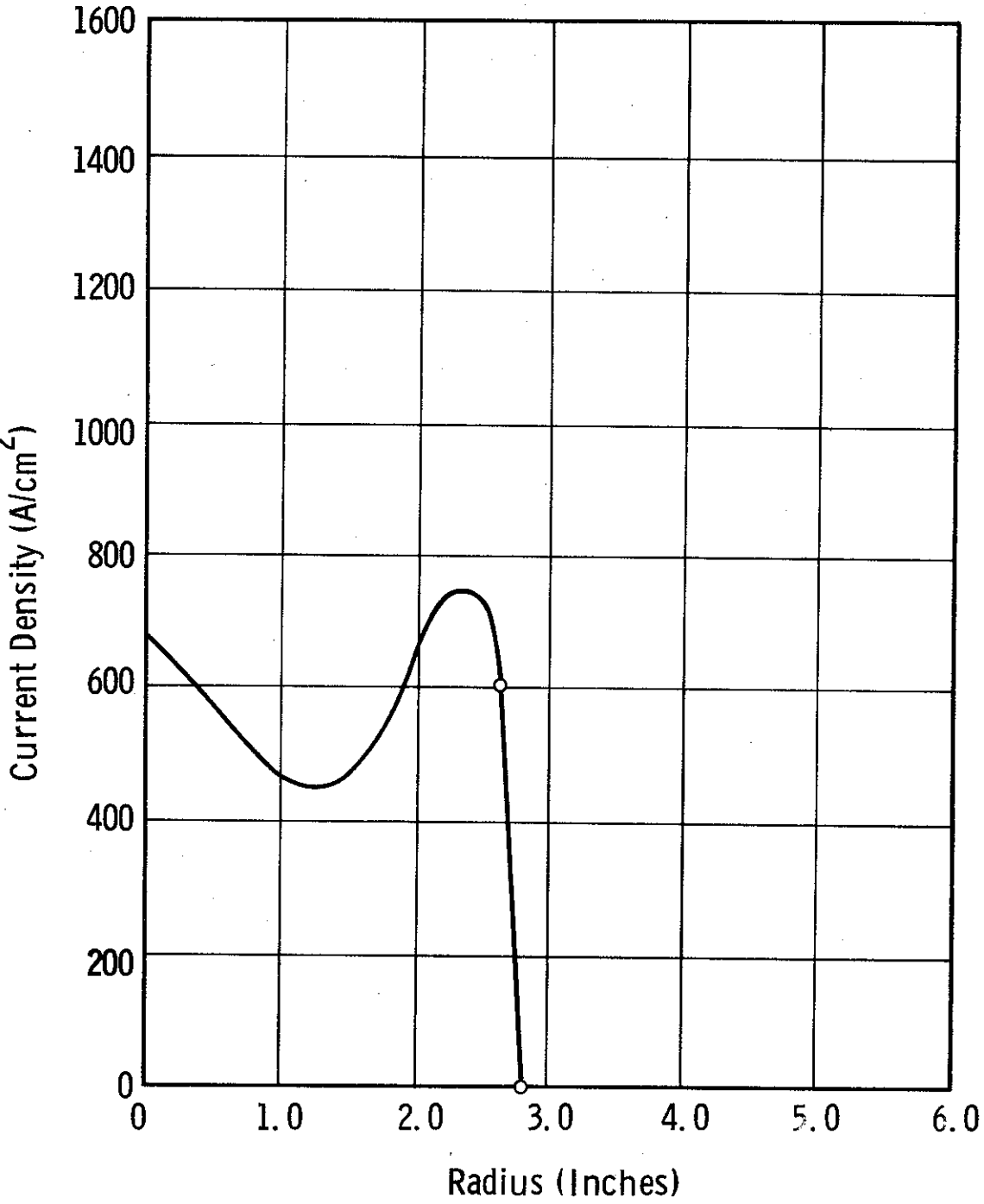

Figure 33. Current Density at Anode Computed for Sphere-Plane Gun with 2" A-K Spacing

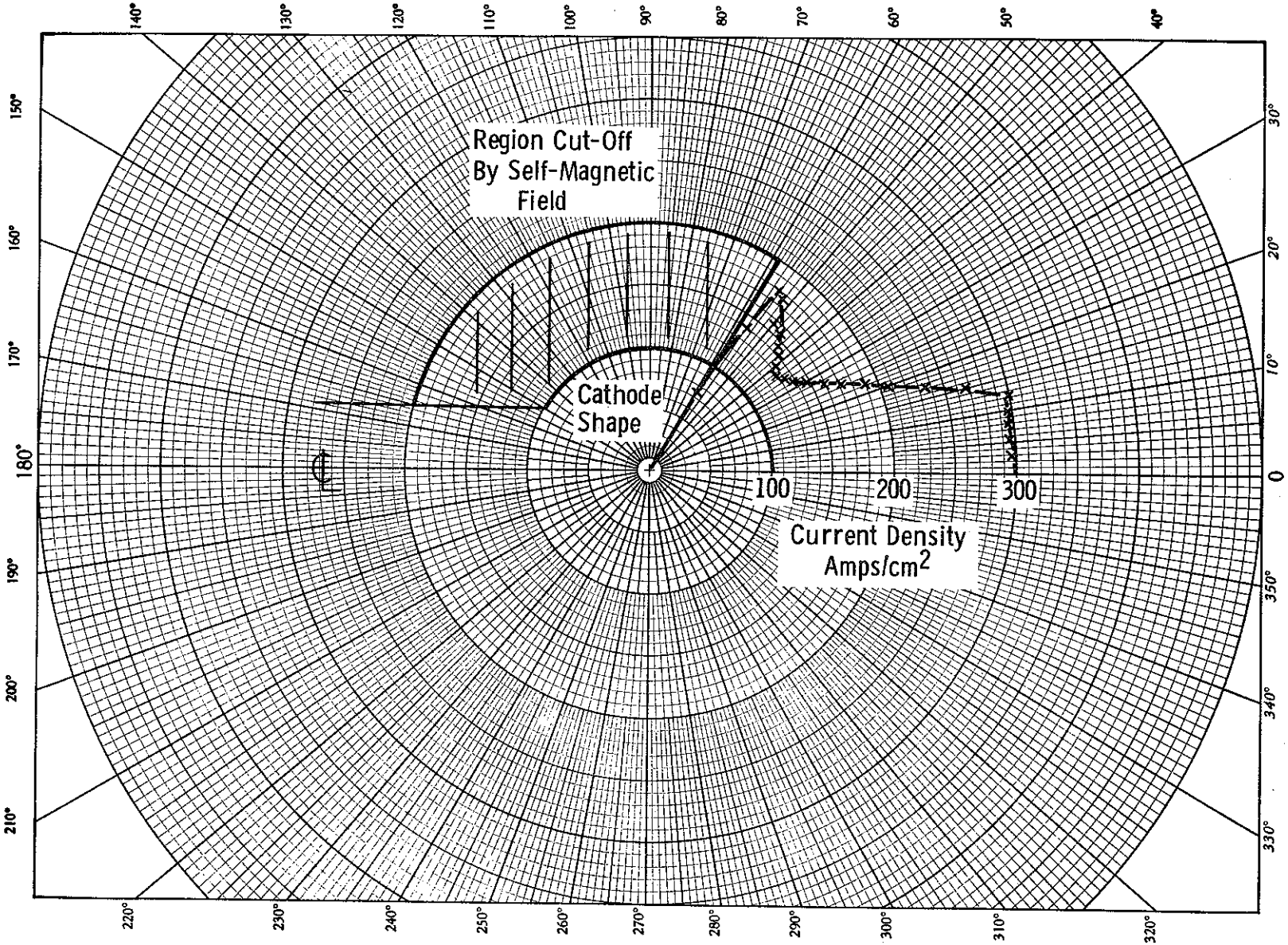

Figure 34. Current Density at Cathode Computed for Sphere-Plane Gun with 2" A-K Spacing

A toroidal cathode, planar anode gun designed by Physics International for which empirical data was available was analyzed using the improved program. Cathode torus minor diameter was 2 inches, cathode-to-anode spacing was 8 inches, anode potential was approximately 4.5 MV with anode current approximately 98 kA. Figures 35 and 36 show a sketch of the gun and anode radiation intensity, respectively.

The Laplacian field distribution was computed as is shown in Figure 37. Note that the spacing from the cathode to the 5% equipotential indicates that the electrostatic field is highest at the top of the toroidal cathode, which would tend to produce the strongest emission from this region.

A good computation for this relatively low impedance gun was difficult to obtain, and proper choice of the initial conditions was essential to avoid wild oscillations and disruptions in the solution. There is some instability in the final solution shown in Figure 38, which is a plot of conduction current versus iteration number. Current limits of 123.1 and 127.9 kA gave a solution self-consistent within $\pm$ 1.9%. One might question whether limits set on the flow forced the solution to some inconsistent value; however, as the plot shows, in iterations 6, 7, 8, 9, 11, and 12 the currents computed were within these limits, and in iteration 10 the current was barely outside the limits.

Plots for iterations 9, 10, 11, and 12 of the flow are shown in Figures 39, 40, 41, and 42. The flows plotted in Figures 39 and 42 would appear to bracket the solution on the small beam, high current side, while those in Figures 40 and 41 bracket it on the large beam, low current side. In the model used, trajectories are launched even if no current is associated with them. Crossed field effects are simulated by gradually reducing the emission current to zero as the self-magnetic field exceeds the value for cutoff, in accordance with Equation (59). Considering the center of the torus as the origin of a polar coordinate system, and the normal to the anode as zero angle, emission from the torus was allowed in the computation from -80° to 230°. The effect of the crossed electrostatic and self-magnetic field limited emission in this computation

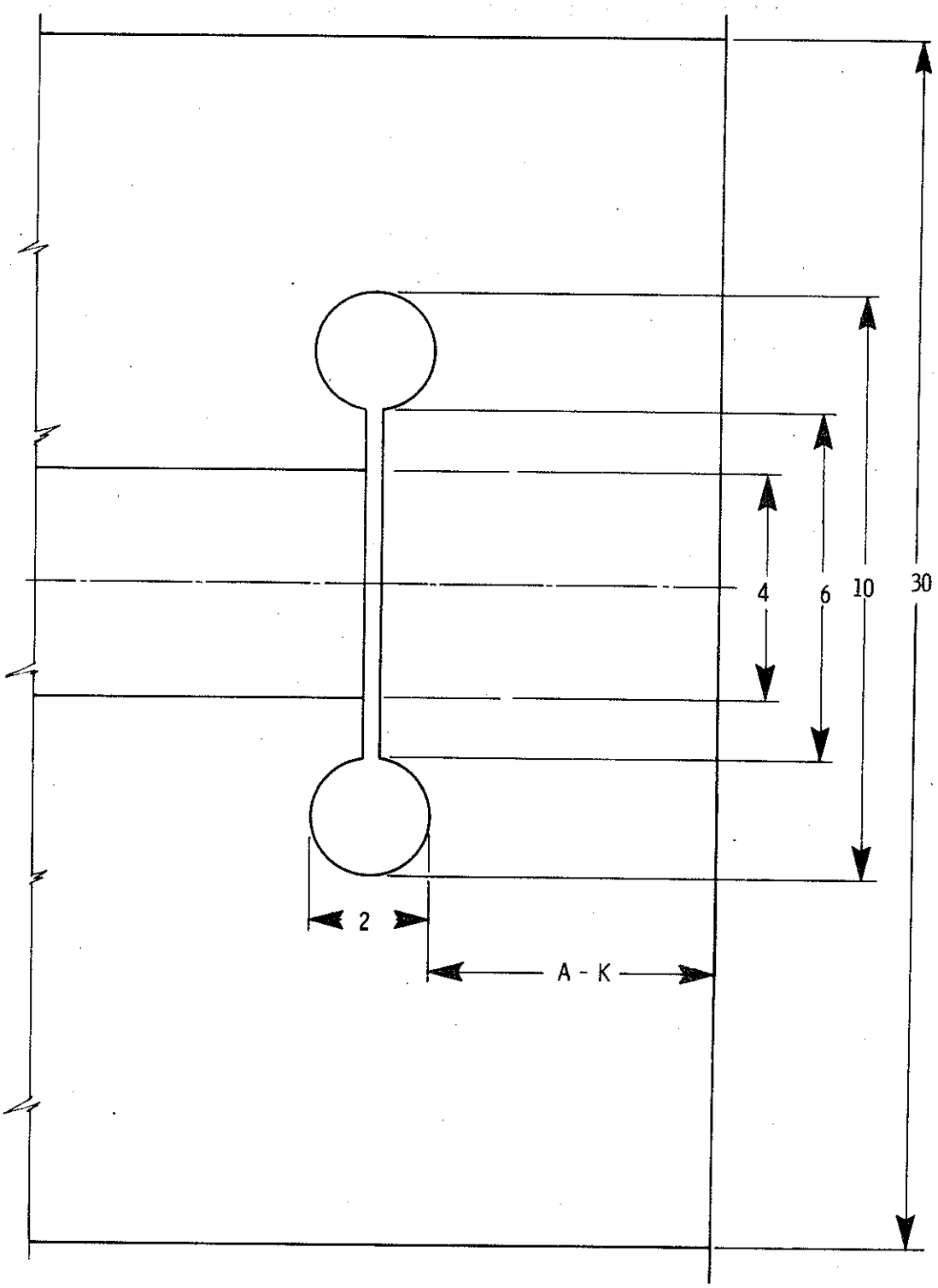

Figure 35. Sketch of Physics International Toroidal Gun
Dimensions in Inches

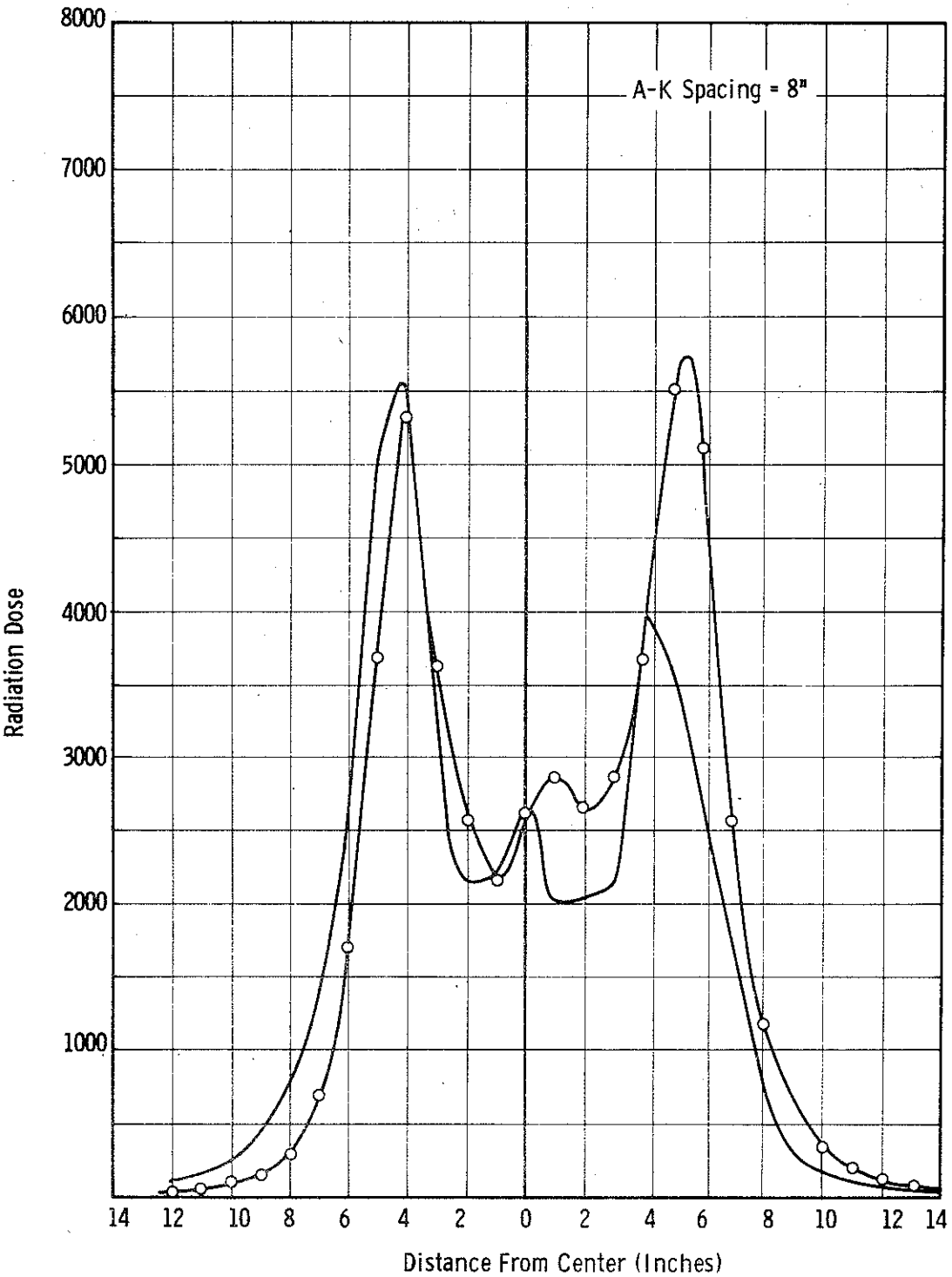

Figure 36. Radiation Intensity Profile for P. I. Toroidal Gun

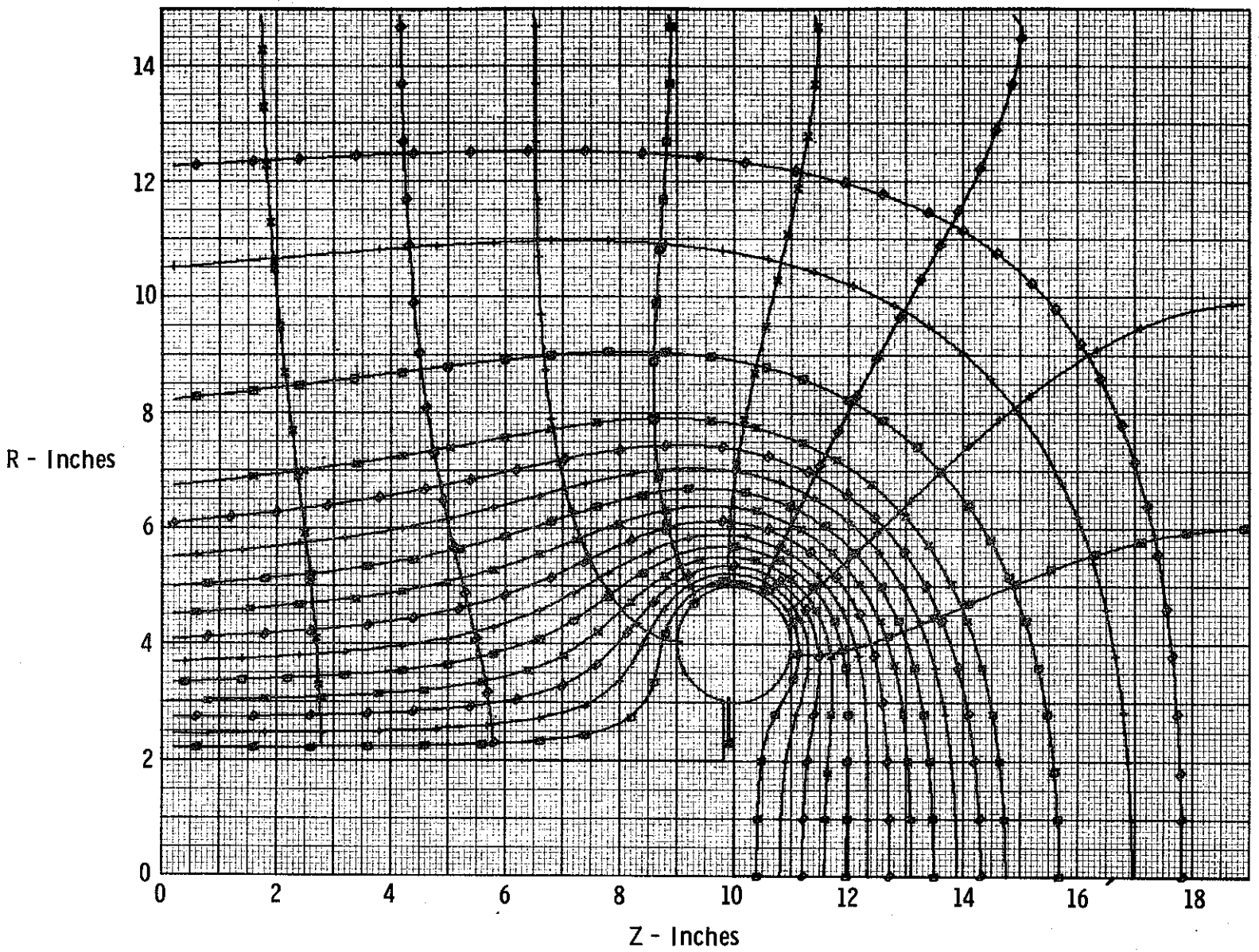

Figure 37. LaPlacian Field Solution for P. I. Toroidal Gun

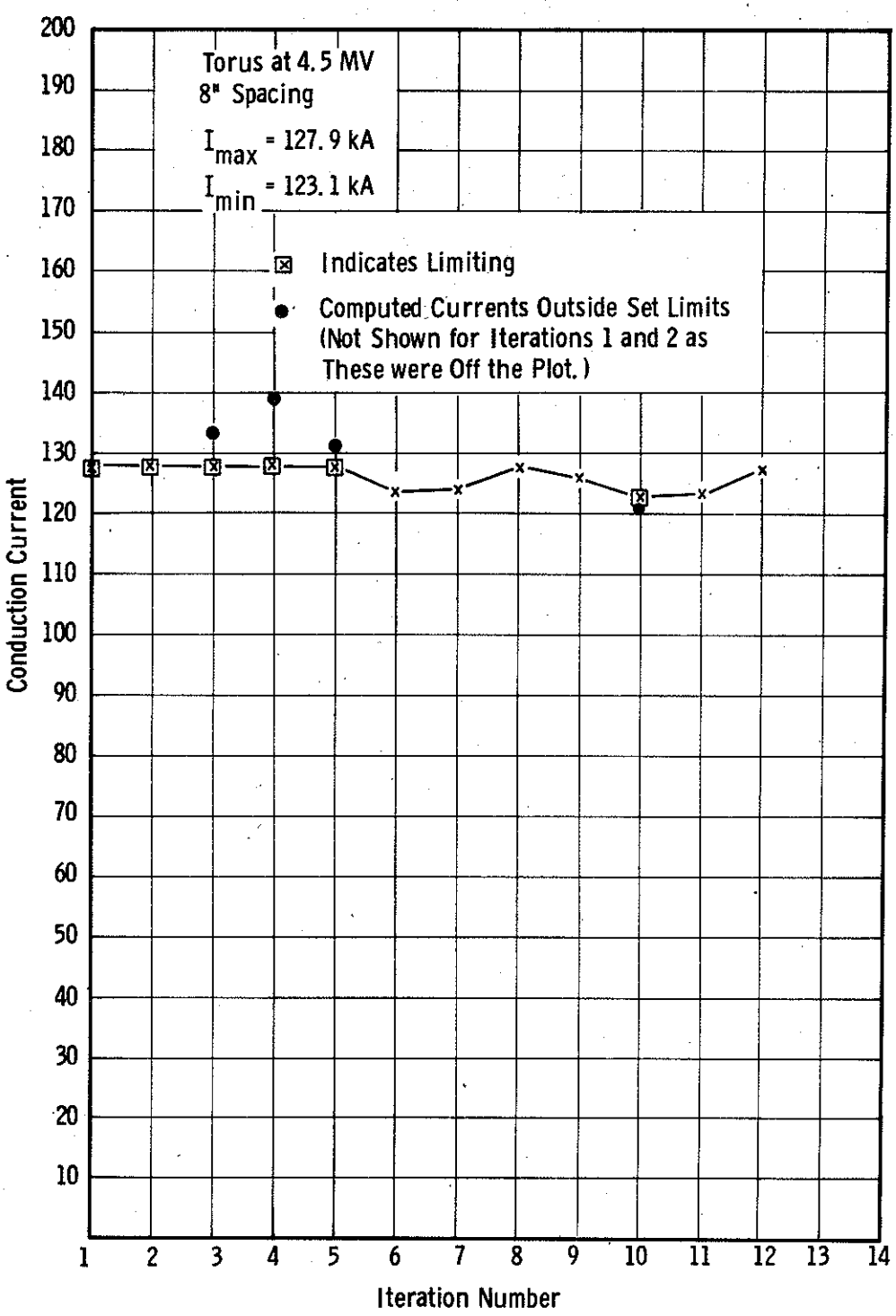

Figure 38. Conduction Current Versus Iteration Number, P. I. Toroidal Gun (Best Solution)

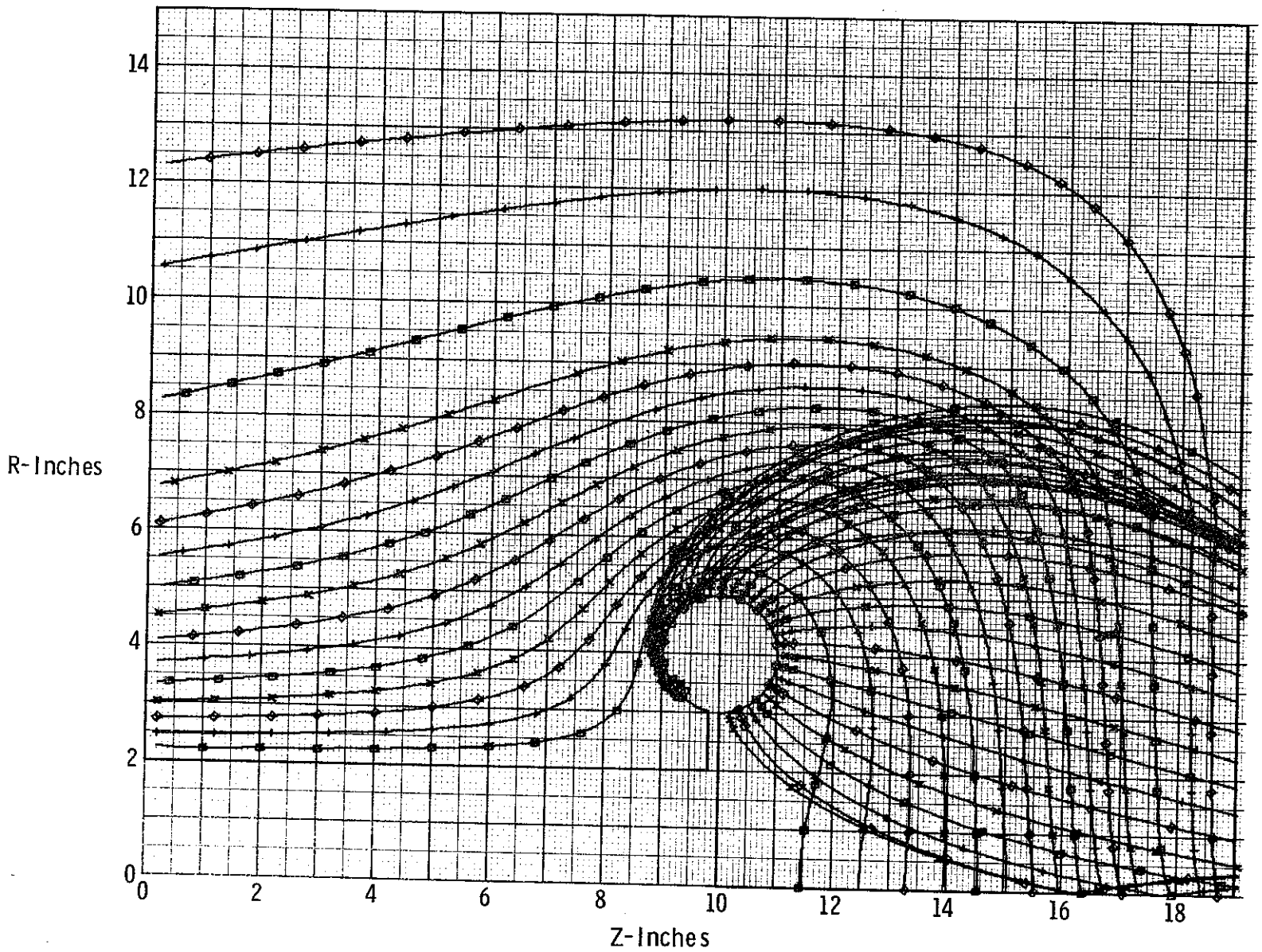

Figure 39. Iteration 9 of the Flow for the P. I. Toroidal Gun
I = 126.3 kA

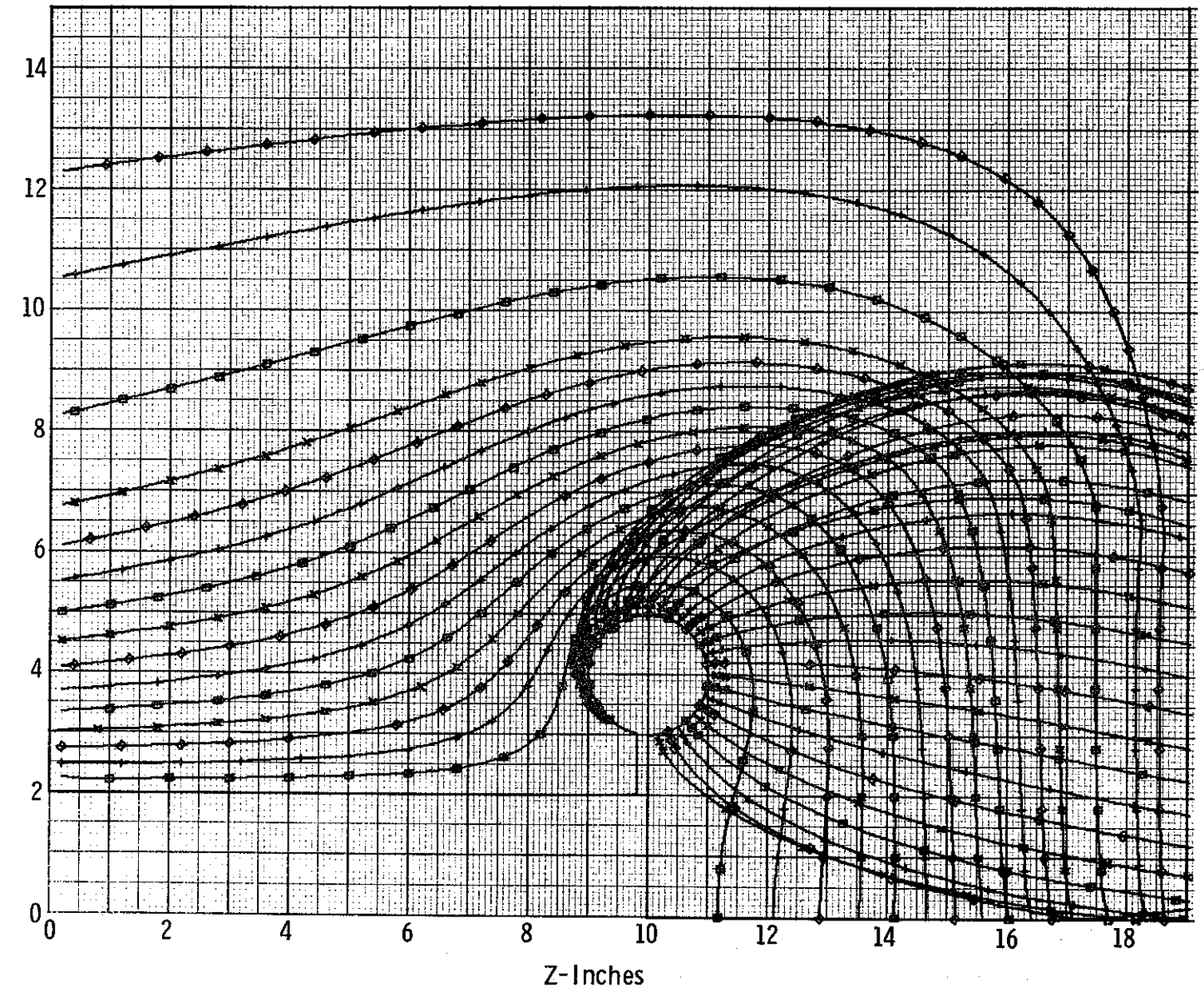

Figure 40. Iteration 10 of the Flow for the P. I. Toroidal Gun
I = 123.1 kA

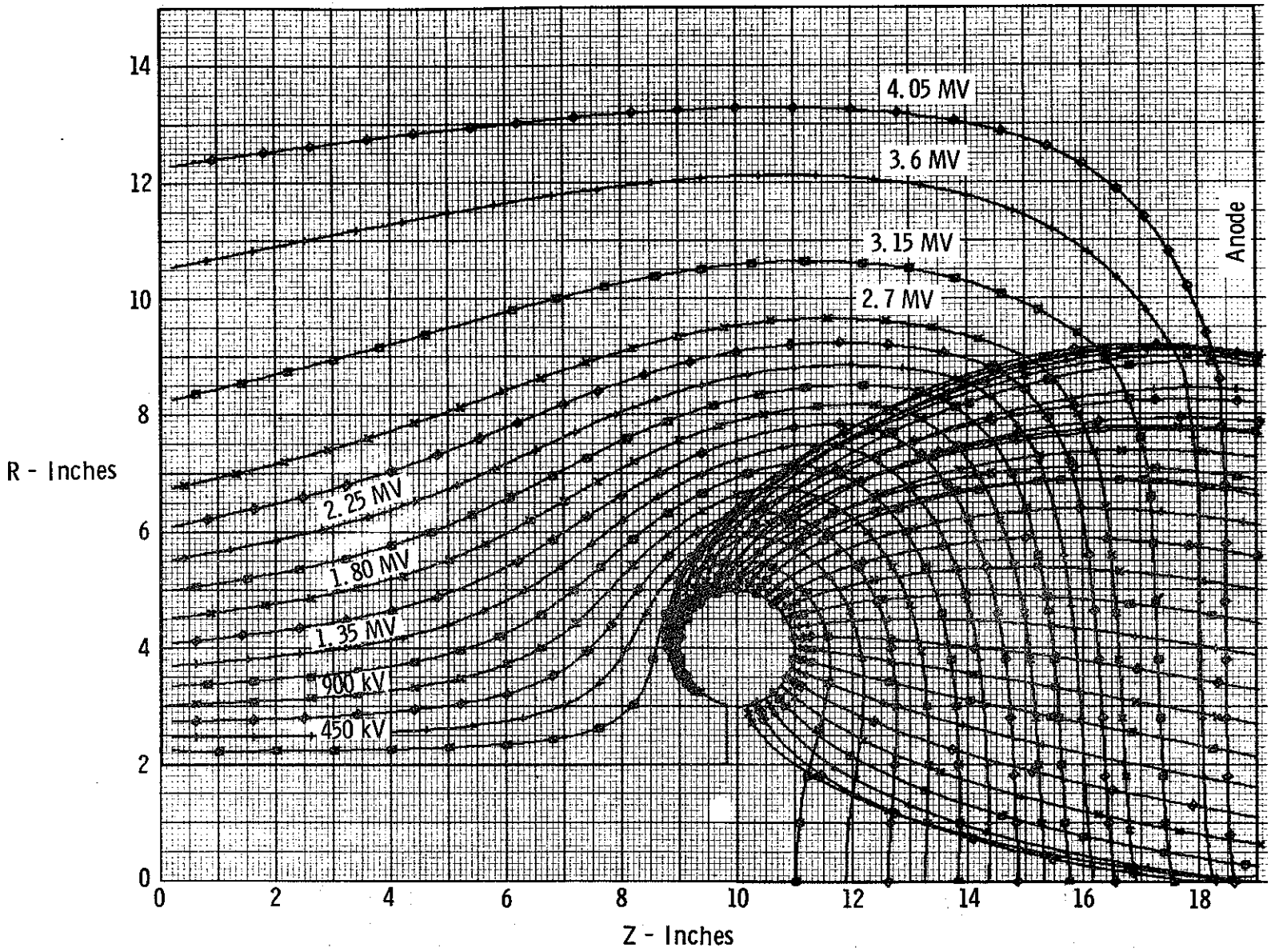

Figure 41. Iteration 11 of the Flow for the P. I. Toroidal Gun
I = 123.4 kA

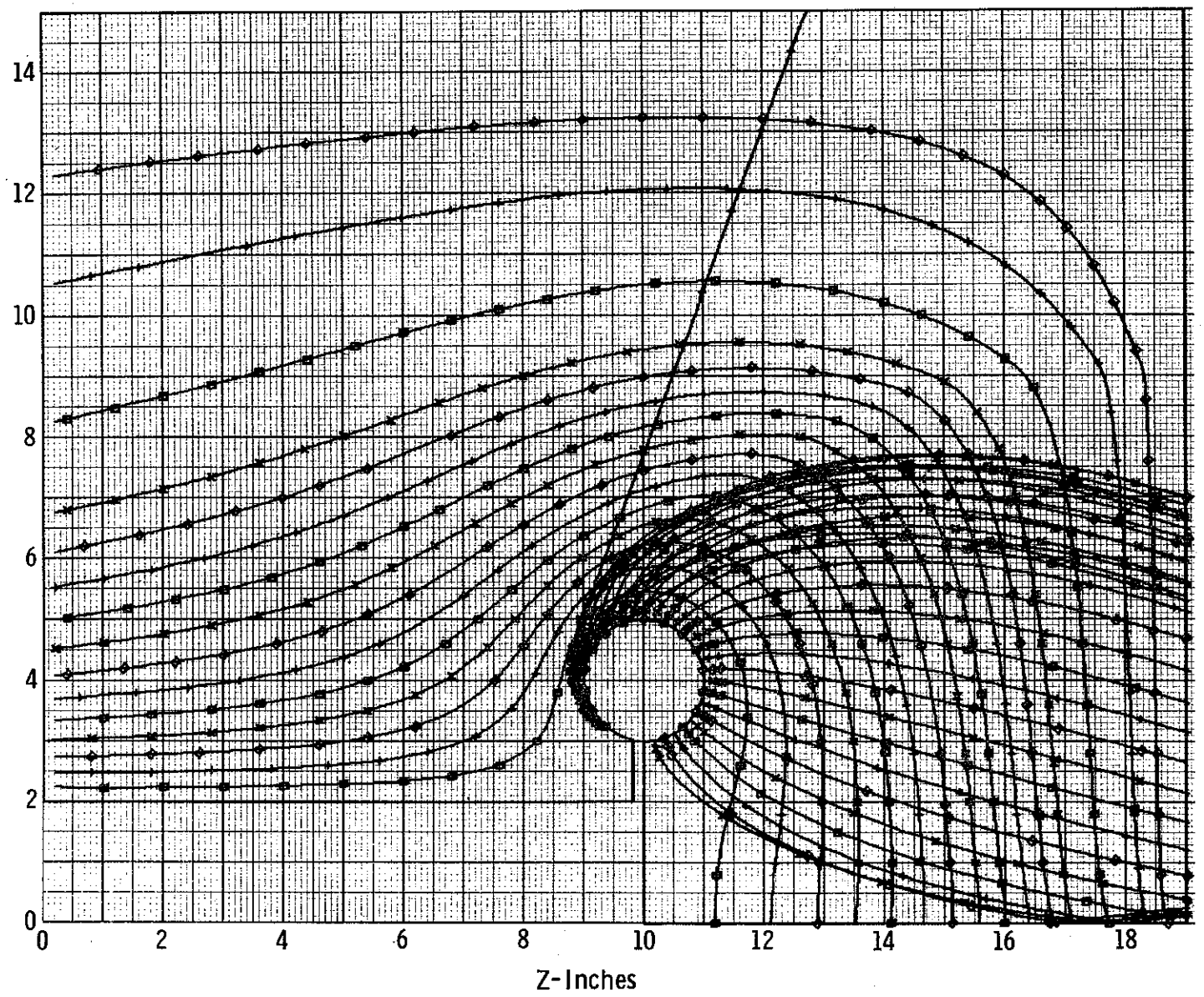

Figure 42. Iteration 12 of the Flow for the P. I. Toroidal Gun
I = 127.9 kA

to the surface included between the angles 170° and -80°. Those trajectories in the region from 230° to 170° (which carry no current) pass very close to the cathode surface. They serve to show the behavior of electrons in the "sheath." In most interations, the trajectory from 230° returns to the cathode. Inaccuracies inherent to finite-difference methods introduced large errors for those trajectories passing very close to the cathode surface. The trajectory shooting out nearly tangent to the cathode surface in Figure 42 (iteration 12) resulted from these numerical errors. There was no current associated with this trajectory, so it could not affect the solution.

Figures 43 and 44 show anode current density versus radial position for, respectively, iteration 10 and 11 of the solution. Qualitatively these plots are similar and resemble the plot of radiation intensity (Figure 36). For iterations 10 and 11, the values of conduction current used were 123.1 and 123.4 kA. The variation in total current is slight, yet the variation in anode current density at the axis and at the beam edge is large.

In Figures 45, 46, and 47 the current density at the cathode is plotted in polar coordinates for iterations 10, 11, and 12. Zero angle is in the direction of the anode. An examination of these plots shows that current density is highest on the top and back side of the cathode surface. The flow from the back of the cathode follows an arc which passes close to the cathode before continuing to the anode. The flow in this region is very complex, since it is the result of very strong cross-field effects approaching but still below magnetron cutoff. In the actual physical flow, the emission current density in this region would be directly affected by cutoff electrons returning to the cathode from the sheath of charge in the region of magnetron cutoff.

In this region, the computed current density reaches a maximum and then has a very pronounced inflection point (at about 130°). It is not clear from the work performed to date whether this should be expected, or is a consequence of inaccuracies in the simulation. It would be desirable to try to further improve the simulation of

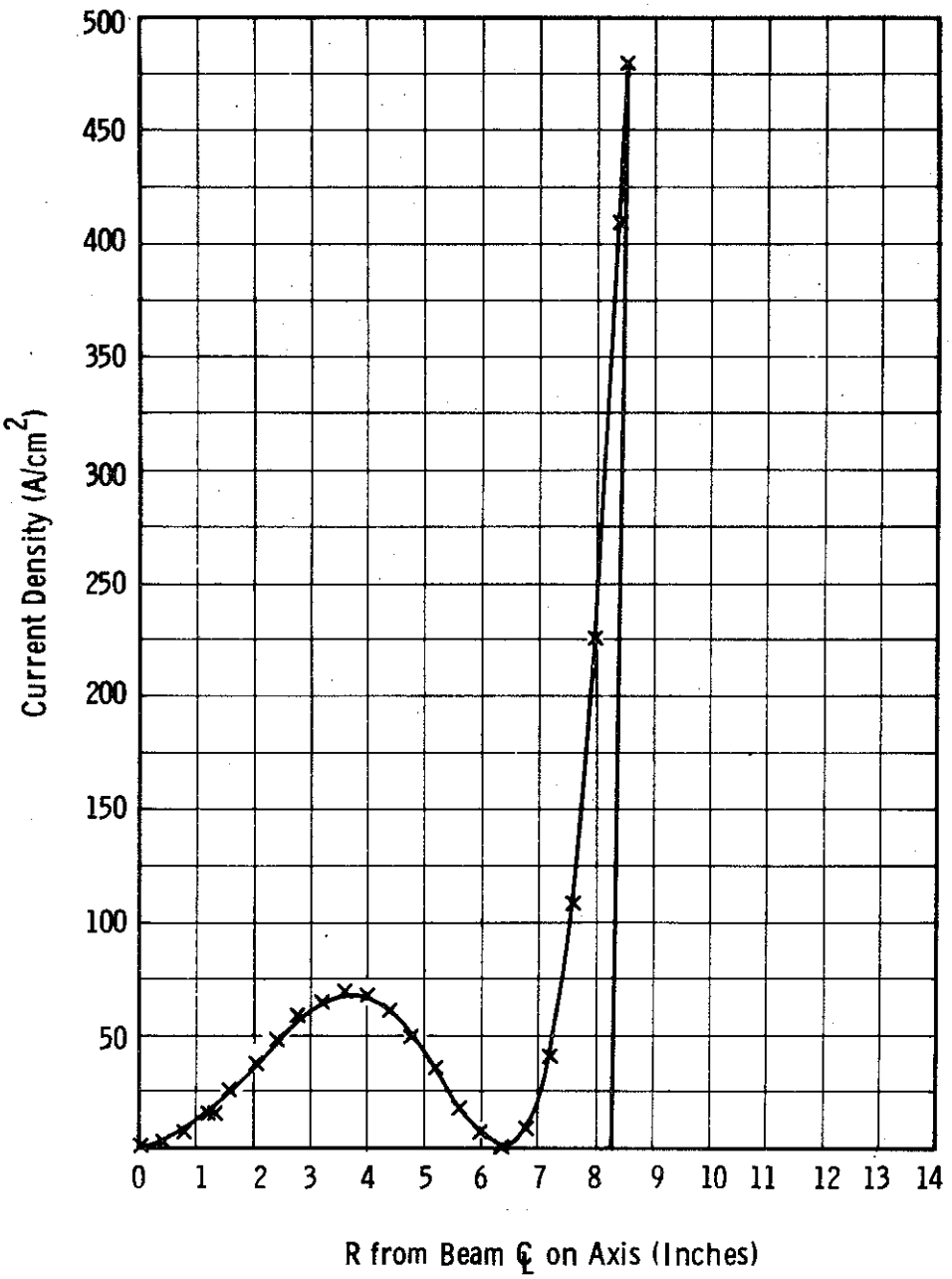

Figure 43. Current Density at Anode Versus Radius, P. I. Toroidal Gun, Iteration 10

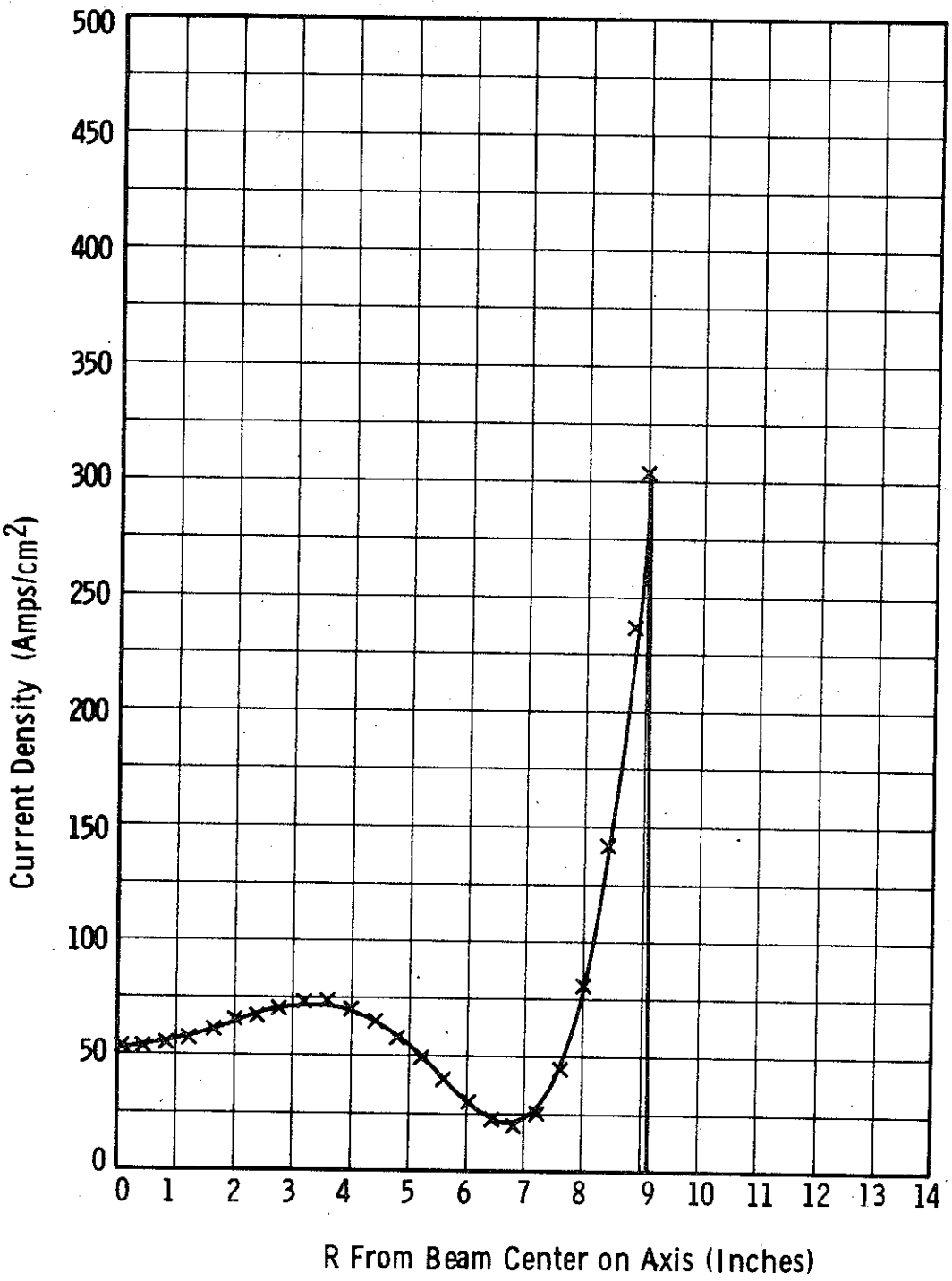

Figure 44. Current Density at Anode Versus Radius, P. I. Toroidal Gun, Iteration 11

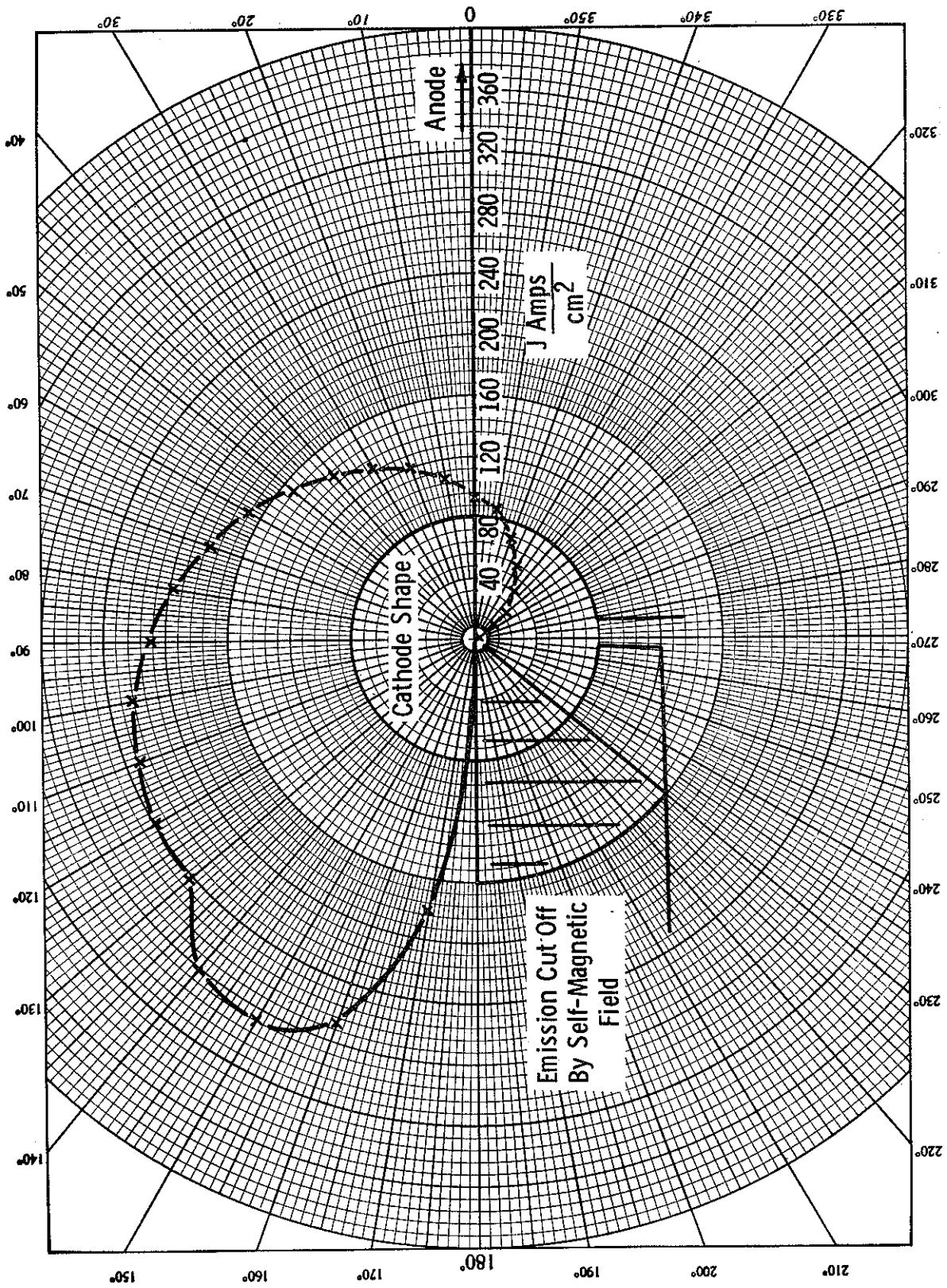

Figure 45. Current Density at Cathode, Iteration 10 for the P. I. Toroidal Gun

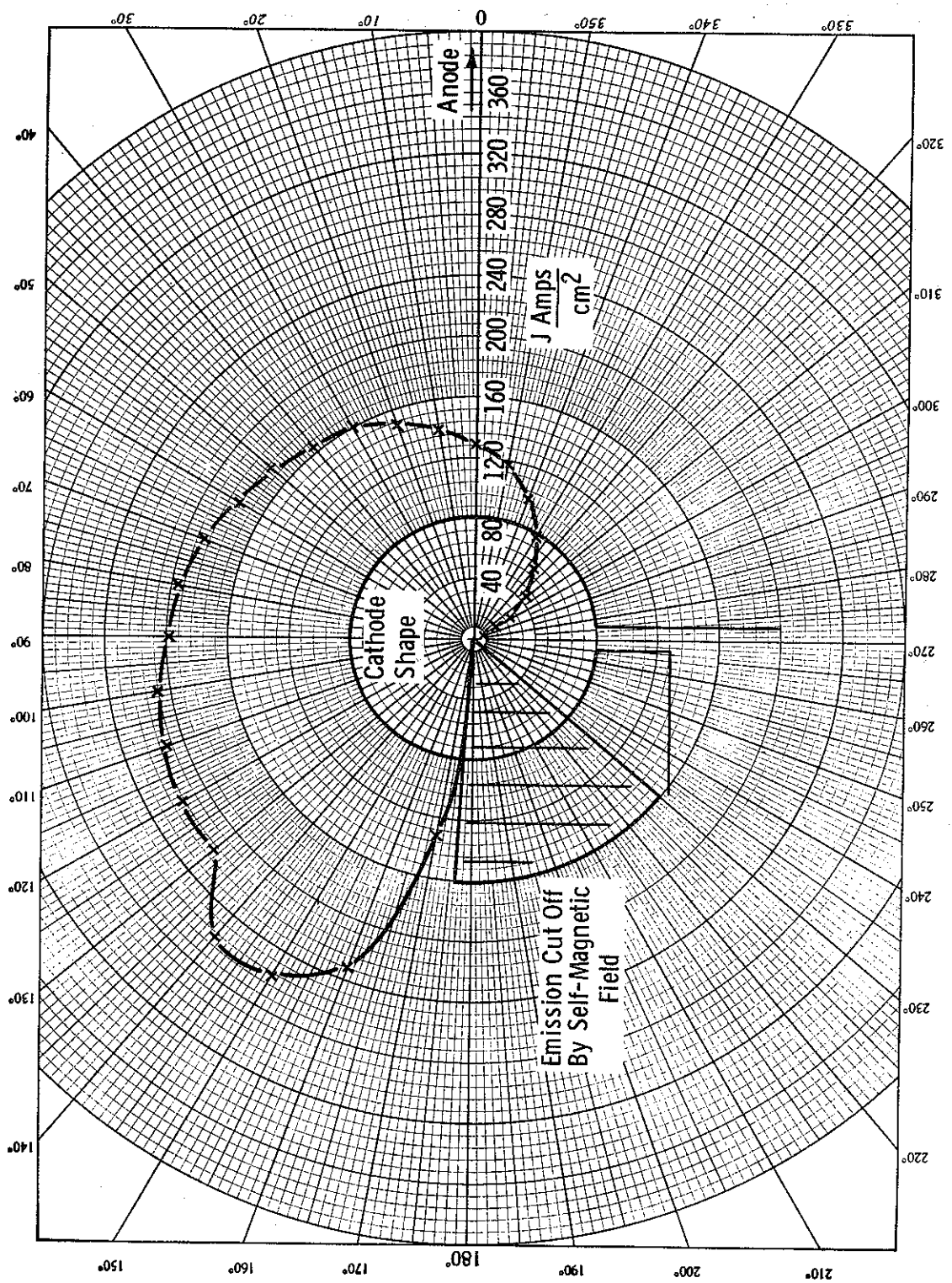

Figure 46. Current Density at Cathode, Iteration 11 for the P.I. Toroidal Gun

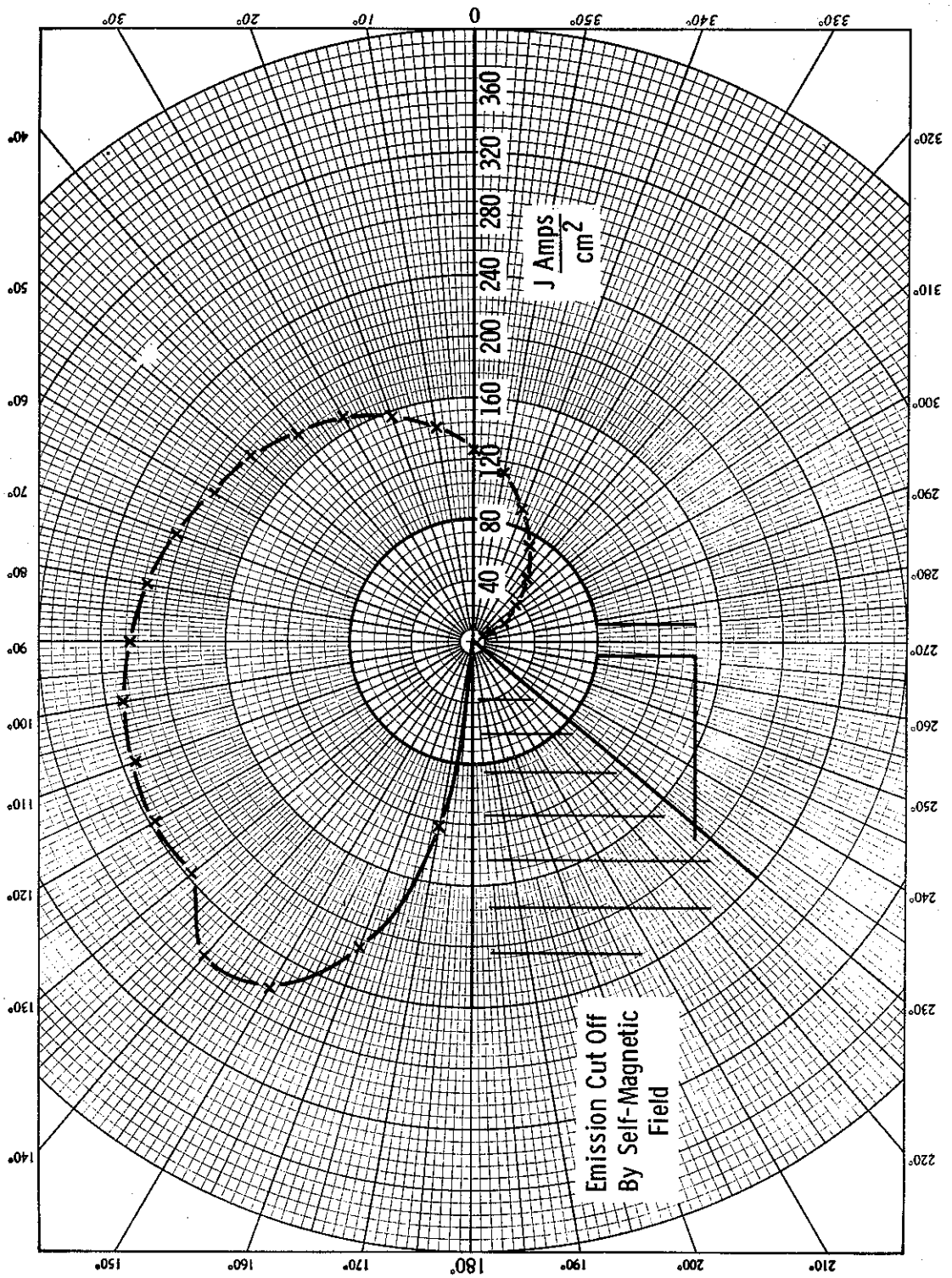

Figure 47. Current Density at Cathode, Iteration 12 for the P. I. Toroidal Gun

cross-field effects on emission to improve the accuracy of the computation, and to determine if this would result in an improvement in convergence. It would also be desirable to determine whether the difficulty of obtaining a converged solution for such high current, low impedance flows is purely mathematical, or whether it is a consequence of an inherent physical instability associated with these flows.

Some insight into the nature of the instability can be gained by comparing Figures 45 through 47. One finds that the variation of current density with angle at the cathode is much more similar between iterations 11 and 12, which had dissimilar beam currents and radii, than between iterations 10 and 11 (which had similar beam currents and radii). Over most of the cathode surface, the current density profile for iteration 12 looks like a scaled-up version of the one for iteration 11, which explains the increase in current. This increase must have been due to the relatively low space charge densities in the larger beams of the preceeding two iterations, 10 and 11 (both have some influence because of space-charge damping). A reduction in the beam size results, due to the increased self-magnetic field produced by the higher beam current. The difference in the shapes of the cathode current density profiles of iterations 10 and 11 are due to the use in each iteration of the matrix of current enclosed (within a given radius) from the previous iteration, scaled by the ratio of the new to the old values of beam current, to determine the self-magnetic field. The error due to a moderate change in beam radius and beam current from a previous iteration, produced for example in iterations 9 or 11, combined with the space-charge damping, must almost offset the tendency for the beam current to change in the next iteration due to the change in overall beam size. This is required to explain the similarity in the results for iterations 10 and 11, 8 and 9, etc. (see Figure 38). The weighted averaging of the space-charge in this case utilized 35% of the values from the preceeding iteration plus 65% of the new values; 35% is high enough for this averaging to have possibly been a significant factor in causing the solution to occur in consecutive pairs of similar iterations. However, both the space-charge and the self-magnetic field errors should be in the direction to reduce the amplitude of the

variation of the pairs of similar solutions about the self-consistent solution (particularly the variation to a smaller beam), and therefore would appear to be desirable until an effective means of improving the convergence is found for computing low impedance relativistic guns.

E. CALCULATIONS RELATED TO GRADED INSULATOR DESIGN

A study was made of the shank and insulator portion of the Physics International torodial cathode gun. The object of this study was to determine if field emission from the shank would cause electron bombardment of the graded insulator. Figure 48 shows the computer solution plot; the first section of the graded insulator has been drawn in for clarity.

Measured anode potential for this gun was 4.5 MV; anode current was 98 kA. To simulate field emission, the beam injection feature of Varian's beam analysis computer program was used. All trajectories were injected normal to the shank surface at a kinetic energy of 6.6 keV. Trajectories 1 through 26 each contain 4 A, trajectories 27 and 28 each contain 1 A, and trajectories 29 through 32 each contain 24.475 kA to simulate flow from the actual cathode. The geometry of the region close to the anode (where the large current was injected) was altered from that of the original gun to simplify the calculation. Injection along the shank back to trajectory 1 seemed deisrable since the electrostatic field in this region was 1.24×10^7 volt/meter. The space-charge potential depression was negligible over the shank surface leading up to the discharge gap. As a result, the cyclotron radii are at their maximum possible values, to provide the pessimistic limiting solution. Note that trajectory 1 passes within 0.100 inch of the spacer.

Each of the trajectories from 1 through 26 either describes a cycloid and returns to the cathode surface, or continues a cycloid curve until it reaches the anode. Only those trajectories in the region of the highest electrostatic field (trajectories 27 through 32) pass directly to the anode, without cycloiding.

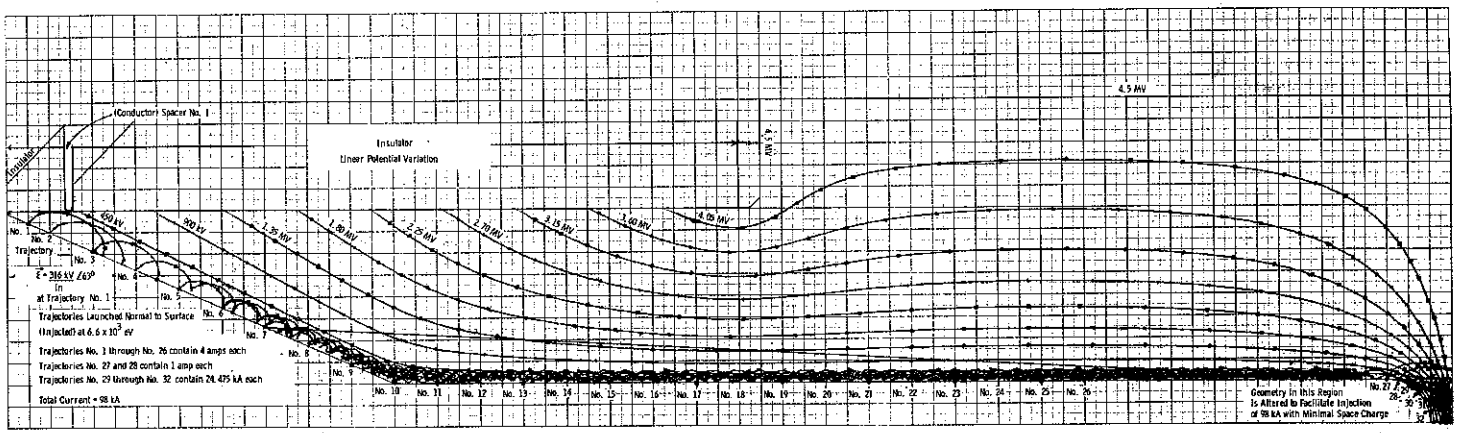

Figure 48. P. I. Toroidal Gun, Insulator Study, Injected Beam, Iteration 2.

To simulate inductive effects at the beginning of the pulse, further calculations were made with the effect of the self-magnetic field scaled by 1/2 and by 1/4 of its steady-state value; the results are shown in Figures 49 and 50, respectively.

F. FIFTEEN MEGAVOLT TOROIDAL GUN COMPUTATIONS

On the basis of previous attempts to design single module electron guns producing currents of greater than one megampere, such as those discussed in the section on planar guns, it was concluded that the best approach to designing such a high current gun (without using an external magnetic focusing field), was to use an array of gun modules. Since each module would include a return conductor for the conduction current, it would be isolated from the self-magnetic field produced in the other modules. Using four such modules, a current of 400 kA in each would yield a total current of 1.6 MA. Studies of radiation patterns for various size beams of varying convergence for such an array were conducted at Physics International. The results indicated that to efficiently provide uniform x-ray illumination in a one meter cubic volume using converging gun modules, the beam radius should be approximately 40 cm (for an idealized beam with uniform current density). The best radiation uniformity was obtained for flow with normal incidence to the anode. The geometries used in the computations to be discussed were based on the above considerations and on design preferences and limitations suggested by Physics International. It was assumed that the optimum computed beam size would fall in the range from 40 to 46 cm, or 16 to 18 inches.

The basic gun module geometry considered is shown in Figure 51; it is somewhat similar to the one shown in Figure 35. The module gun voltage is 15 MV, and several dimensions are considered open to optimization. These include the cathode-to-anode spacing (S), the torus minor diameter (D_t), and the mean torus diameter (D_M).

Computations were made using a number of variations of these parameters. The combinations are listed in Table I.

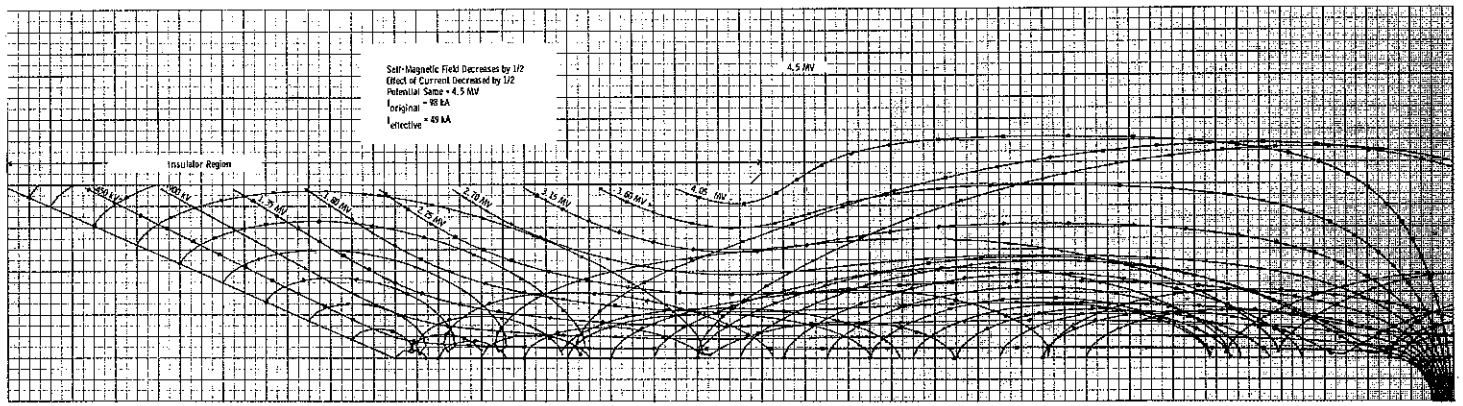

Figure 49. P. I. Toroidal Gun, Insulator Study, Injected Beam, Iteration 1, Self-Magnetic Field Decreased by 1/2.

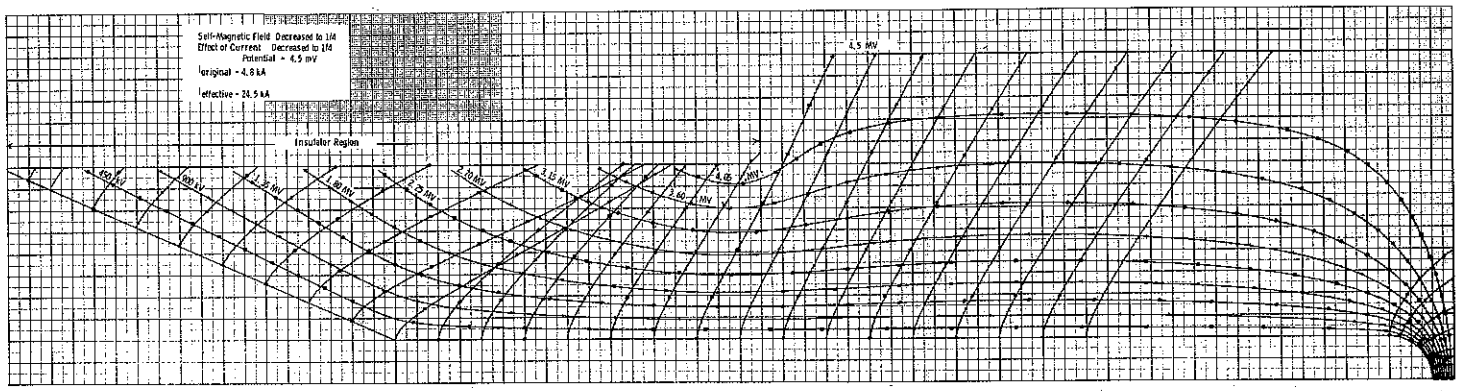

Figure 50. P. I. Toroidal Gun, Insulator Study, Injected Beam, Iteration 1, Self-Magnetic Field Decreased to 1/4.

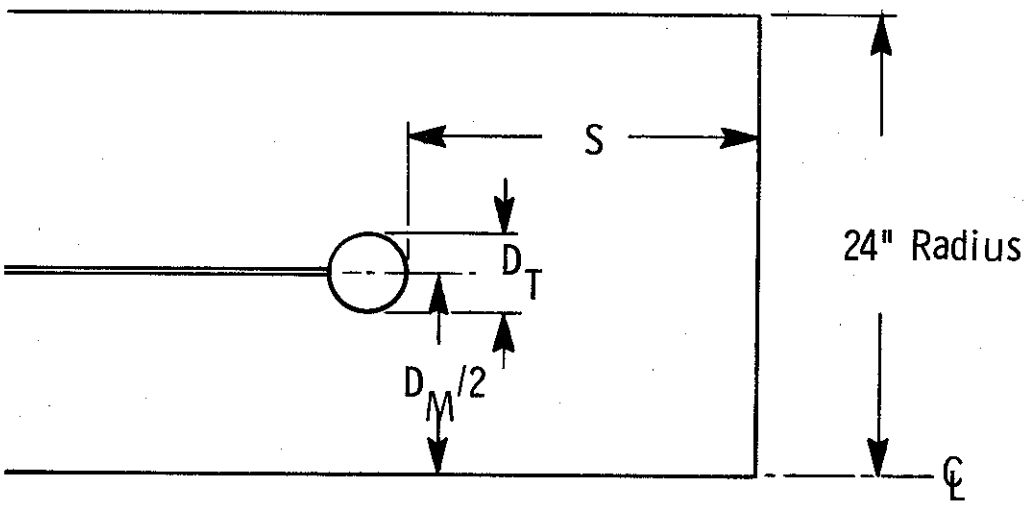

Figure 51. Basic Gun Module Geometry Used in 15 MV Gun Calculations

TABLE I

VALUES OF PARAMETERS USED IN COMPUTATIONS

Mean Torus Diameter D_M (in.)	Torus Minor Diameter D_t (in.)	Cathode-to-Anode Spacing S (in.)
21	4	12, 14, 18, 24
21	3	24
21	2	18, 24
14	4	10, 14

The behavior of the iterative computations for these guns was very unstable. Despite considerable effort for some of the cases in Table I, no completely self-consistent solutions were obtained. However, the solutions give approximate information on beam current and beam flow at the anode. Use of the perveance limiting feature proved invaluable for determining the range in which the solution for a given gun must exist, and for obtaining a number of iterations for the flow. When the upper limit on perveance (and therefore current) was set too low, the space-charge potential depression was less than that for the self-consistent solution. As a result, the computed perveance (and current) would be consistently higher than the upper limit set. An example of this behavior is shown in Figure 52 in a plot of the computed current and the current limit from a calculation for the 15 MV gun module, with values of D_M, D_t, and S of 21, 4, and 12 inches. The value of the computed current for the first iteration is off the plot and therefore not shown. A second curve plotted in the figure is the result for the same gun when the upper current limit is prescribed too high. For this case, the space-charge potential depression becomes excessive and drives the potential to negative values over a substantial portion of the cathode, cutting off possible emission from that portion in the next iteration. If the calculation is continued, the emitted current computed in the next iteration may be much too low, and

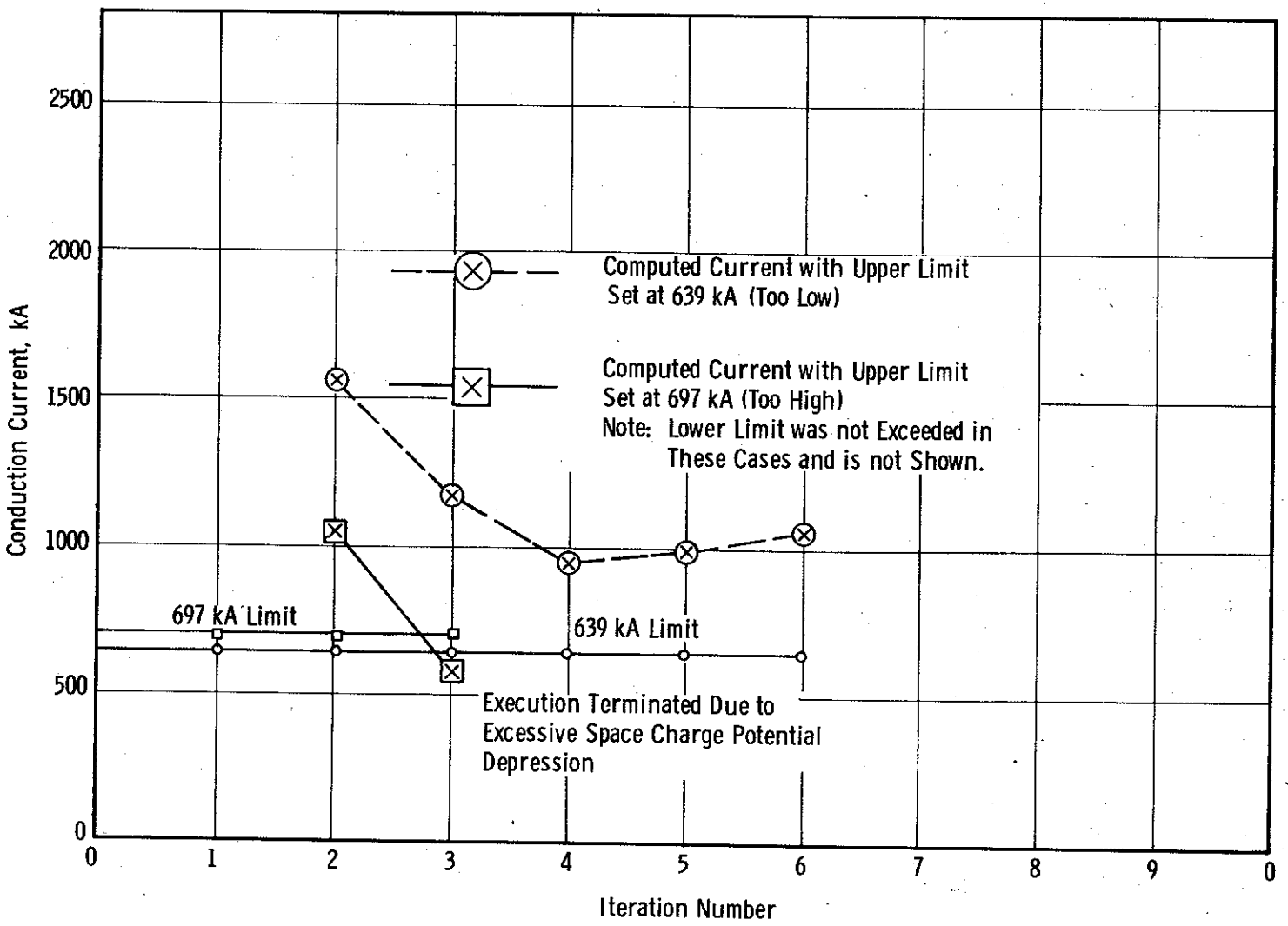

Figure 52. 15 MV Gun, Computed Current Versus Iteration for Current Limited Cases D_M = 21", D_T = 4", S = 12 "

the iterative solution then becomes very unstable. The computation is usually made to terminate if more than about one-third of the trajectories are cut off.

Thus, by trial-and-error adjustment of the upper perveance limit the range in which the self-consistent value should be found can be determined, and corresponding approximations (however crude) to the current flow can be computed. In particular, the relatively well behaved results, when the current limit is set too low, establish an upper limit to beam size and a lower limit to beam convergence at the anode for the self-consistent solution. A lower limit to beam size is not necessarily established by the non-self-consistent solution obtained with the current limit too high due to errors in the self-magnetic field distribution (derived from the preceeding iteration) and in the electric field (which will be too high when the computed current is higher than the self-consistent value).

The first computations were performed for values of D_M, D_t, and S of 21, 4, and 24 inches. A plot of the flow that perhaps is most representative is shown in Figure 53. In this case, the upper perveance limit was set slightly low. The actual flow should therefore be slightly more convergent. The self-consistent beam current is estimated to be in the range of 523 to 580 kA for this gun. The flow should be converging only moderately at the anode, very likely in the desired range of beam radius of 16 to 18 inches. The computed flow tends to be too large by an additional amount due to the presence of a small error in the calculation of the self-magnetic field above the cathode; this error was eliminated in the final calculations performed.

In Figure 54, the most representative flow is shown plotted for the 12 inch spacing case with D_M and D_t as they were in Figure 53. The plot shown is for iteration 6 for the low current limit case of Figure 52. The self-consistent space-charge limited current is much higher than the desired 400 kA for this case, as expected since it was already somewhat high with twice the axial spacing. The cathode current density is much more uniform than for the large spacing case, as can be inferred by comparing the spacing from the cathode to the first equipotential plotted in the two

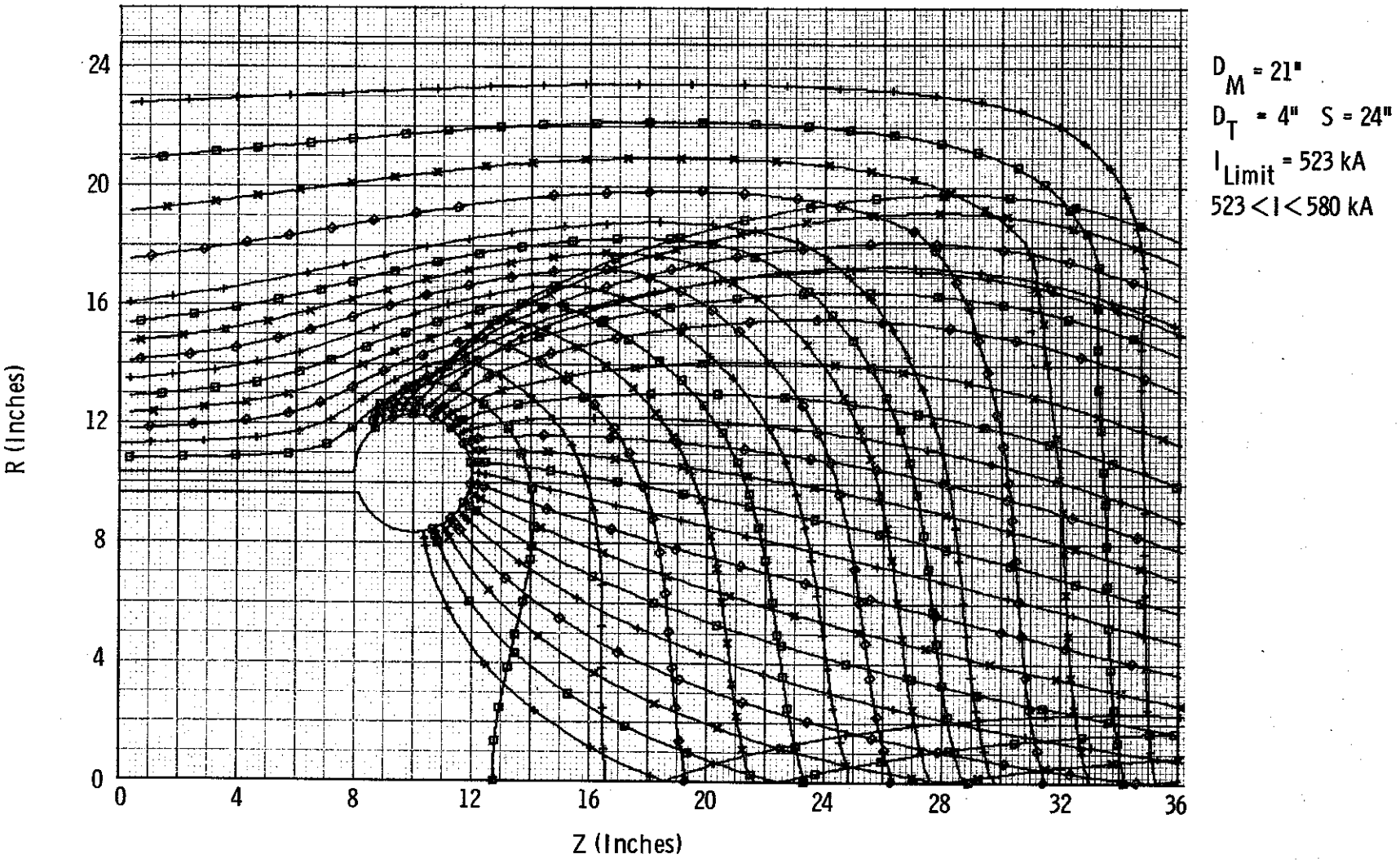

Figure 53. 15 MV Gun Calculation

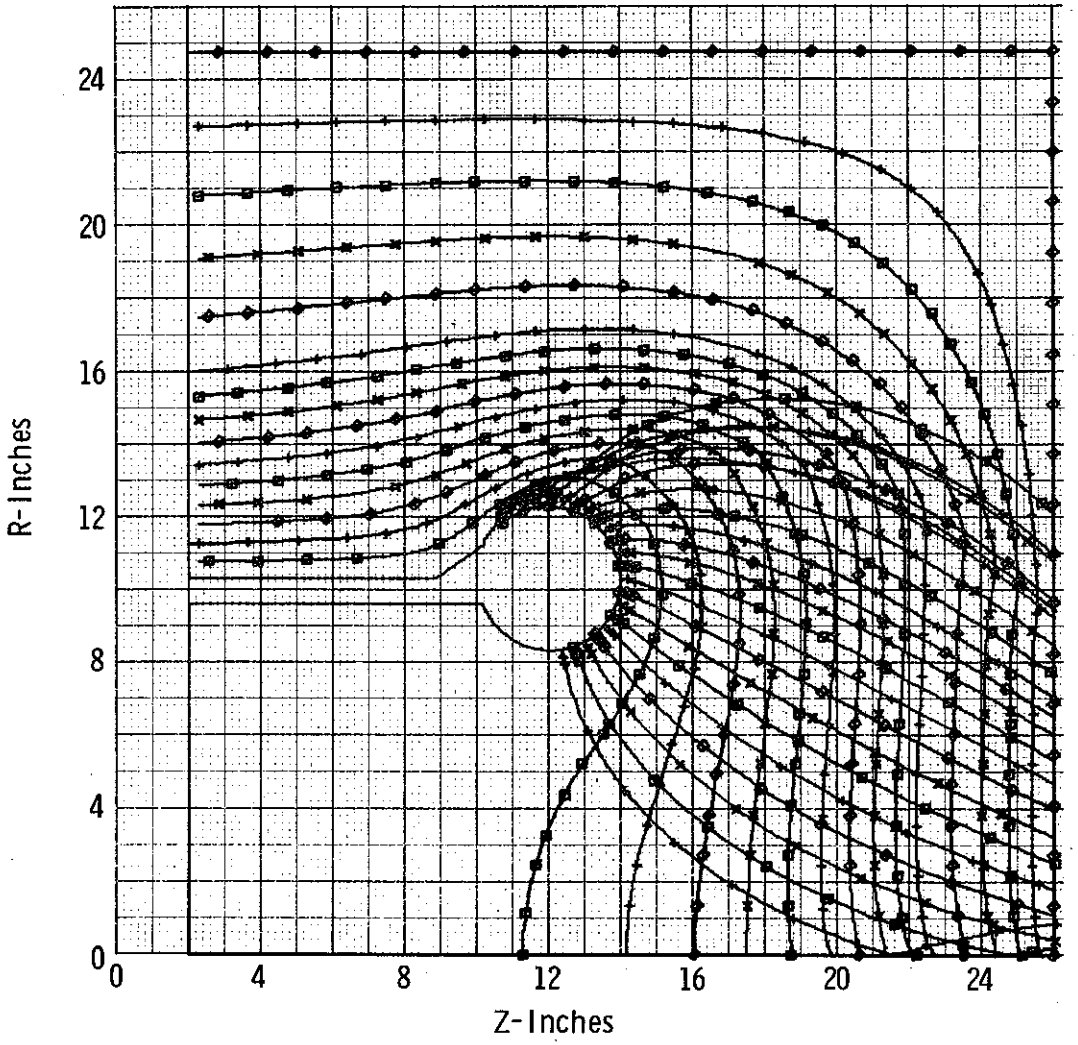

Figure 54. 15 MV Gun Calcuation

figures. The emission tends to be uniform in this case since the distance from the cathode to the anode is nearly the same as to the outer conductor, whereas in the first case it is much greater. With the higher self-magnetic field for this case, the beam size at the anode is much smaller, no more than 12 inches in radius. The convergence angle is also greater at the anode. Thus, if such a gun actually operates fully space-charge limited, a lower perveance design than that for this case is clearly desirable.

The ranges for the self-consistent space-charge limited current for the cases with D_M equal to 21 inches and D_t equal to 4 inches and 2 inches are plotted in Figure 55. Toward the end of these studies it was learned that spacings greater than about 20 inches were not considered practical by Physics International for the converging module geometry being utilized. Thus, a geometry utilizing a relatively small value of D_t appears to be desirable to keep the beam current from being too large. Ranges for self-consistent current versus torus minor diameter for D_M equal to 21 inches and S to 24 inches are plotted in Figure 56. From this curve it would appear that a value of from 1 to 3 inches would be optimum for providing a space-charge limited current of from 400 to 500 kA. With an 18-inch spacing these values would increase by about 10%, from the data in Figure 55.

The two computations made with D_M reduced to 14 inches (a dimension considered as an alternate to 21 inches by Physics International) were both done with an upper limit on current of 523 kA. The resultant behavior suggested that the self-consistent current would be higher than this value with a 10-inch spacing, and lower with a 14-inch spacing. Comparing to the curve for D_t equal to 4 inches in Figure 55, this indicates that the current drops as D_M is reduced, as one would expect. A flow for the 10-inch spacing case is shown in Figure 57. The convergence of the beam at the anode in the figure is probably slightly less than would occur for a self-consistent flow. From this calculation it would appear that the beam radius would be less than 6-1/2 inches, much less than the desired 16 to 18 inch value. The beam would also

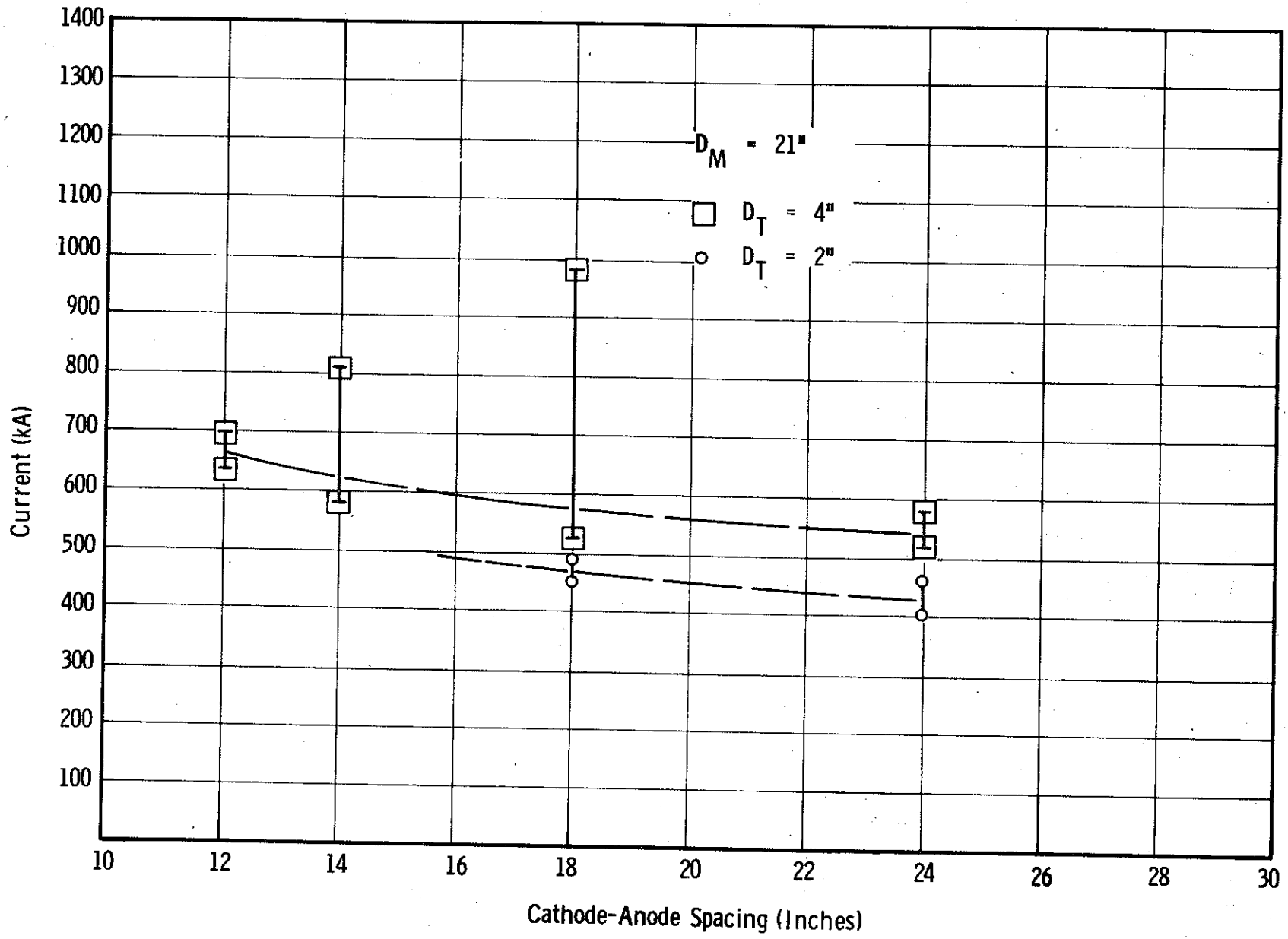

Figure 55. 15 MV Gun, Possible Range for Space Charge Limited Current Versus Cathode-Anode Spacing

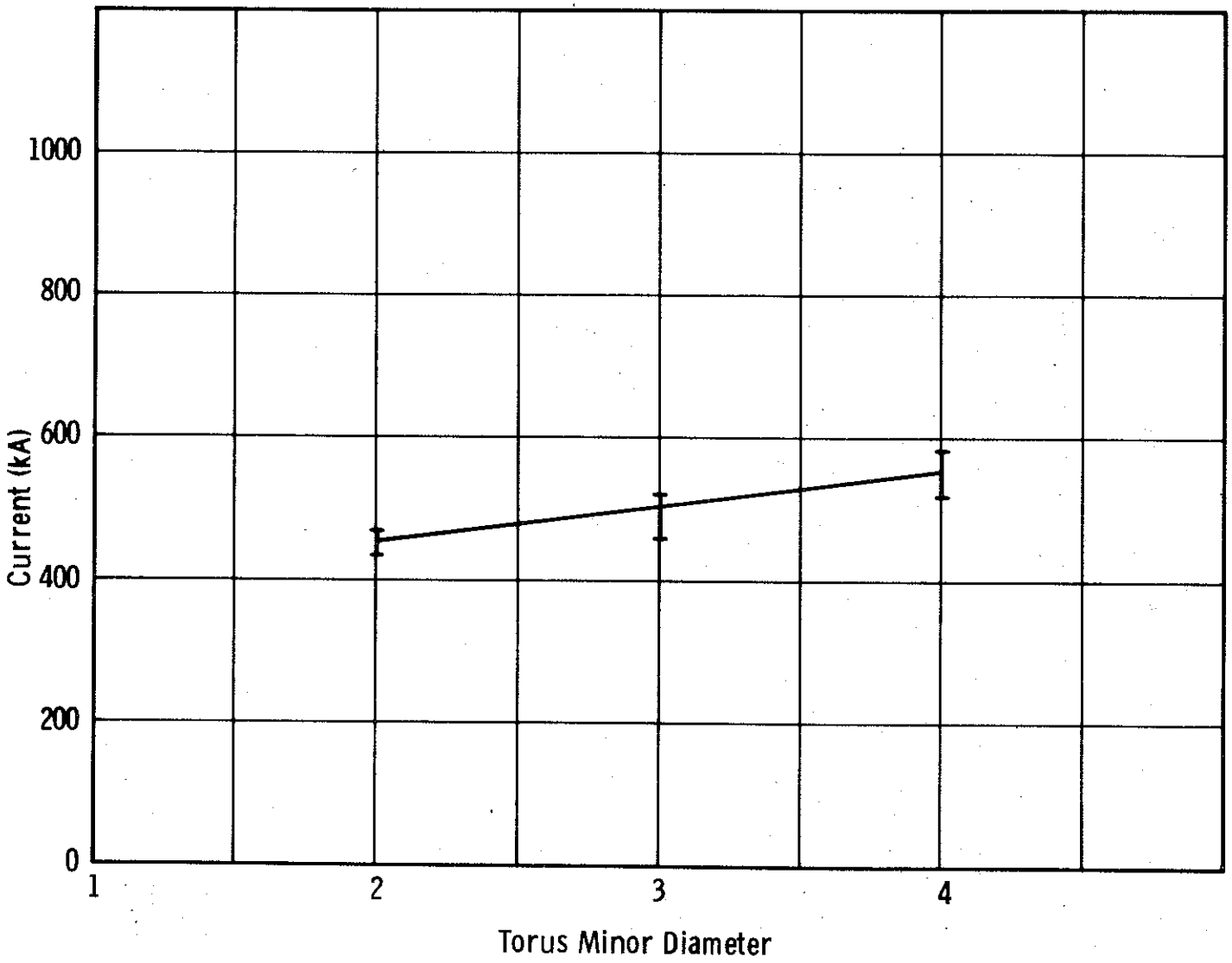

Figure 56. 15 MV Gun, Possible Range for Space Charge Limited Current Versus Torus Minor Diameter, D_T
D_M = 21", S = 24"

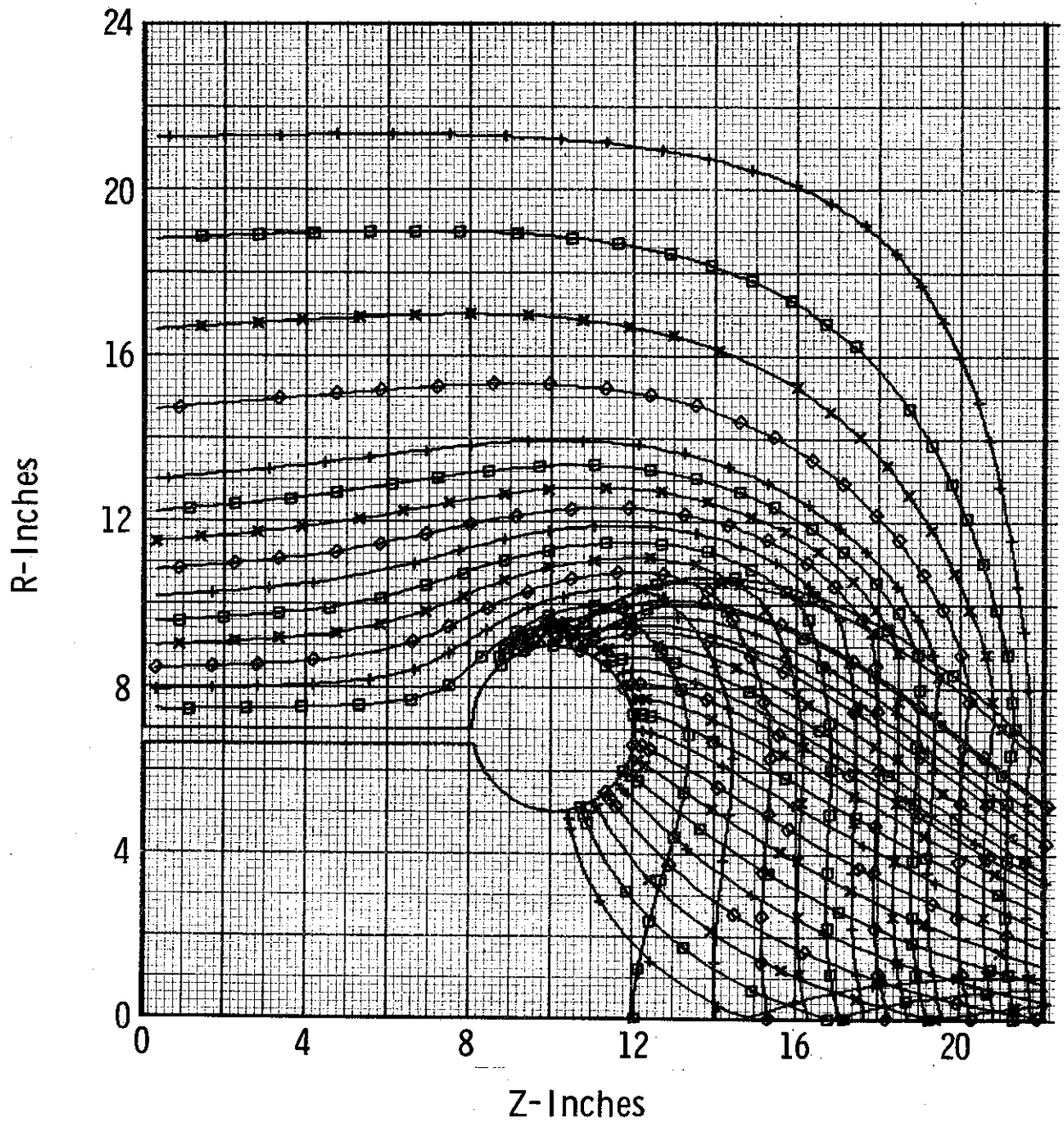

Figure 57. 15 MV Gun Calculation

be converging relatively steeply at the anode. It would thus appear that the optimum value of D_M is substantially larger than 14 inches, and probably somewhat closer to 21 inches.

A representative flow solution for a case with 21 inches for D_M, 2 inches for D_t and a 24-inch spacing is plotted in Figure 58. The upper current limit was 465 kA and the computed beam current for the iteration shown (number 4) was 447 kA. The computed beam radius at the anode was about 17 inches, and the beam was converging moderately at that plane. The solution had not converged but was space-charge limited.

Considerable effort was expended in an attempt to obtain a self-consistent solution for a 15 MV toroid with D_M = 21 inches, D_t = 2 inches, and S = 18 inches. The results of this study are presented in Figures 59 - 73.

It was not possible to obtain a completely self-consistent solution for this case as the flow was quite unstable. Since these investigations represent an entirely new realm of currents and voltages, it is as yet unclear if these instabilities are introduced through our basic assumptions or numerical procedures, or are in fact physically real.

Figures 59 - 63 show the flow pattern for iterations 5 - 9 for a typical case. By iteration 9, the beam has become very unstable so that the lower portion of the cathode is cut off due to negative electric fields, and a number of trajectories are cycloiding in the vicinity of the axis near the anode. This is somewhat surprising as the perveance (Figure 69) appears to be stabilizing within the chosen limits prior to iteration 9. The high values of the perveance obtained on the initial iterations are due to the fact that the solution is started using a Laplacian field (no space-charge). This technique was often used on the gun computations because of the difficulty in choosing a reasonable initial space-charge guess. Moreover, approaching the actual current from "above" seems to help the stability problem.

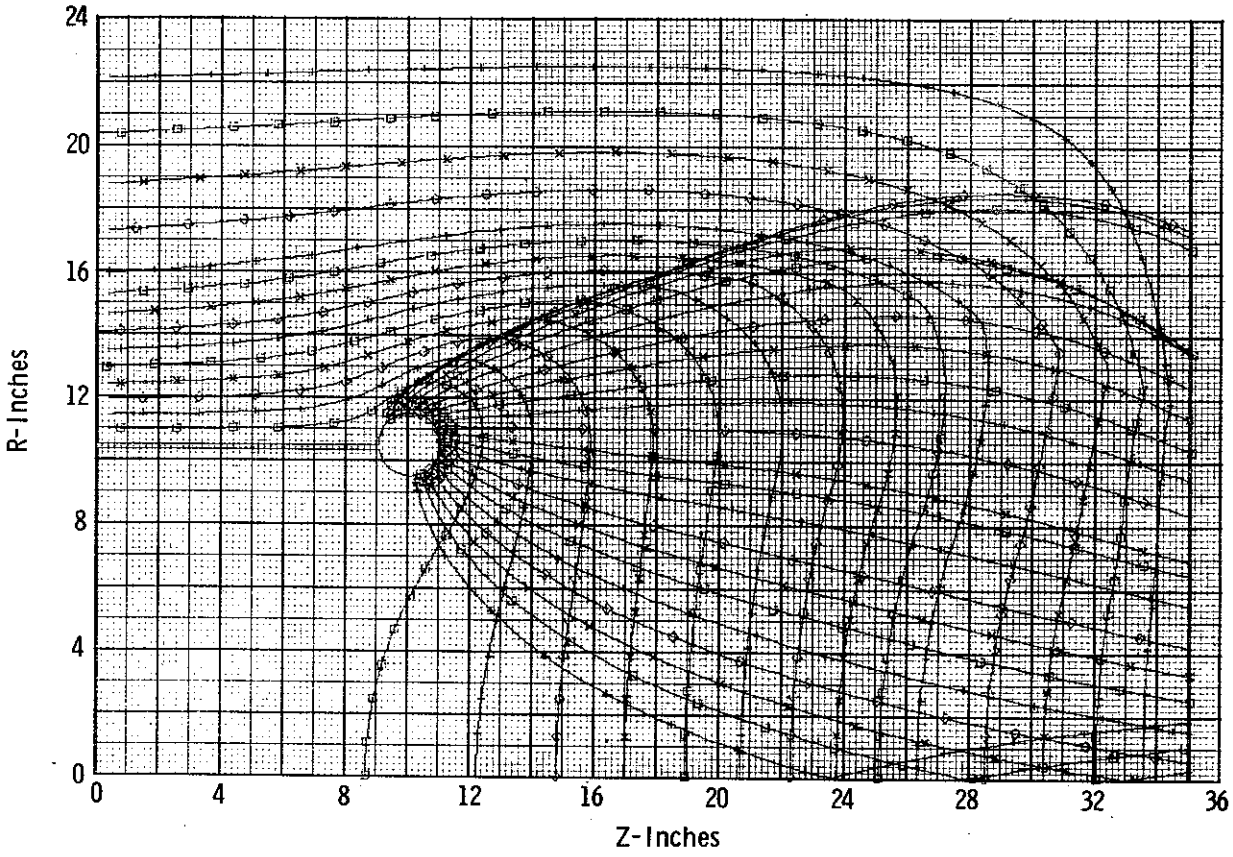

Figure 58. 15 MV Gun Calculation

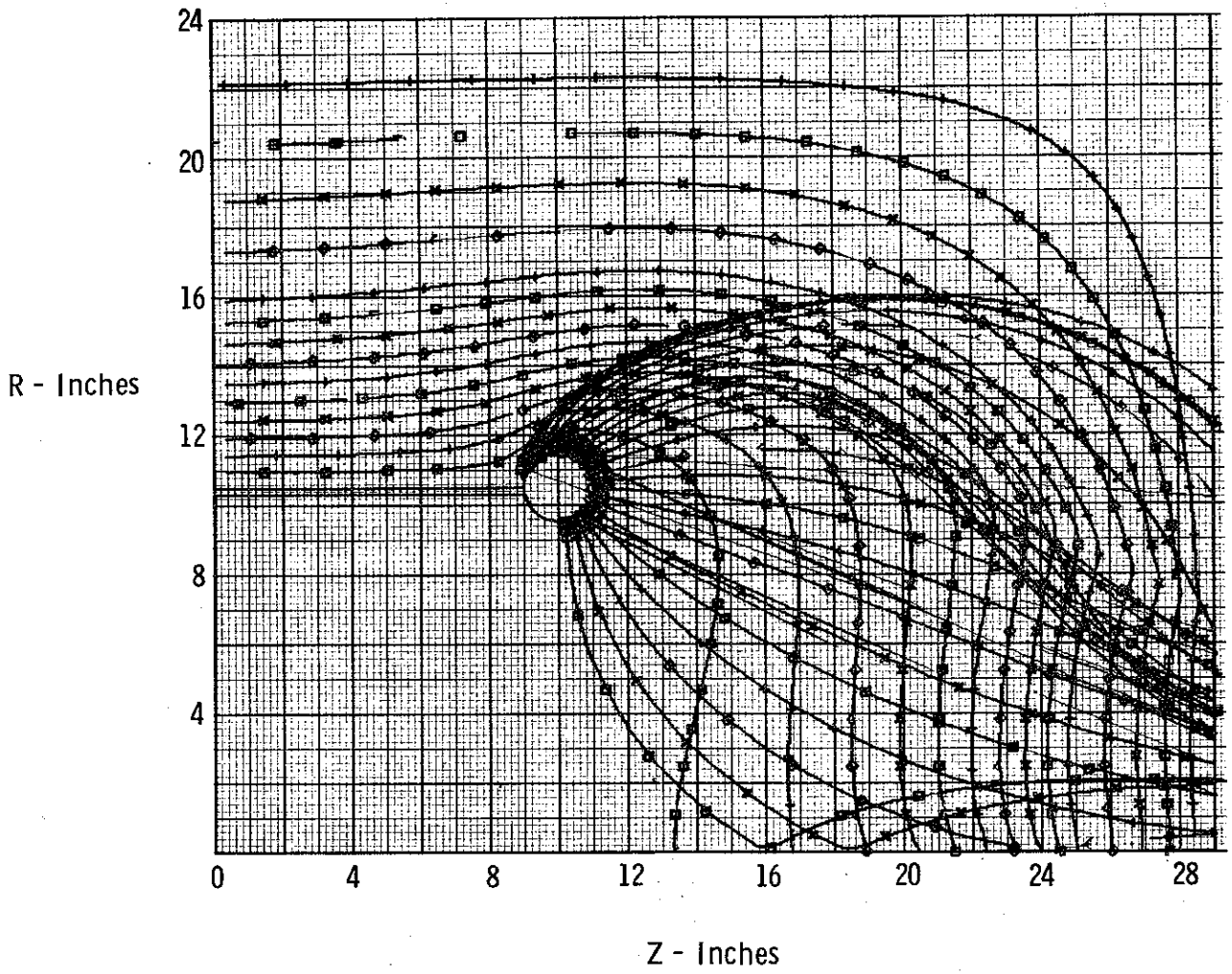

Figure 59. 15 MV Gun, Iteration 5
D_M = 21" D_T = 2" S = 18"
I = 454 kA

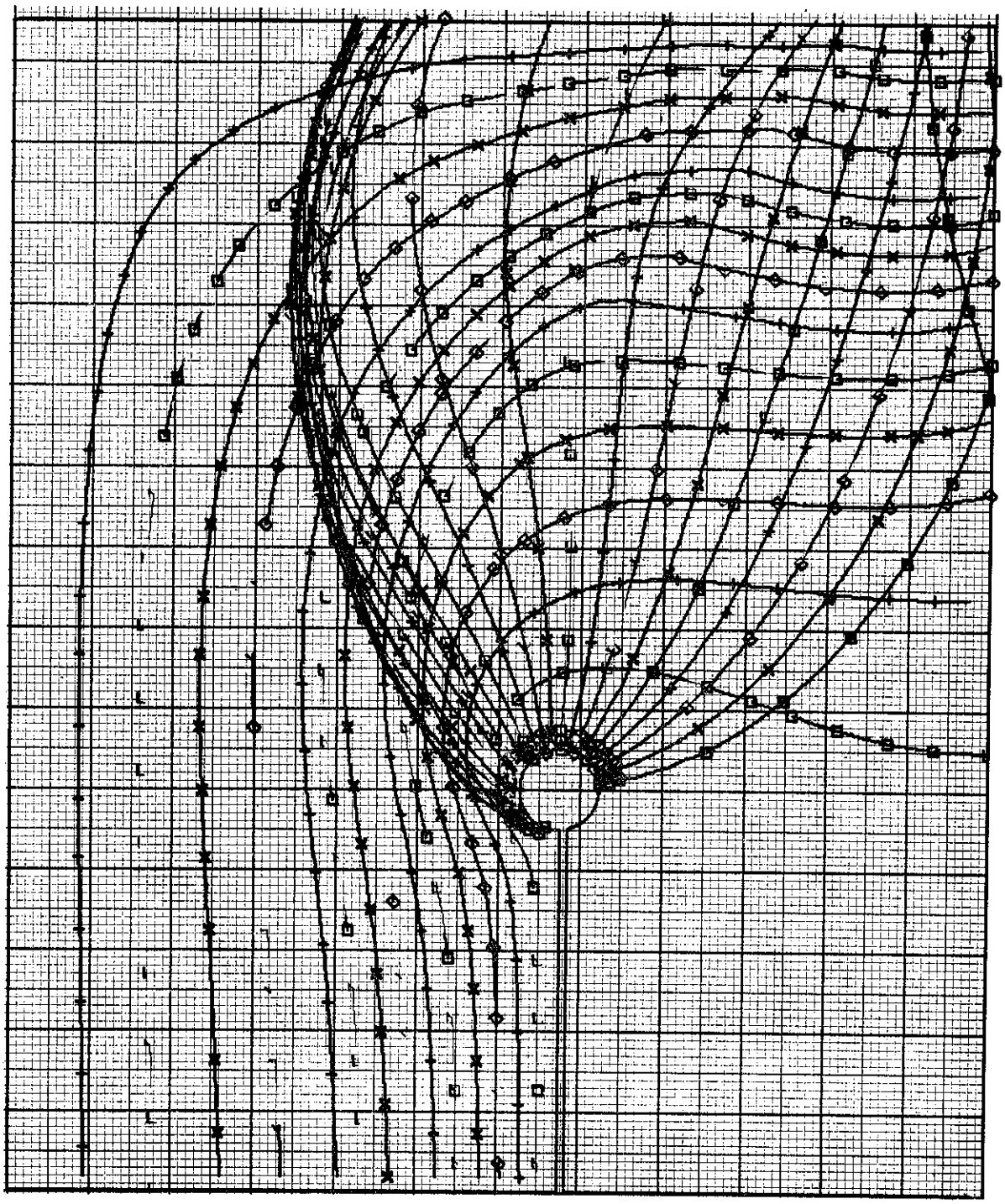

Figure 60. 15 MV Gun, Iteration 6.
D_M = 21" D_T = 2" S = 18"
I = 460 kA Scale: 1/4

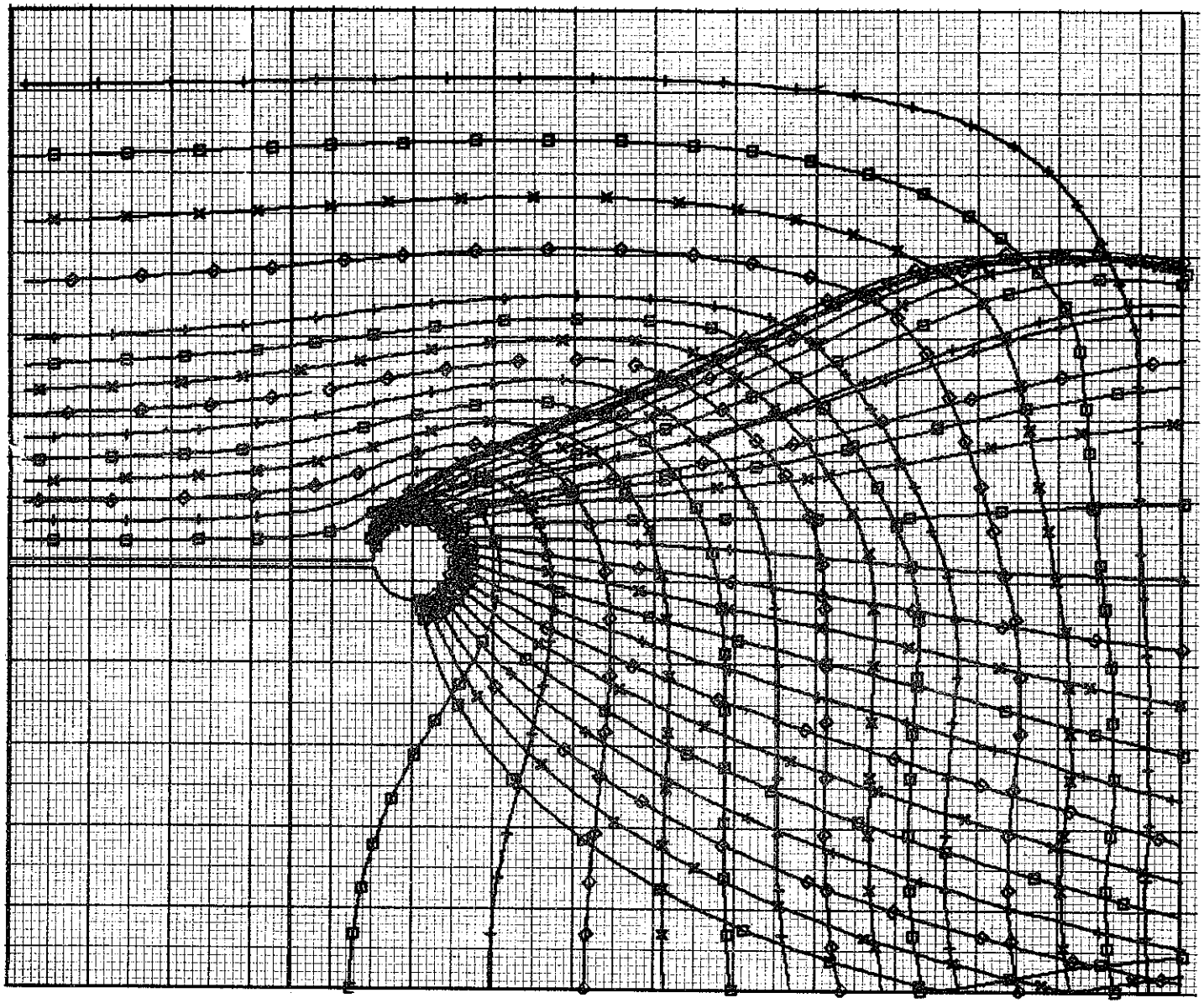

Figure 61. 15 MV Gun, Iteration 7.
I = 489 kA
D_M = 21" D_T = 2" S = 18"
Scale: 1/4

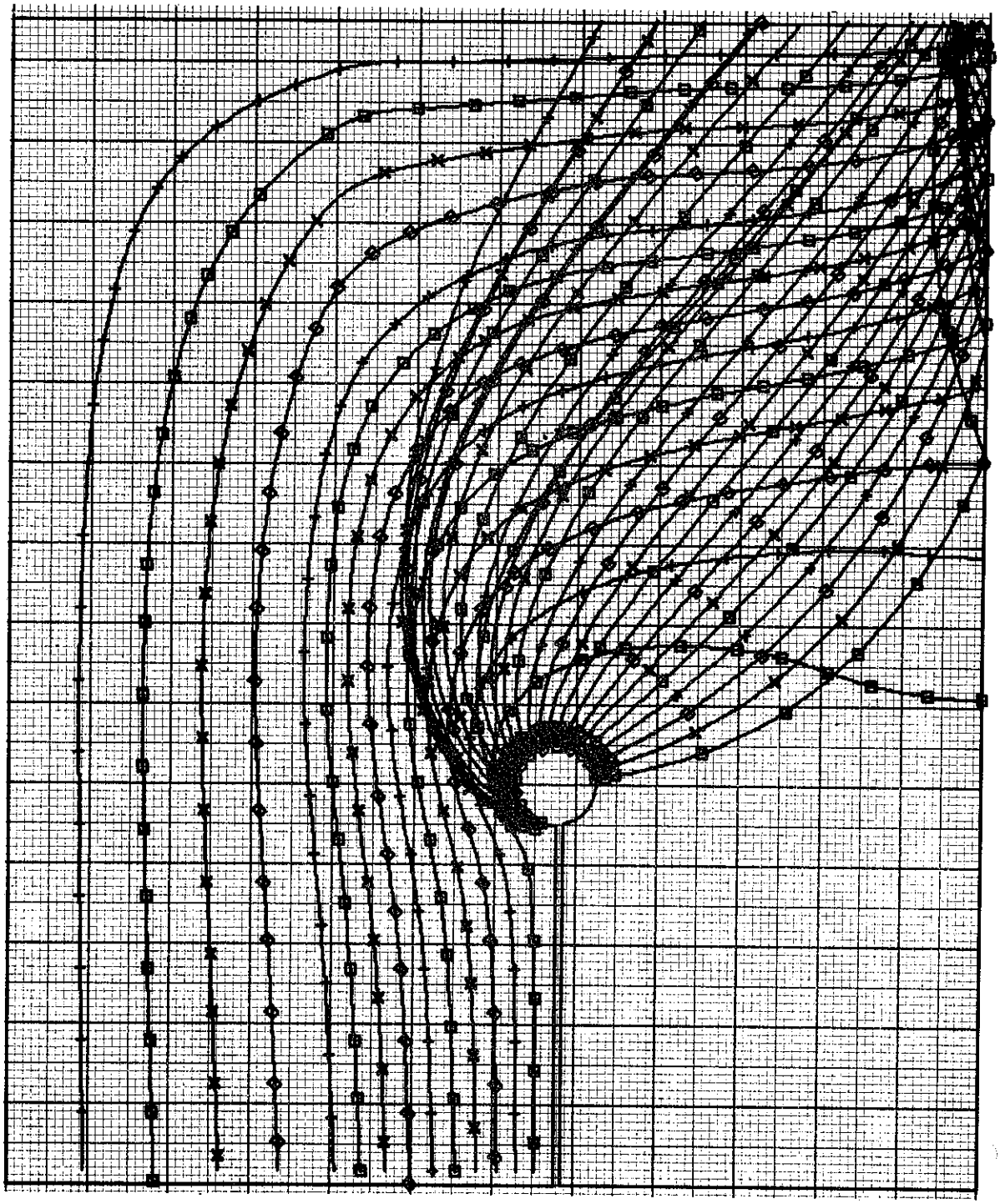

Figure 62. 15 MV Gun, Iteration 8.
I = 469 kA D_M = 21" D_T = 2" S = 18"
Scale: 1/4

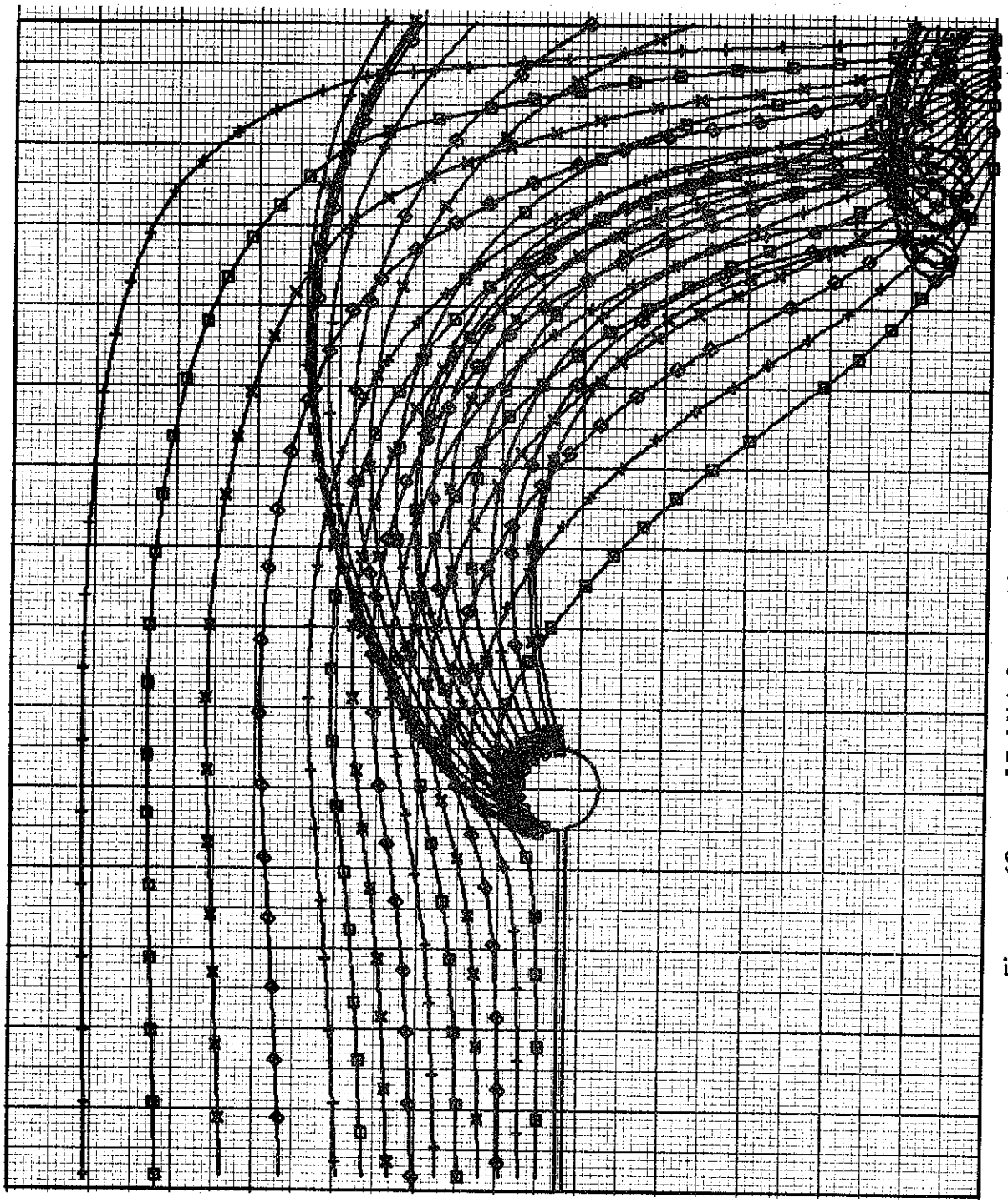

Figure 63. 15 MV Gun, Iteration 9.
I = 422 kA, D_M = 21" D_T = 2" S = 18"
Scale: 1/4

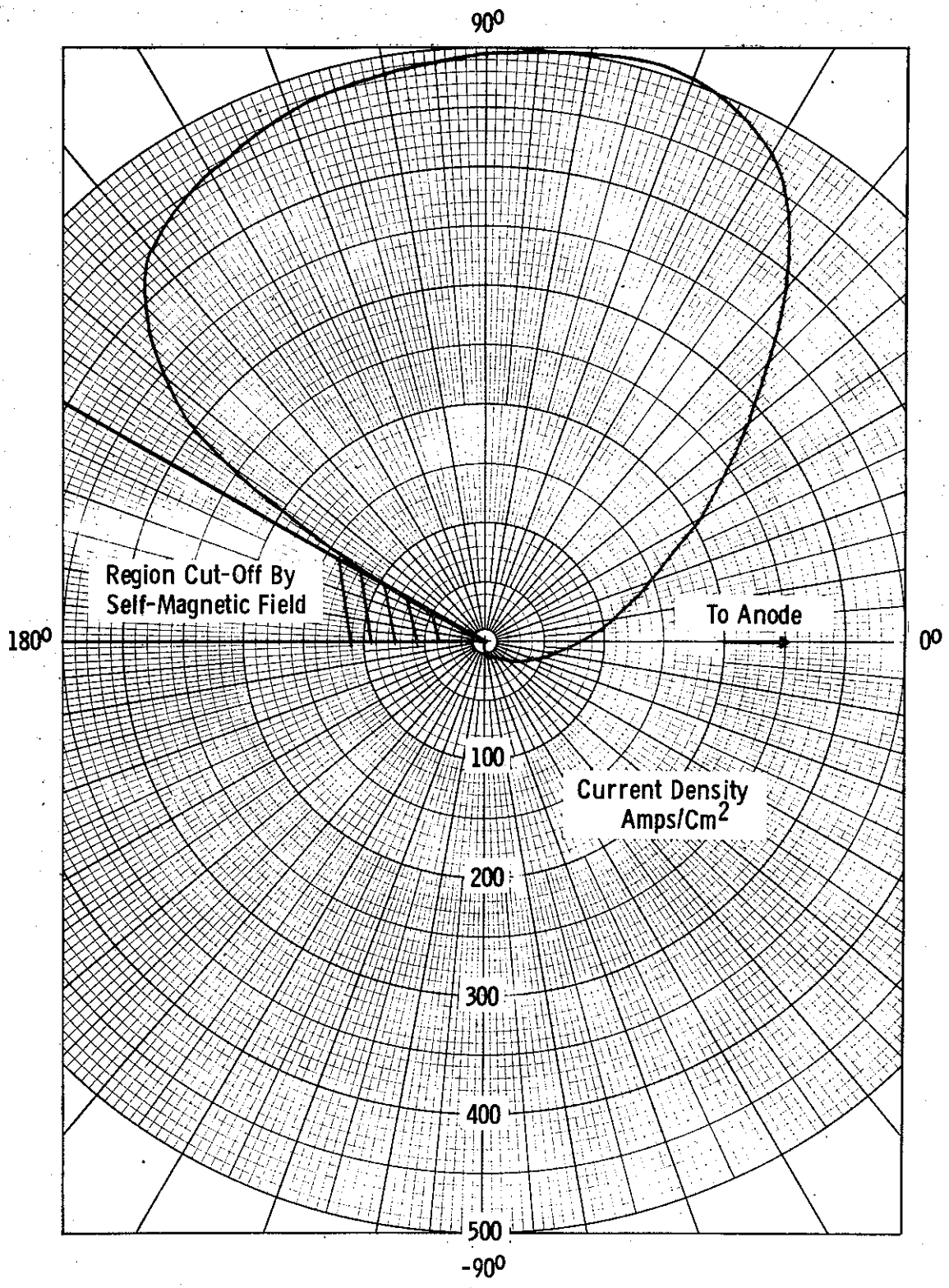

Figure 64. 15 MV, 18" Gun Polar Plot of Current Density at Cathode, Iteration No. 5

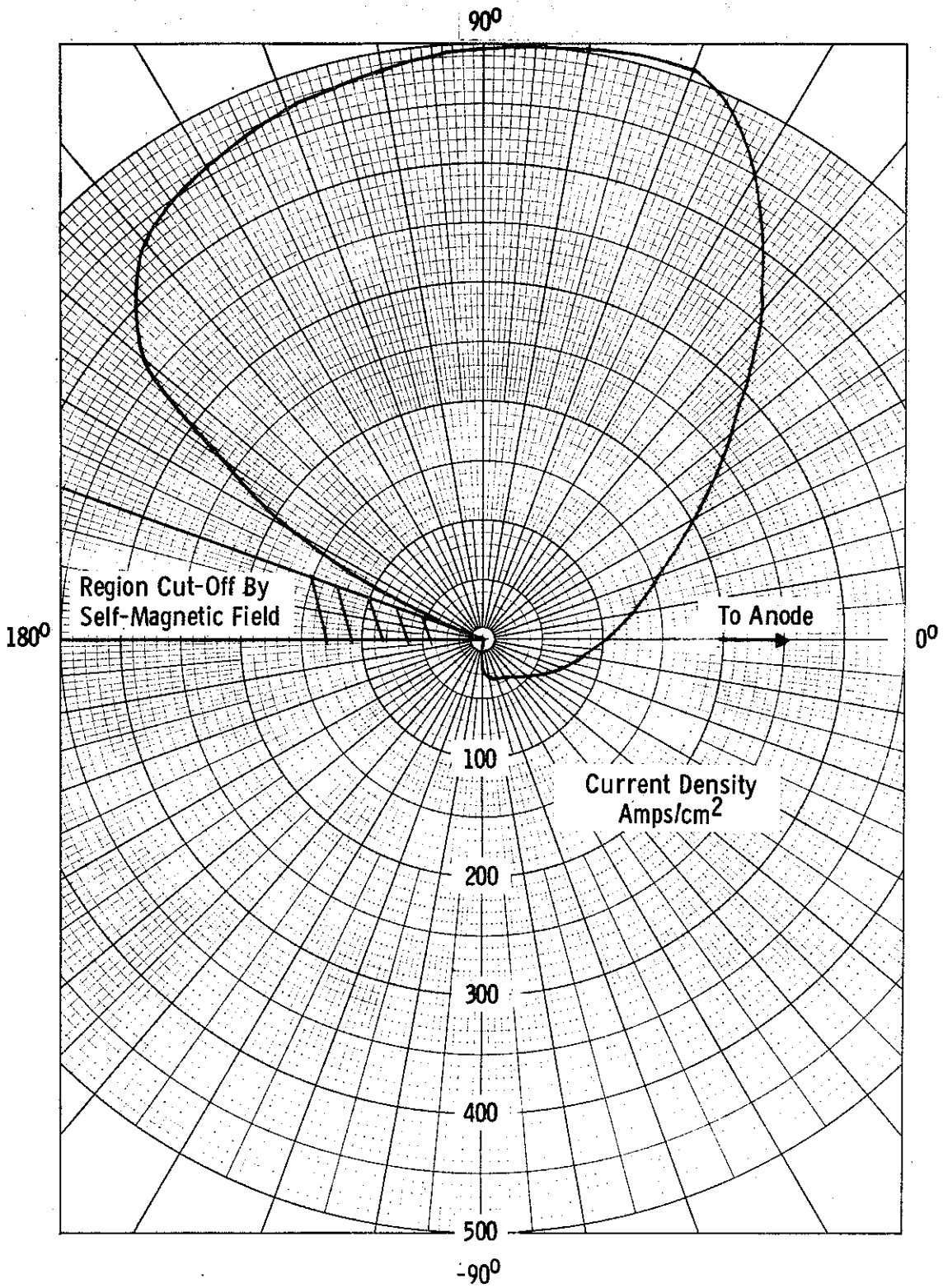

Figure 65. 15 MV, 18" Gun
Polar Plot of Current Density at Cathode.
Iteration 6

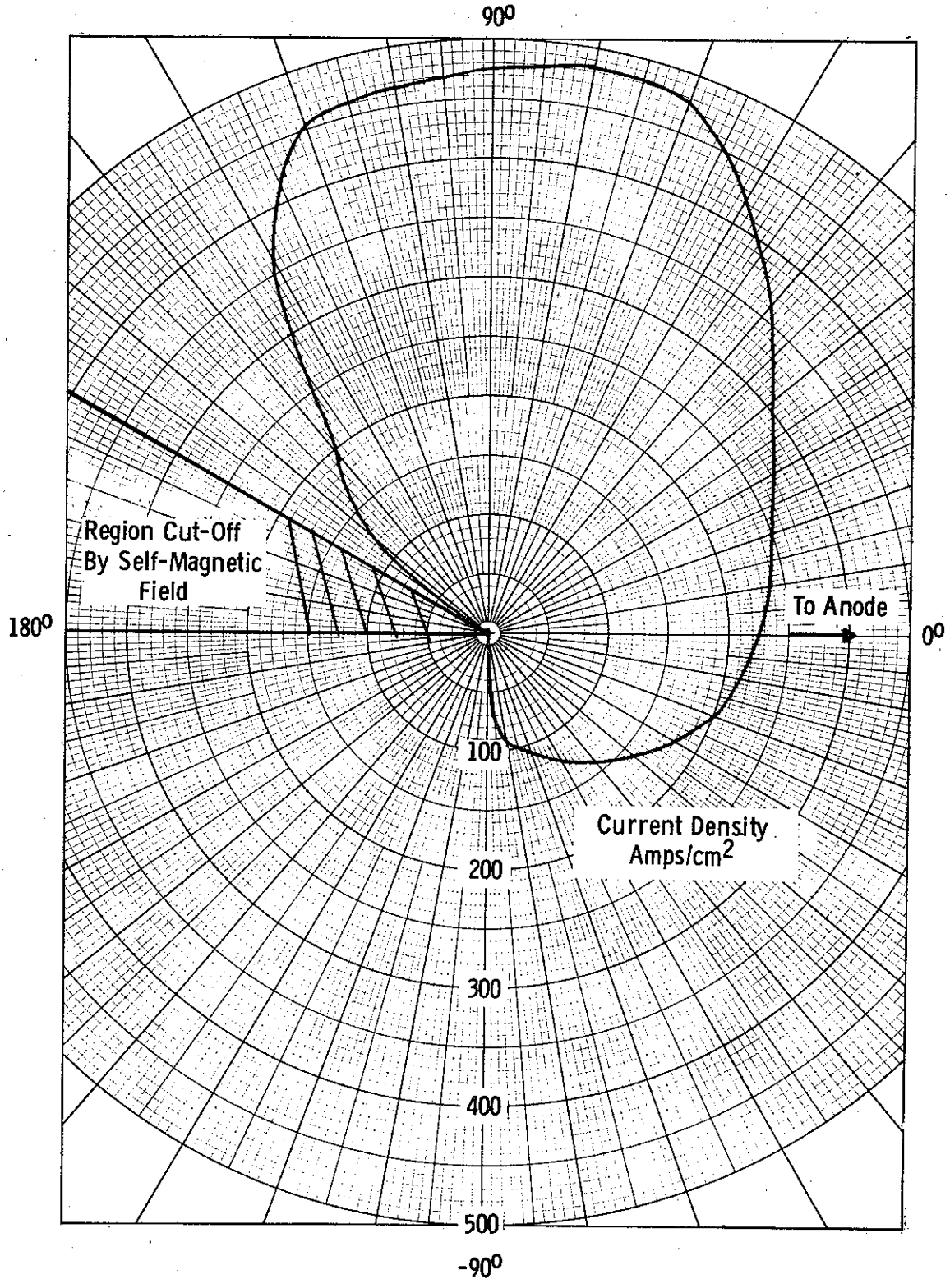

Figure 66. 15 MV, 18" Gun Polar Plot of Current Density at Cathode, Iteration No. 7

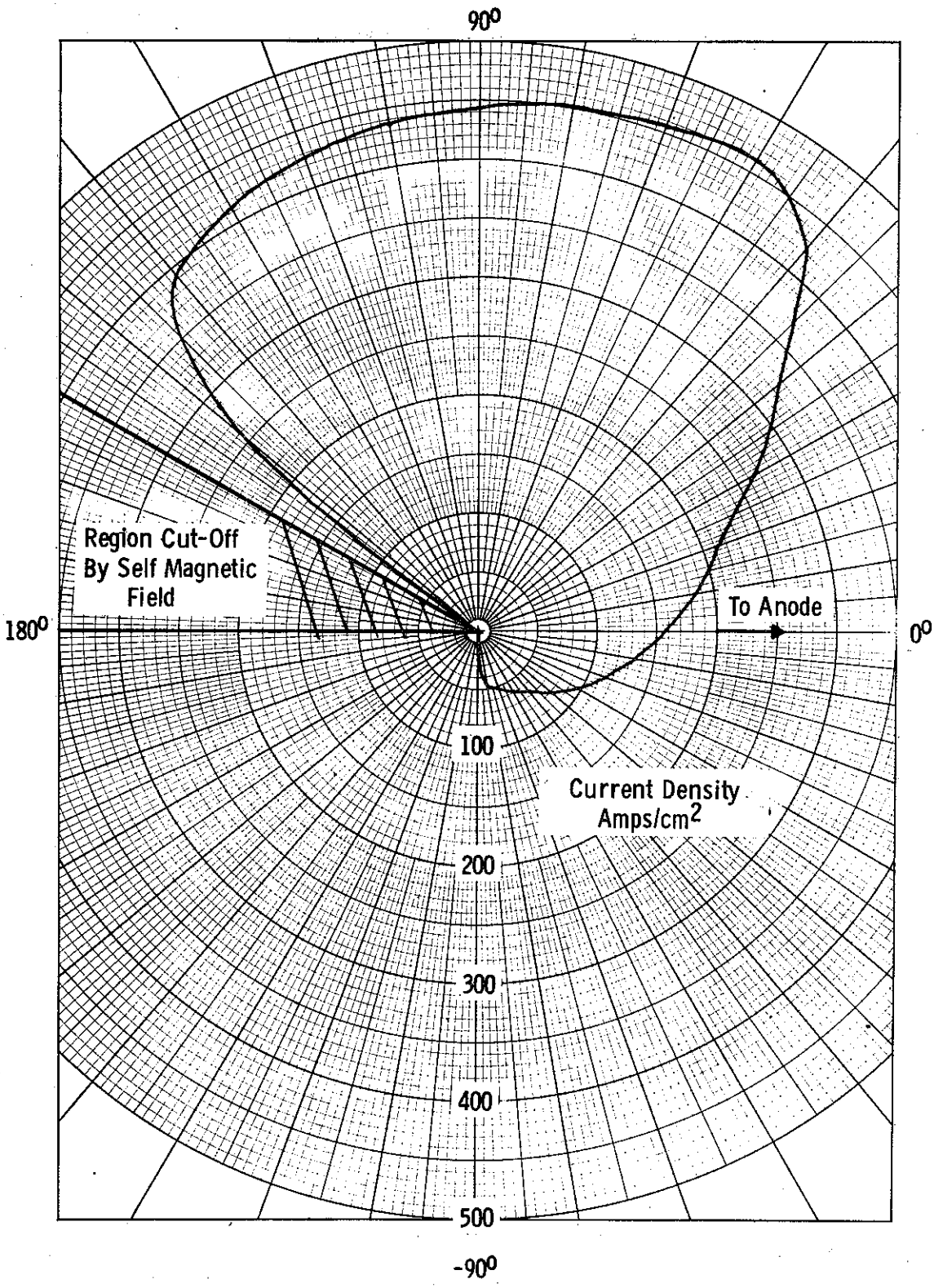

Figure 67. 15 MV, 18" Gun Polar Plot of Current Density at Cathode, Iteration No. 8

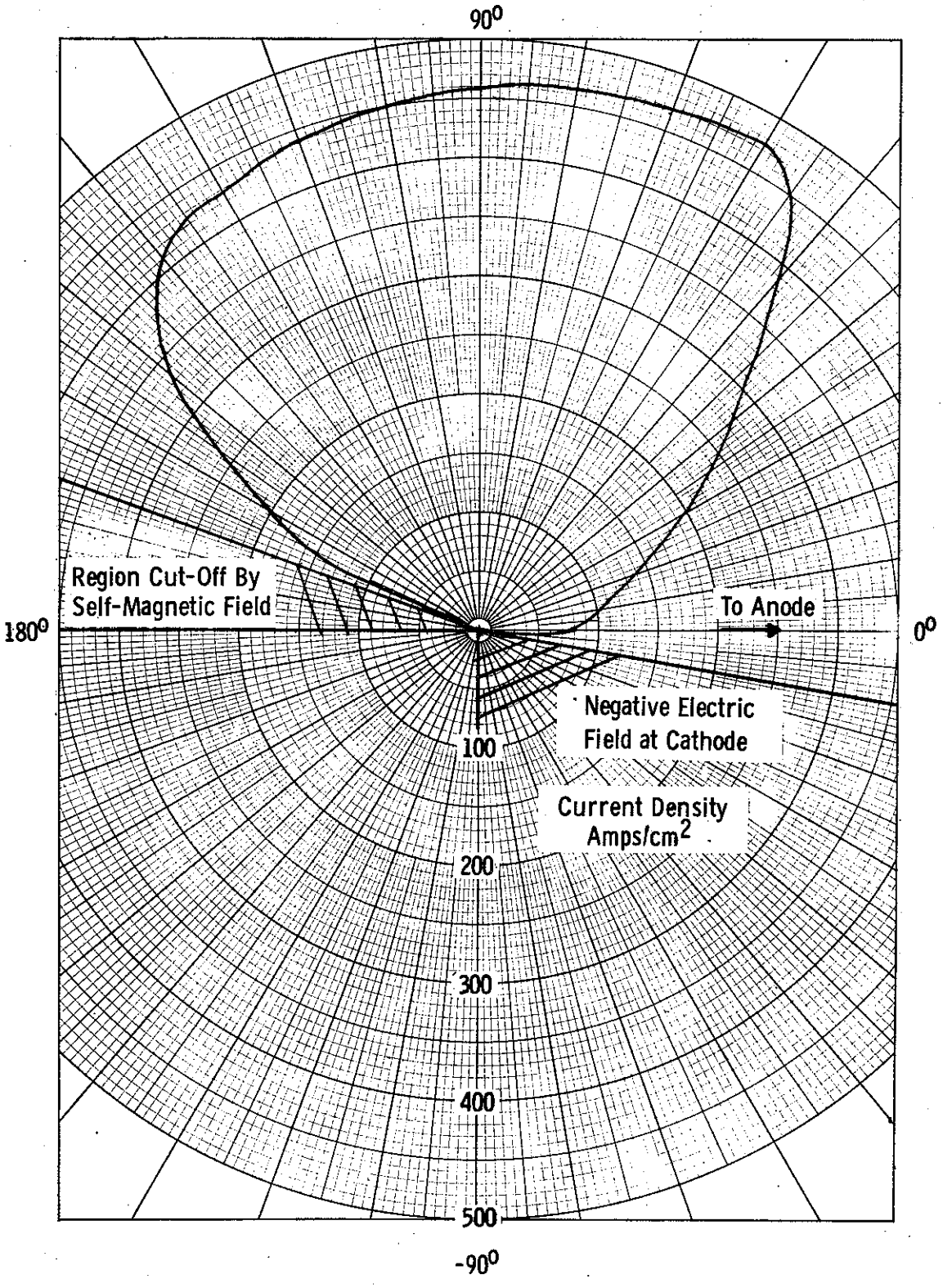

Figure 68. 15 MV, 18" Gun Polar Plot of Current Density at Cathode, Iteration No. 9

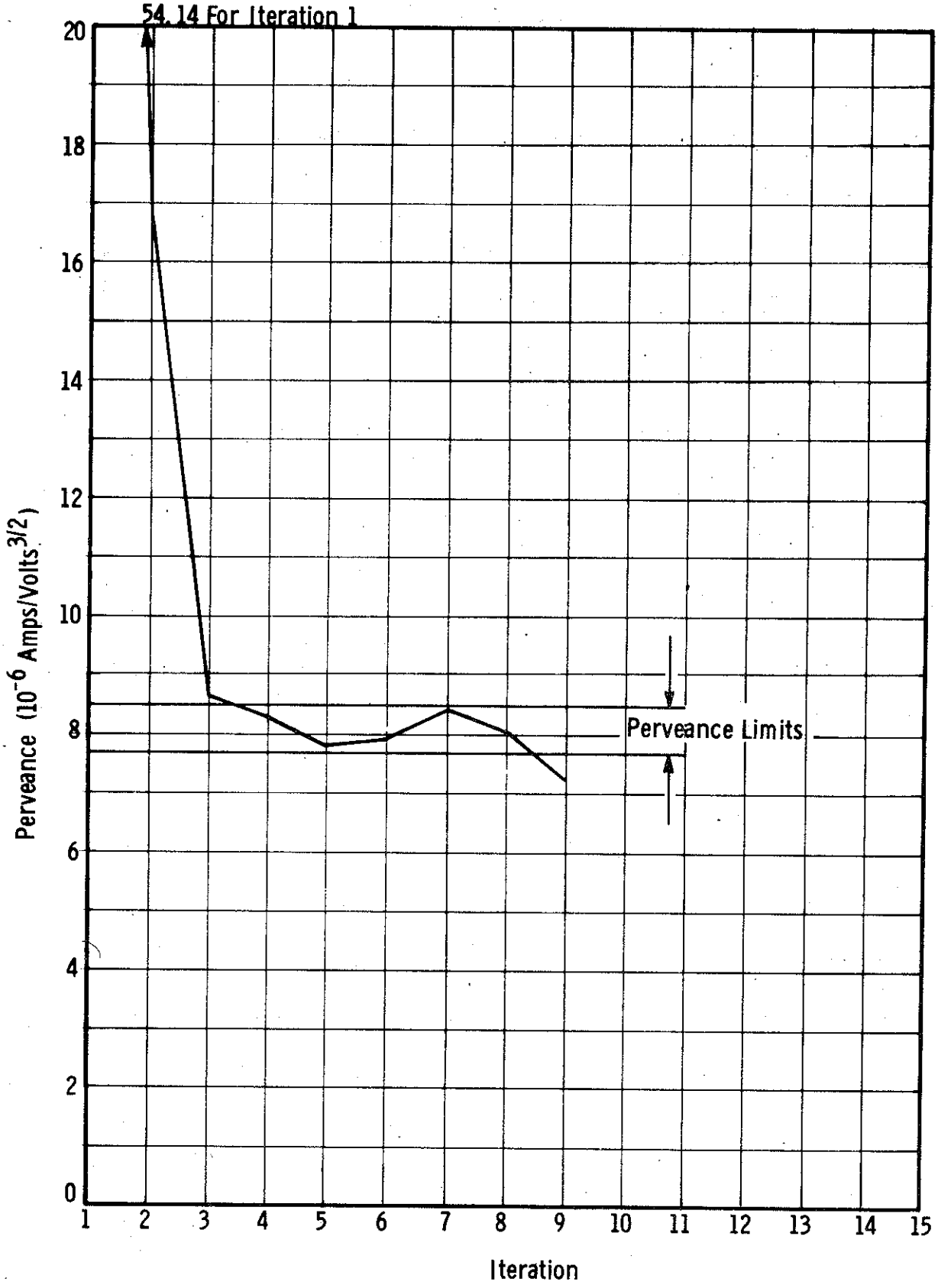

Figure 69. 15 MV, 18" Gun. Computed Perveance vs Iteration Using Perveance Limits of 8.5 and 7.8

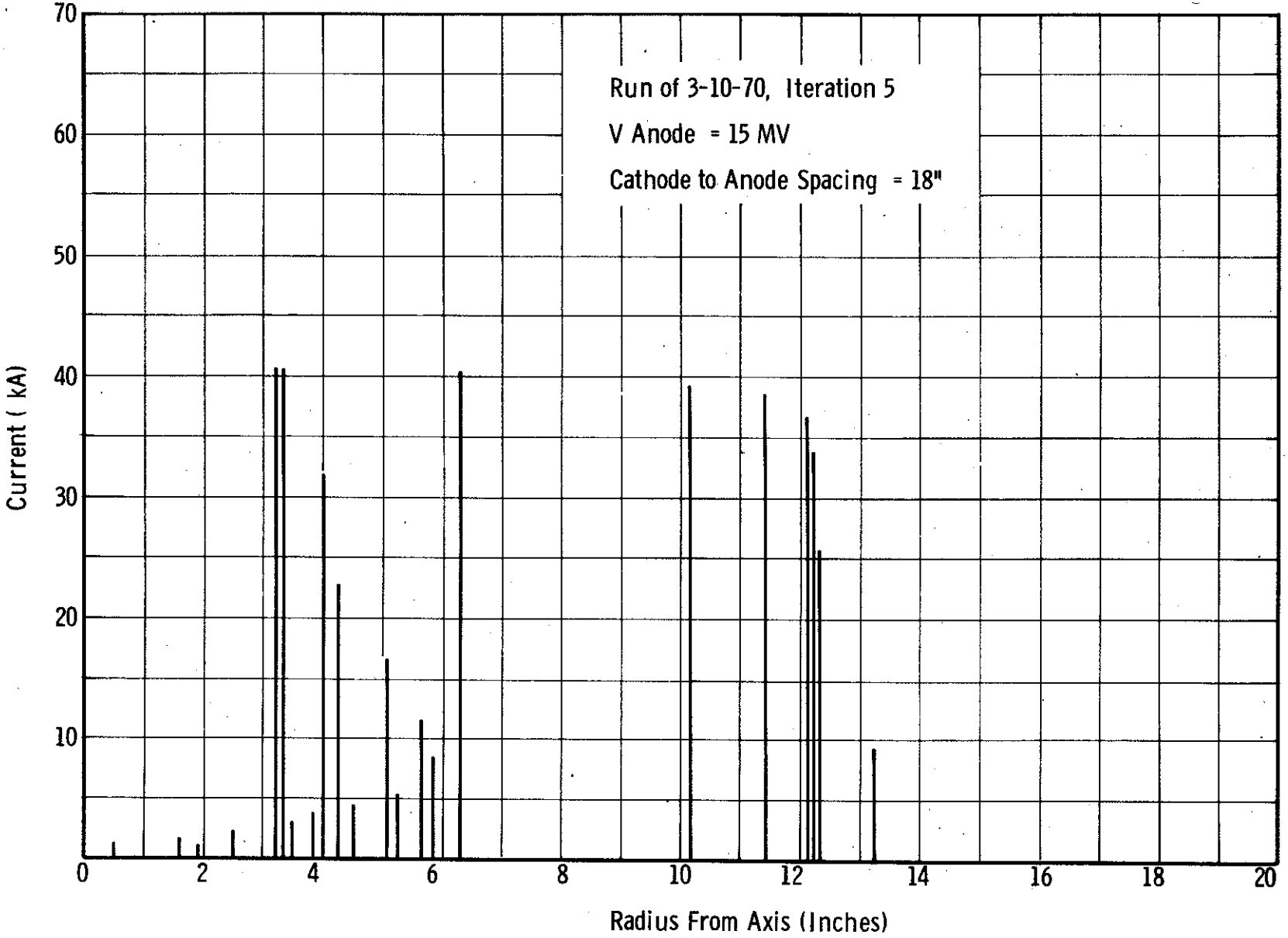

Figure 70. Physics International Toroidal Gun
Trajectory Current Contributions vs Radius at Anode

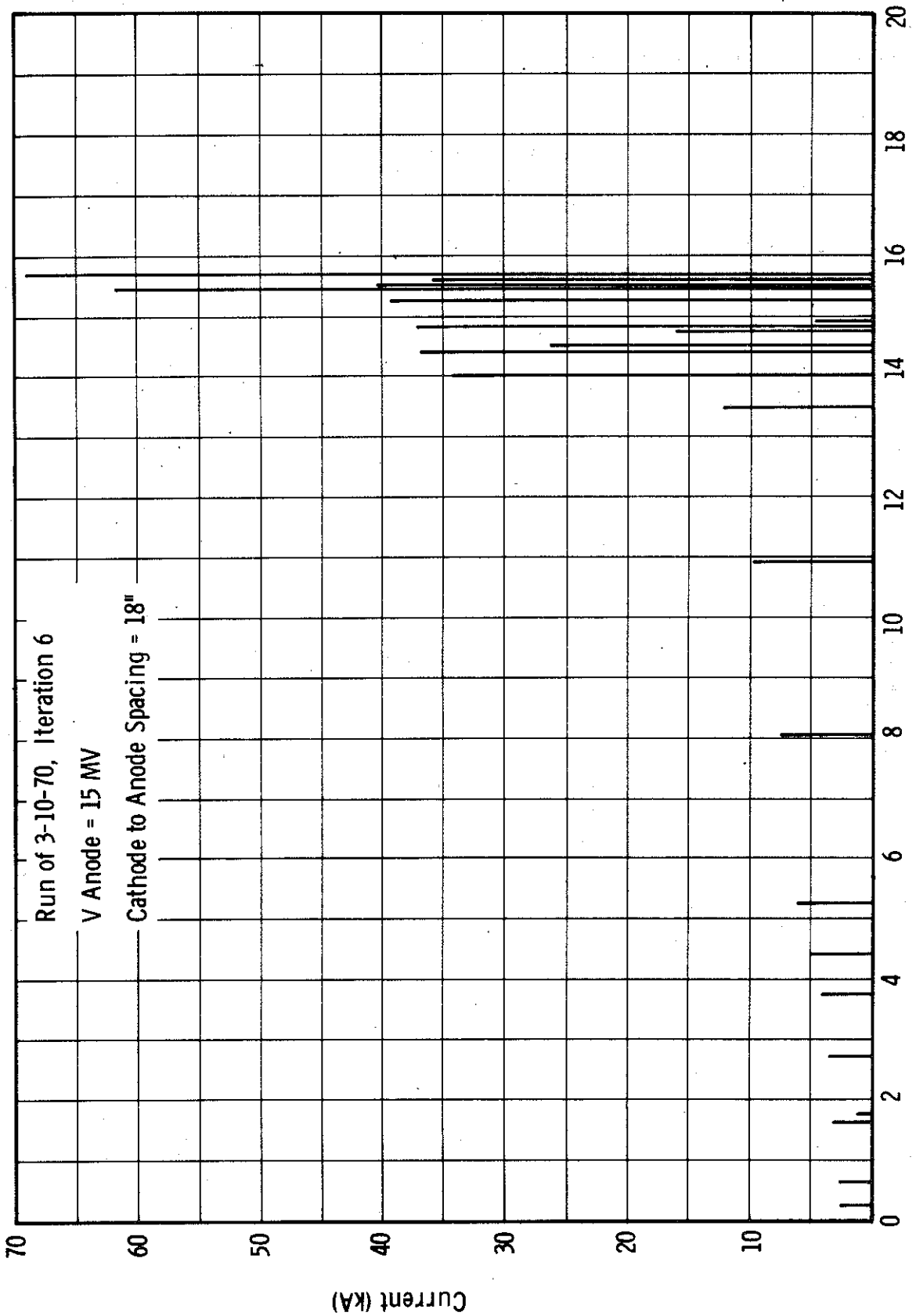

Figure 71. Physics International Toroidal Gun. Trajectory Current Contributions vs Radius At Anode.

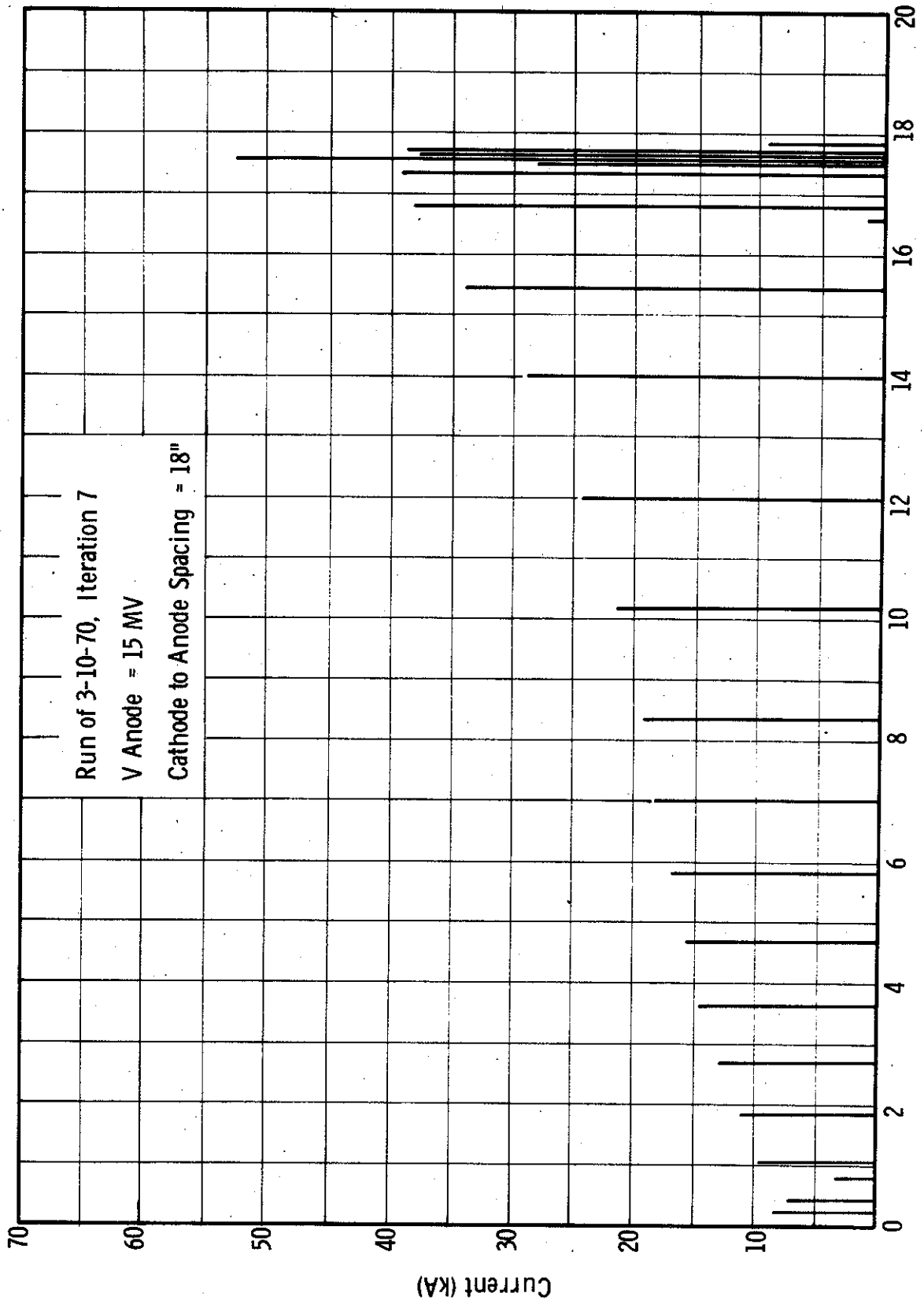

Figure 72. Physics International Toroidal Gun
Trajectory Current Contributions vs Radius at Anode

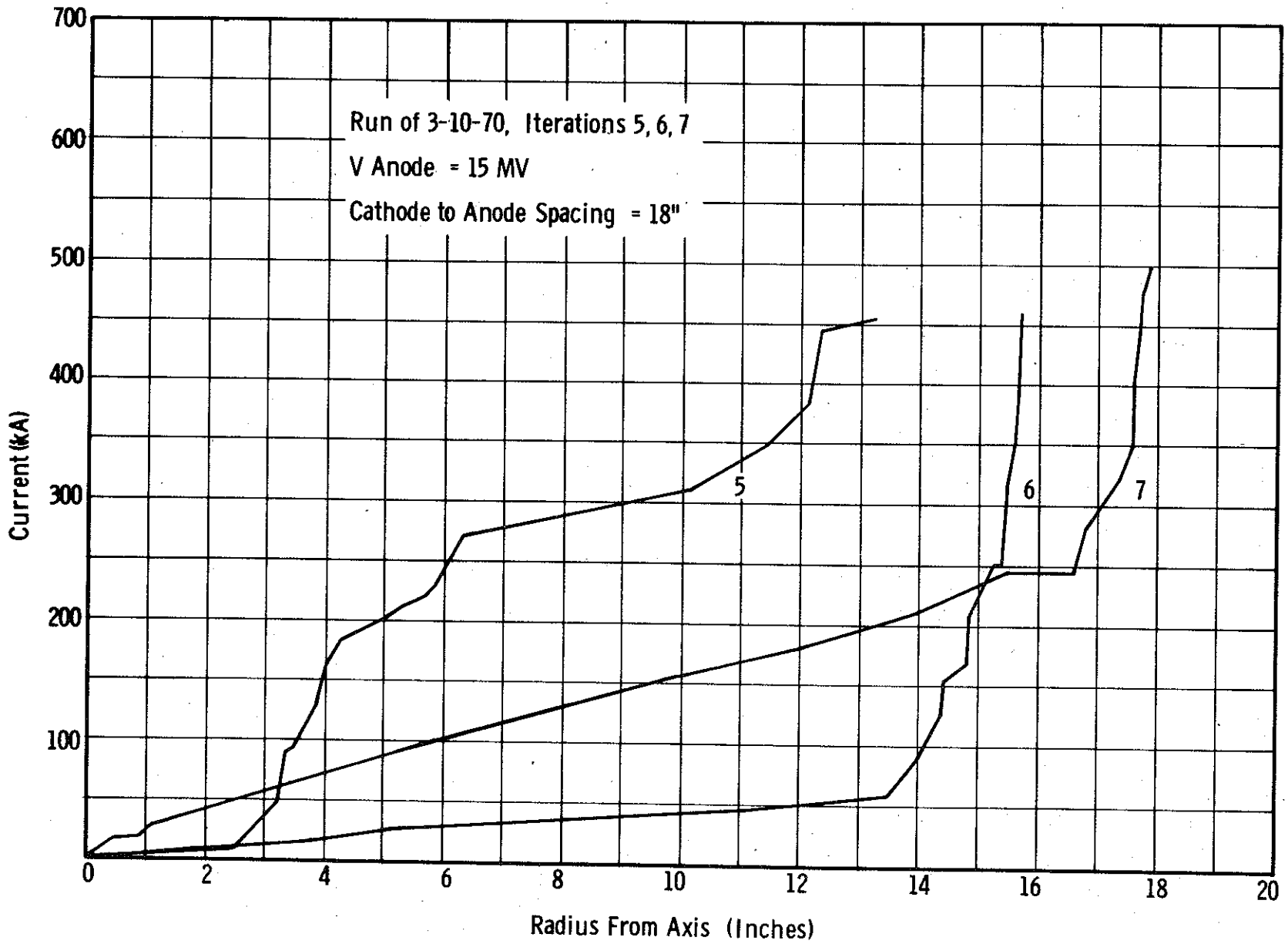

Figure 73. Physics International Toroidal Gun
Current Enclosed vs Radius at Anode

In Figures 64-68, polar plots of the current density at the cathode are given for iterations 5-9. The maximum current density occurs between 60° and 90° and is relatively stable. The bottom region of the cathode, however, is very unstable, the current density initially growing, then diminishing, and finally being entirely cut off. The trajectory current contributions at the anode for iterations 5-7 are given in Figures 70-72 and the sum of these contributions is given in Figure 73. This is a further graphic display of the unstable nature of the solution. Indeed, even though a 50% space-charge averaging is used, the major part of the beam essentially avoids that region through which it passed on the previous iteration.

Because of the instability present in the computer solutions, several different approaches were used in an attempt to achieve self-consistency.

The sensitivity of the solution to both changes in the mesh size and in the boundary potentials along $Z = 0$ was tested. In both cases, the solutions were essentially unchanged.

Another interesting experiment involved the use of "minor iterations" on the self-magnetic field. Since the self-field forces appear to be dominant at these current levels, it was decided to make several trajectory iterations while holding the electric fields and current emission fixed, and allowing only the self-magnetic field to change. This produced an extremely unstable situation. After one or two iterations, the beam would either collapse to the axis or become hollow out to a large radius, depending upon the starting conditions. The dependence on starting conditions is illustrated by the following arguments: Suppose that the total current I_t is held fixed at a value larger than that required for stable flow. The self-magnetic field $B_\theta \sim I_t/r$ will then collapse the beam to the axis. On the other hand, if I_t is held at a value smaller than that required for stable flow, the self-magnetic field will diminish itself and the beam will move away from the axis.

Finally, a calculation was made in which the self-magnetic field B_θ was replaced by αB_θ, and α was gradually increased from 0.65 to 1.0 after a number of iterations. It was hoped that by "turning on" B_θ gradually, and approaching the correct beam size from above, the instability could be avoided. The full self-field was reached on iteration 7 and by iteration 9 the solution had much the same appearance as Figure 63. There was insufficient opportunity, however, to fully explore this approach and it may yet prove to be of value.

IV. REMOVAL OF ENERGY STORED IN A CAVITY RESONATOR BY INJECTION OF AN ELECTRON BEAM

A. ANALYSIS

1. General Description

This section will be concerned with cavity resonators formed by metallic conducting walls which essentially completely enclose a vacuum region containing stored energy. The energy is in the form of time varying electric and magnetic fields. The transfer from completely electric to completely magnetic energy occurs twice during each period of the resonant frequency. To the extent that the cavity is an efficient system for storing energy, the total stored energy can be gradually built up over a relatively long time from a low power source. If, then, an electron or other charged particle beam is suddenly injected into the cavity, the energy can be transferred to the electron beam to produce a relatively short high power beam pulse. In this manner a power gain has been achieved with a corresponding reduction in pulse length.

Considerable insight into the operation of such a system can be obtained by considering the equivalent circuit model shown in Figure 74. The figure indicates a two-wire transmission line of characteristic impedance Z_o, having a length $L = 3\lambda/2$, with a short circuit termination at each end. It is assumed that the section of line is lightly coupled to an rf source of wavelength λ. If the line has very low loss, the voltage can be described by the equation[5]

$$V = V_1 \cos(\omega t - \beta z) + V_1 \cos(\omega t + \beta z) \tag{69}$$

where the first term represents a wave traveling in a positive z direction and the second term a wave traveling in the negative z direction; β is the propagation constant defined by $\beta = \omega/c$. In the steady state situation, any power loss in the line is compensated

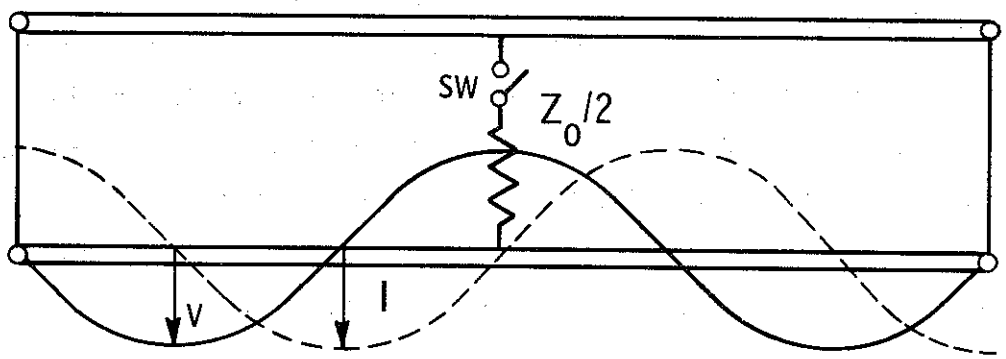

Figure 74. Equivalent Circuit Model for Beam and Cavity Resonator

by a small amount of power flowing from the source, and the line voltage amplitude remains constant with time. The switch and the resistor in the figure simulate the loading effect of an injected electron beam. If at some instant of time the switch is closed, then the resistor of magnitude $Z_o/2$ is connected across the two-wire line midway between the ends. A resistor of that value matches both halves of the line, i.e., waves traveling toward the midway point are completely absorbed in the resistor. The voltage developed across the resistor will be sinusoidal with time for a time interval of $\tau = \beta L$ and then will abruptly drop to a value near zero depending on the weak coupling to the rf source. The phase and amplitude of the resistor voltage will be the same as the voltage at the midpoint of the line prior to the switch closure. The total time duration of the resistor voltage is the propagation time for a wave to travel from the midpoint to one end and back to the midpoint.

For the case shown in the figure, the total time duration of the resistor voltage is 1.5 rf cycles. If the line length had been chosen at $1/2\lambda$ instead of $3/2\lambda$, the total pulse time for the resistor voltage would be 0.5 rf cycle.

In a practical embodiment of such a system, the two-wire transmission line would probably be replaced by a waveguide or a radial transmission line. Such lines have dispersive properties which will change the behavior of the system. A particle beam behaves like a resistor only to a limited extent. Such effects as space-charge, beam cross sectional area, and particle transit time through the resonator structure will need to be considered in predicting the performance of practical systems. Since it is proposed that a vacuum be used as the energy storage medium, field emission and multipactor effects must also be considered.

2. TM_{010} Cylindrical Cavity

The TM_{010} cylindrical cavity has a number of properties which are ideal for an energy storage system to be discharged by an electron beam. The fields in the cavity are given by[5]

$$E_z = E_m J_o (kr) \cos (\omega t) \tag{70}$$

$$H_\phi = j \sqrt{\epsilon/\mu}\ E_m J_1 (kr) \cos (\omega t) \tag{71}$$

where J_o and J_1 are Bessel functions, E_m is the electric field amplitude, and k is the wave vector defined by

$$k = 2\pi / \lambda \tag{72}$$

The cavity resonant frequency depends only on the diameter according to the relation

$$kD = 2\, p_{o_1} \tag{73}$$

Where D is the diameter and p_{o_1} is the first root of J_o.

Since the electric field is axial and has maximum amplitude on the axis, the cavity is well suited for injection of an axial election beam at one end of the cavity. The length of the cavity can be selected to satisfy transit time requirements or output kinetic energy requirements since the length does not affect the resonant frequency.

The TM_{010} cavity can be considered as a section of radial transmission line shorted at the outer edge. When the beam is injected on the axis, it will form an essentially resistive termination for the radial line. To avoid reflection from the resistive termination, the beam impedance would normally be chosen to match the line impedance. Certain difficulties arise in attempting to do this.

Voltage, current, and impedance for the radial line are defined in the following manner:

$$V_z = E_z L \tag{74}$$

$$I_r = 2\pi\, r H_\phi \tag{75}$$

$$Z_o = V_z / I_r = E_z L / 2\pi\, r H_\phi \tag{76}$$

For the radial line, the characteristic impedance defined above is not constant, as in a conventional transmission line, but rather varies in the following manner[5] :

$$Z_o \frac{\lambda}{L} = \sqrt{\frac{\mu}{\epsilon}} \quad \frac{1}{kr} \sqrt{\frac{J_o^2 (kr) + N_o^2 (kr)}{J_o^2 (kr) + N_1^2 (kr)}} \tag{77}$$

The impedance given by this equation is plotted in Figure 75. Transit time effects require that the cavity length be typically less than a quarter wavelength ($L \leq \lambda/4$). When $L = 0.1\lambda$, the radial line impedance varies from 16.5 Ω at the outer wall ($kr = 2.405$) to infinity at the axis. It is obvious that an infinite resistance at the axis will not remove any energy from the cavity. Furthermore, it does not appear possible to determine the proper beam impedance by matching arguments alone.

To determine the proper beam impedance, we will equate the output electron beam energy to the cavity stored energy. We will assume that the beam voltage is a sinusoid with a time duration of one half rf cycle and a peak amplitude equal to the cavity voltage on the axis reduced by a transit time factor M. If it is assumed that the beam has constant resistance, then the current is also a half sinusoid. The total energy in the output beam pulse is

$$\begin{aligned} U_b &= \int V_b I_b \, dt \qquad (78) \\ &= \frac{1}{\omega} \int_0^{\pi} V_m I_m \sin^2 (\omega t) \, d(\omega t) \\ &= \frac{1}{4f} V_m I_m \end{aligned}$$

where $$V_m = M E_m L \tag{79}$$

The stored energy in the cavity is

$$U_c = \frac{1}{2} \epsilon \int_v E_z^2 \, dv \tag{80}$$

where V indicates an integral over the entire cavity volume. Then we have

$$U_c = \pi \epsilon \int_0^{D/2} E_m^2 \, J_o^2 (kr) \, r dr \tag{81}$$

$$= \frac{1}{8} \pi \epsilon E_m^2 D^2 L J_1^2 (P_{o_1})$$

Equating the beam energy to the cavity energy we get

$$\frac{V_m}{I_m} \frac{1}{M^2} \frac{\lambda}{L} = \sqrt{\frac{\mu}{\epsilon}} \frac{2\pi}{P_{o_1}^2 J_1^2 (P_{o_1})} \tag{82}$$

The quantity $V_m/I_m M^2$ is the equivalent loading impedance of the beam presented to the cavity including the transit time reduction factor, M. The Bessel function root has the value of $P_{o_1} = 2.405$. The right hand side has a value of 1520 ohms. A comparison of the beam impedance given above and the radial line impedance given in Figure 75 indicates that impedance matching is achieved by making the beam diameter such that $kr \approx 0.04$. The effect of space-charge in the beam has not been considered in this choice of beam diameter. Space-charge will be considered in a later section.

The amount of rf power required to maintain the cavity stored energy prior to injection of the beam is related to the Q of the cavity by the following equation

$$P = \frac{\omega U_c}{Q} \tag{83}$$

where P is the steady state input power to maintain the stored energy U_c. For the TM_{010} cavity the Q is given by[5]

$$Q = \frac{\lambda P_{o_1}}{\delta \pi (2 + D/L)} \tag{84}$$

where δ is the skin depth, given by

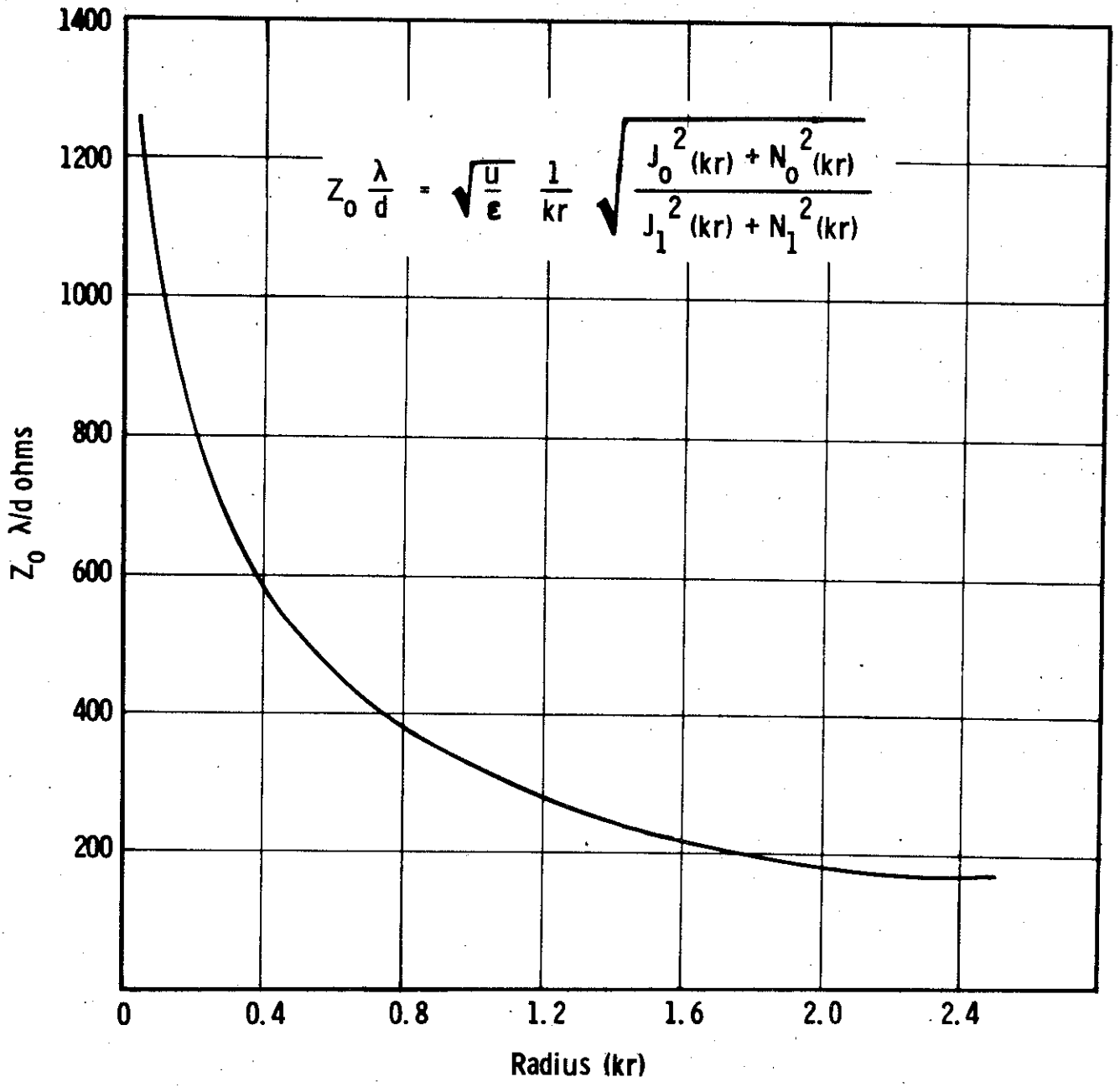

Figure 75. Characteristic Impedance of a Radial Transmission Line

$$\delta = \frac{1}{\sqrt{\pi f \mu \sigma}} \tag{85}$$

and σ is the conductivity of the cavity walls.

The total energy which must be supplied by an rf source to fill the cavity will always be greater than the amount of stored energy just prior to the beam pulse because of losses during the fill time. Storage efficiency will be defined as the ratio of the available cavity energy to the total energy supplied by the source. This storage efficiency will depend on the degree to which the cavity stored energy is allowed to reach its steady state value. If we define a fill time as

$$t_f = \frac{2Q}{\omega} \tag{86}$$

then for $t = 0.4\ t_f$ the storage efficiency is 60%[6], and for $t = t_f$ the efficiency is 41%.

3. Electric Field Limitations

In determining the maximum electric field that can be sustained between metal electrodes in a vacuum environment, two effects must be considered. These are field emission[7] and multipactor[8]. The current density of field emitted electrons increases very rapidly for local electric field strengths greater than 10^9 V/m. In general, the local electric field at a surface, on a microscopic scale, is much greater than the applied field calculated on a macroscopic basis. The ratio of local to applied field, called the field enhancement factor, has a value of the order of 100 for most surfaces. Therefore, the applied field must be kept near 10^7 V/m or less to completely avoid field emission. By careful processing of the surface, it is possible to operate at fields of 5×10^7 to 10^8 V/m[7,9].

The energy storage density for electric field storage is given by

$$U_v = \frac{1}{2} \epsilon E^2 \tag{87}$$

For a field strength of 10^7 V/m which results in negligible field emission problems, the energy storage density is 443 joules/m^3. For a field of 10^8 V/m, which is probably a practical upper limit when there are fields normal to a surface, the storage density is 44,300 joules/m^3. When energy is stored in an rf cavity resonator, the above storage densities have to be reduced because the electric field has reduced amplitude in some sections of the cavity. For the TM_{010} cavity, the effective energy density reduction can be obtained from equation (81). The resulting reduction factor is J_1^2 (P_{o_1}) which has a value of 0.27. Other rf resonators have similar factors.

The multipactor effect is a resonance phenomenon involving secondary emission of electrons. Considerable analysis is available for the case of rf electric fields between parallel plane electrodes. A multipactor discharge can occur when electrons emitted at one electrode are accelerated by the rf field to cross the gap to the other electrode in a time comparable to one, or more, rf half cycles. In that case, secondary electrons at the second electrode will be accelerated back to the first electrode by the rf field of reversed phase, and the process can continue for many cycles. If the secondary emission coefficient at the surfaces is greater than unity, then a high current discharge can build up thereby dissipating the energy in the rf fields.

For parallel plane electrodes with a given gap spacing there is generally a range of electric field strengths over which multipactor will occur[8]. The minimum field boundary of the multipactor region is given approximately by

$$E_{min} = \frac{\omega^2 L m}{e\sqrt{4 + \pi^2 (2n+1)^2}} \tag{88}$$

where n is the order of the multipactor discharge (2n + 1 = the number of rf half cycles per electron transit). The maximum field boundary is given by

$$E_{max} = \frac{\omega^2 L m}{2 e} \tag{89}$$

In most cases it is sufficient to consider only the n = 0 order of discharge. In that case, multipactor can occur over about a two-to-one range of electric field.

Multipactor can be inhibited (or enhanced) in a number of ways. These include surface coatings to reduce the secondary emission coefficient, variations in the planar geometry to prevent cumulative effects, and magnetic fields to alter electron trajectories.

4. Space-Charge Effects

Space-charge depression of potential will impose a limit on the current density which can travel across the cavity. An estimate of the current density limits can be obtained by neglecting the time variation of the fields, neglecting any injection velocity, and considering the cavity as a space-charge limited parallel plane diode. For the non-relativistic case, the Child-Langmuir law applies:

$$J = \frac{4}{9} \epsilon \sqrt{\frac{2e}{m}} \frac{V^{3/2}}{L^2} \tag{90}$$

where J is the maximum current density, e is electronic charge, and m is the mass.

If there is a finite initial velocity of the injected beam, the above equation is modified to the form

$$J = \frac{4}{9} \epsilon \sqrt{\frac{2e}{m}} \frac{V^{3/2}}{L^2} \left(1 + \sqrt{\frac{V_i}{V}} \right)^3 \tag{91}$$

where V_i is the beam voltage at injection. If the injection voltage is ten percent of the final voltage, the limiting current density is increased by less than three percent; hence, the effect of initial velocity is negligible.

For relativistic beams, an approximate solution for the case of zero initial velocity can be written in the form[4]

$$J = \frac{2m_o c^2}{e L^2} \sqrt{\frac{\epsilon}{\mu}} \left(1 + \sqrt{\frac{eV}{m_o c^2 + 1}} - 0.8471 \right)^2 \qquad (92)$$

It is of interest to relate maximum current density to maximum electric field strength. If we substitute L = V/E into the Child-Langmuir law, we get

$$J = \frac{4}{9} \epsilon \sqrt{\frac{2e}{m}} \frac{E^2}{\sqrt{V}} \qquad (93)$$

or

$$J = 2.33 \times 10^{-6} \frac{E^2}{\sqrt{V}}$$

For $E = 10^7$ V/m and $V = 5 \times 10^5$ V, we get $J = 3.3 \times 10^5$ A/m^2 or 33 A/cm^2. If E is increased to 5×10^7 V/m, then we get a maximum current density of 825 A/cm^2. It is concluded that current densitites can be used which are large compared to those obtainable from conventional thermionic emitters.

5. Transit Time Reduction Factor

When an electron passes through a region containing an rf electric field, the change in energy of the electron is generally less than the product of the distance traveled and the peak electric field because of the sinusoidal time variation of the field. The ratio of the energy gained in electron volts to the field-distance product is generally called the transit time reduction factor. Considerable information is already available[10] for the case where the change in energy is small compared to the initial electron energy. However, for the system of interest here, the energy gain will be large compared to the initial energy.

The case of a uniform rf field between planar electrodes at z = 0 and z = L will be considered. Nonrelativistic equations for which a closed form solution can be readily obtained will be used. The force equation is then

$$m \frac{dv}{dt} = -e E \cos(\omega t - \phi) \qquad (94)$$

where ϕ is the relative phase of the field at t = 0. If we assume that v = 0 and z = 0 at t = 0, then integration of the force equation gives

$$mv = \frac{eE}{\omega}\left[\sin(\omega t - \phi) + \sin\phi\right] \tag{95}$$

and another integration gives

$$mz = \frac{eE}{\omega^2}\left[\cos(\omega t - \phi) - \omega t \sin\phi - \cos\phi\right] \tag{96}$$

The velocity at the position of z = L will vary depending on the initial phase, ϕ. It can be shown by differentiation or by physical arguments that maximum energy gain occurs when $\omega t_L = 2\phi$ where t_L is the time for which z = L. Substitution of this optimum ϕ into the above equation gives

$$mv_L = -\frac{2eE}{\omega}\sin(\omega t_L/2) \tag{97}$$

and

$$mL = -\frac{eE}{\omega^2}\omega t_L \sin(\omega t_L/2) \tag{98}$$

We can eliminate ωt_L between these equations with the result

$$\sin\frac{\omega L}{v_L} = -\frac{m v_L \omega}{2eE} \tag{99}$$

Now we are in a position to evaluate the reduction factor which is by definition

$$M = -\frac{m v_L^2}{2eEL} \tag{100}$$

Substitution of equation (99) into this definition gives the result

$$M = \frac{\sin\left(\frac{\omega L}{v_L}\right)}{\left(\frac{\omega L}{v_L}\right)} \tag{101}$$

It is of interest to compare this result to the result when there is negligible energy gain across the gap. For the case of negligible energy gain we would have[9]

$$M_o = \frac{\sin\left(\frac{\omega L}{2v}\right)}{\left(\frac{\omega L}{2v}\right)} \tag{102}$$

where v is the velocity which is essentially constant throughout the gap. Hence, we can apply results for the constant velocity gap to the accelerating gap case, provided we use the average velocity in the gap rather than the final velocity.

Transit time reduction factors calculated using equation (101) for a 3.25 cm gap are shown in Figure 76 as a function of beam voltage. An exact point using a computer analysis which is relativistically correct is also shown for comparison. The error in the nonrelativistic analysis is not large in this range of voltage.

B. EXPERIMENT

1. Design Considerations

The goal of this experiment was to demonstrate the feasibility of using rf energy storage to produce short pulse, high energy electron beams. Since it was a feasibility demonstration, the emphasis was not placed on achieving particular values of current or voltage, but rather on minimizing the cost and complexity of performing the experiment.

The TM_{010} cylindrical cavity was chosen as the most appropriate cavity configuration. It was decided that a non-reentrant cavity would be used. A frequency of 720 MHz was chosen as the resonant frequency. This frequency was a compromise between lower frequencies which would make the short pulse instrumentation easier, and higher frequencies which would decrease the size and cost of the experimental device. At 720 MHz, the Techtronix 519 oscilloscope can be used as a monitor for single pulse operation. To use more conventional oscilloscopes would

require going down in frequency by about an order of magnitude which would increase the size of the experimental device by one order. Furthermore, a pulsed power source of 20 kw peak was readily available for the range of 685 to 985 MHz while high power sources at lower frequencies were not on hand.

The choice of 720 MHz as the resonant frequency determines the cavity diameter at 32 cm from equation (73). The choice of cavity length is somewhat arbitrary. If we assume a constant power input of 20 kW, then increasing the cavity length will increase output beam voltage up to a point where transit time effects culminate. However, the increased cavity lengths in the range of 2.5 to 12.5 cm were considered. A length of 3 cm was finally chosen.

The Q for the TM_{010} cavity was given by equation (84). Assuming copper cavity walls with full conductivity, the calculated skin depth from equation (85) is 2.43×10^{-4} cm, and the ideal cavity Q is 1.01×10^{4}. The cavity fill time based on the ideal Q is about five microseconds. Using the ideal Q and assuming the rf pulse is long compared to the fill time, the cavity stored energy and peak electric field strength were calculated using equations (81) and (83). The results are shown in Table II along with other calculated parameter values. The transit time reduction factor was determined from Figure 76, using the calculated values of electric field. Beam voltage was calculated from equation (79). The required current in the Table is the peak value of current required to discharge all the cavity energy in one rf half cycle which is obtained from equation (82). The maximum current density is based on the nonrelativistic Child-Langmuir law.

The required beam area was obtained by dividing the required current by the maximum current density. It is observed that for low input power the required beam area increases rapidly. Hence, it becomes impractical to perform the experiment at very low power level. A beam radius of 7 cm was chosen as a compromise solution, one which would allow operation at power levels as low as about 5 kW but would not be impractically large.

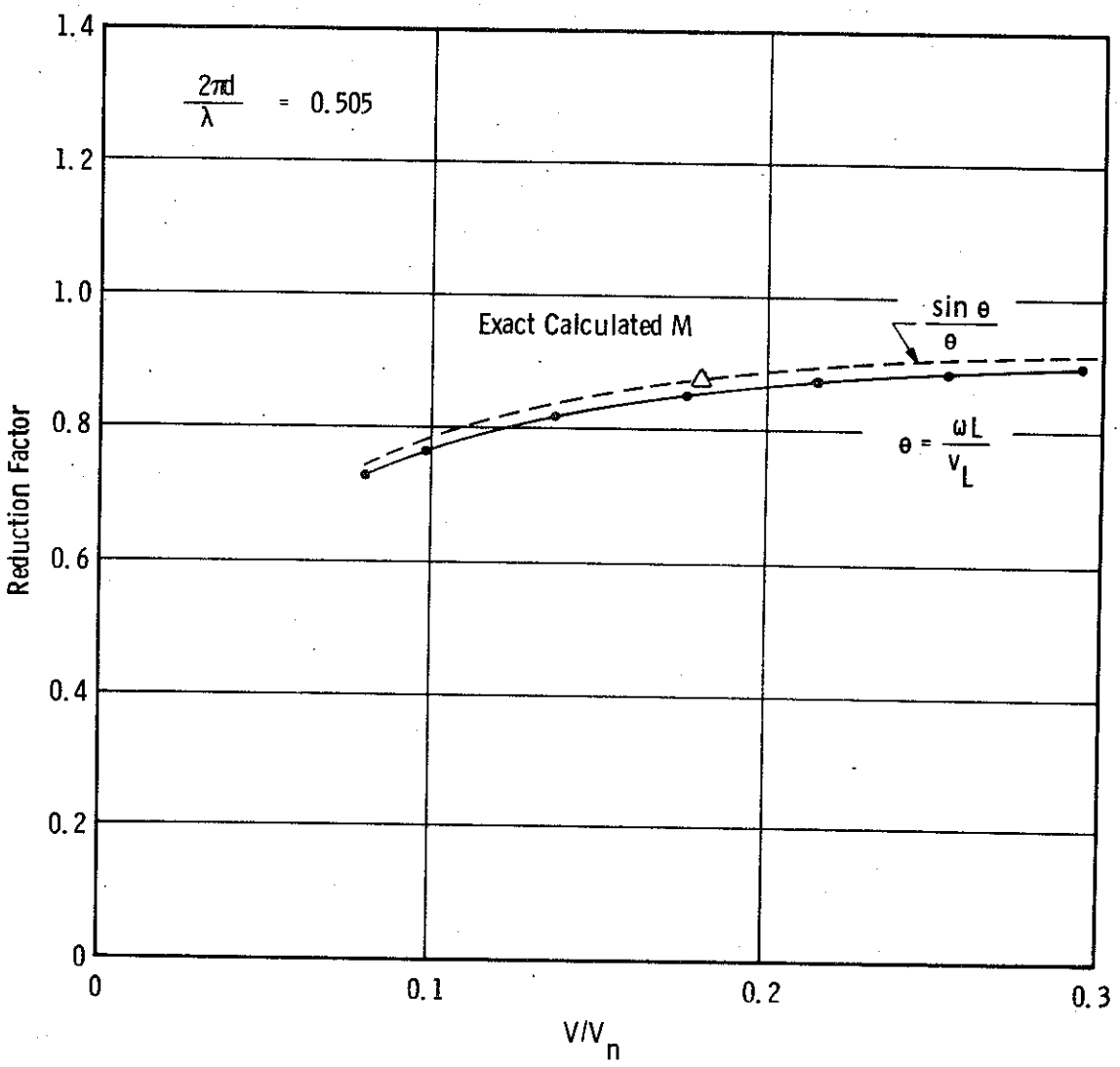

Figure 76. Transit Time Reduction Factor

A grid structure was used to inject the electron into one end of the cavity. Ideally the grid should be non-intercepting for the electron beam, but appear as a conductor to the rf currents in the cavity. Since the current in the TM_{010} cavity is entirely in the radial direction, a structure made up of radial hairpin elements was used. It can be seen in the photograph in Figure 78.

TABLE II

Input Power, P - kw	2.5	5	10	15	20	25	30
Stored Energy, U-joules	.0054	.0107	.0215	.0322	.043	.0537	.0645
Electric Field, E - kV/cm	14.1	19.9	28.2	34.5	39.8	44.4	48.8
Transit Time Factor, M	.765	.828	.876	.90	.91	.915	.918
Beam Voltage, V - kV	35.0	59.6	80.1	101	117	132	145.5
Required Current, I_{req} - A	455	590	795	944	1090	1200	1310
Current Density, max - A/cm^2	1.69	3.63	6.1	8.18	10.1	12.1	13.8
Required Beam Area - cm^2	269	163	130	115	108	99	95

As a source of injected electrons, a field emission-planar cold cathode structure was considered. Some feasibility tests indicated that it might not be possible to achieve the desired rise time of about 0.5 nsec using this approach and it was, therefore, abandoned in favor of a conventional oxide thermionic cathode. The grid-to-cathode spacing was chosen at 0.140 inch such that grid voltages in the range of 2.5 to 3.5 kV would be required to perform the experiment.

It is probable that the amount of current required from the cathode structure will depend on the timing of the gun pulse relative to the phase of the fields in the cavity. If beam injection begins when the cavity fields are just beginning the accelerating phase, then the full current is required off the cathode. However, if injection begins when there are decelerating fields in the cavity, then there will be a

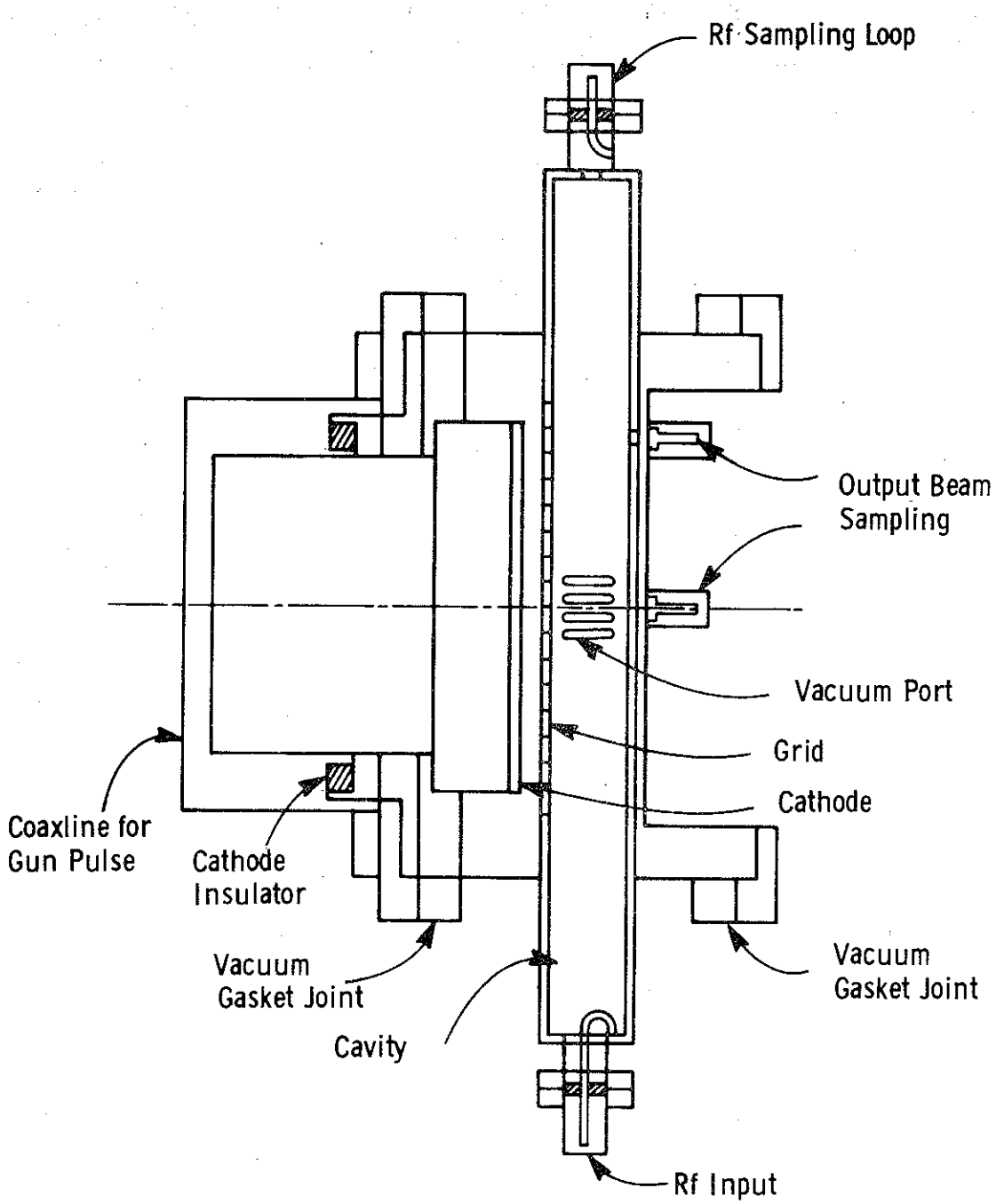

Figure 77. Cavity for Beam Generation

buildup of additional charge in the grid-cathode space due to electrons reflected by the cavity fields. This reflected charge may be available to contribute to the beam current when the cavity fields change to an accelerating phase. In this way the effective injection current might be as much as twice the cathode current.

To monitor the output beam, it would be desirable to measure beam voltage, current density, and total current. However, to measure all of these in the same device appeared to be impractical. It was decided that the most convenient way to measure peak voltage would be through a measure of the maximum x-ray photon energy with a scintilator, photodetector, and pulse height analysis. It was decided that to measure current density a number of sampling holes would be drilled in the output end of the cavity. The holes would lead to coaxial collectors which could be used to measure both peak current density and wave shape. It was decided that total current, as such, would not be measured. However, a sampling loop to monitor the rf magnetic field in the cavity would give an indication of the rate of energy removal by the beam and hence, an indication of the total current-voltage product.

With regard to multipactor effects in the cavity, the minimun field for multipactor effects can be calculated from equation (88). For a 720 MHz cavity with a 3 cm gap, we get a minimum field of 9.4 kV/cm. The operating fields in Table II are either in or above the multipactor range. Therefore, we must take some measures to inhibit multipactor. To accomplish this, a pattern of slots was cut in the ends of the cavity to geometrically inhibit the multipactor discharge. Field emission effects should not be expected since the cavity fields are well below that threshold.

2. Description of the Experimental Device

A sketch of the experimental device is shown in Figure 77. The inside dimensions of the cavity are 12.913 inches diameter and 1.181 inches length. The

walls of the cavity are 5/8-inch thick stainless steel and are copper plated to minimize rf loss. The rf input power is coupled in with a magnetic loop connected to 1-5/8 inch coax line with a brazed aluminum coaxial vacuum window. The orientation of the coupling loop was adjusted for an overcoupled condition with a voltage standing wave ratio of 1.53. An rf sampling loop was also included so that the field strength in the cavity can be continuously monitored. The sampling loop was weakly coupled so that the power sampled is 33 dB below the power level in the cavity. The sampling loop is fitted with a smaller aluminum coax window and a type N connector.

The cavity is evacuated through a number of rectangular slots in the cylindrical wall. The slots lead to a 1-1/2 by 3-inch rectangular pipe which is connected to a 50 ℓ/sec VacIon® pump. The pump has a side port with a valve which was used to connect a fore pump during processing.

One end of the cavity has the grid structure for injection of the electron beam. The grid is made of molybdenum ribbon bent into hairpin shapes and brazed into a cylindrical retaining ring. The grid ring is fastened to the cavity body with a second ring held with eight screws. A copper gasket is used between the grid ring and the cavity to obtain good electrical contact. This assembly can be seen in Figure 78 which is a photograph of the partially assembled device.

The cathode structure which is shown schematically in Figure 77 is fastened to the cavity with a ConFlat® vacuum flange joint. The cathode is 1/8-inch nickel with a conventional triple carbonate coating. The cathode is indirectly heated with a bifilar tungsten heater. The cathode diameter is 5.520 inches and the cathode-to-gun spacing was set at 0.140 inch. Hastalloy B material was used for heat shields around the cathode and filament. A thermocouple was installed to measure cathode temperature.

The cathode and its surrounding structures were designed to form the termination of a twelve ohm coaxial transmission line. Since beam pulse rise times

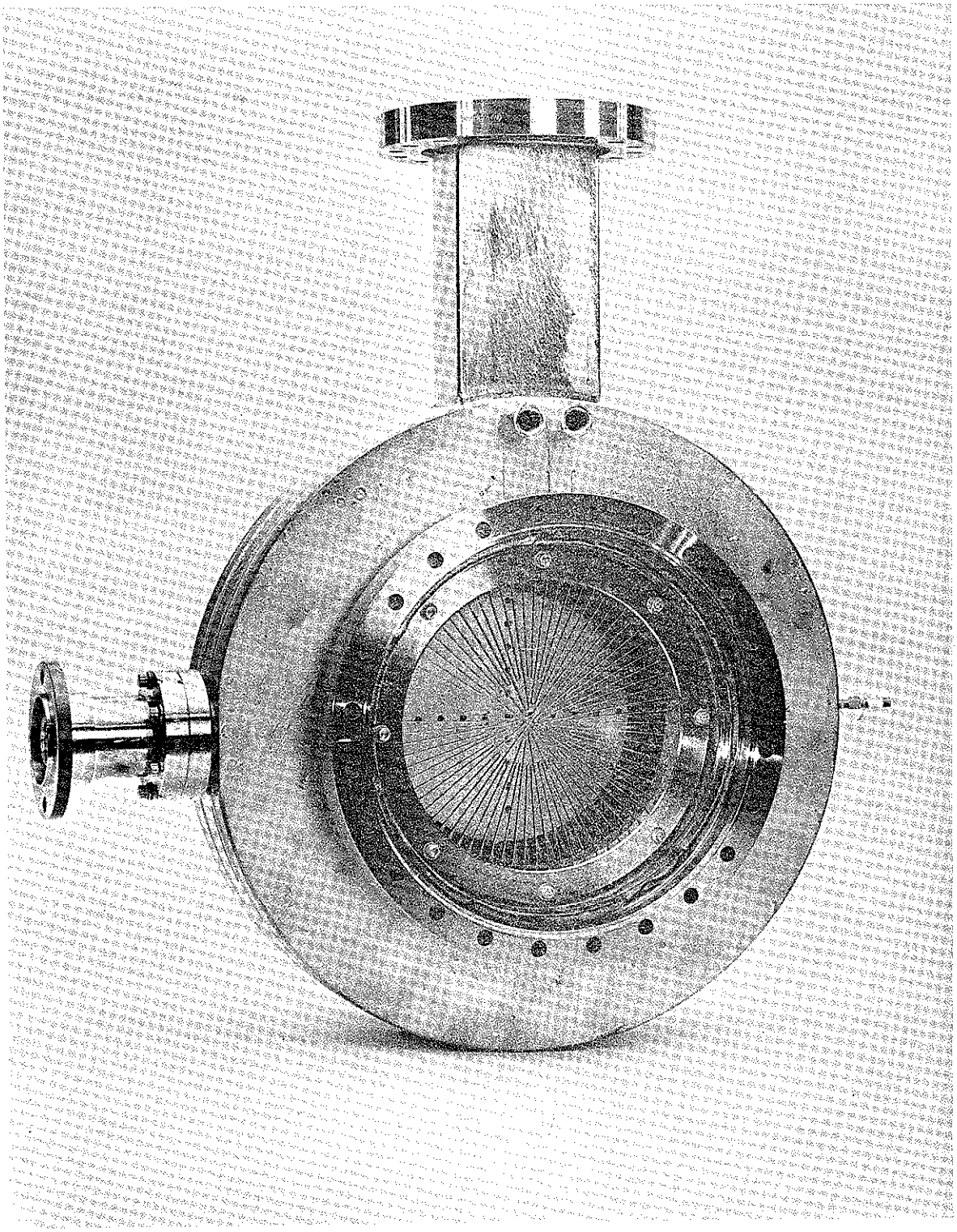

Figure 78. Partially Assembled Cavity Structure

of the order of 1 nsec were desired, efforts were made to preserve a relatively constant impedance coaxial geometry. However, a number of mechanical considerations required departures from the ideal geometry. Figure 79 shows the cathode structure in a stage of partial completion.

The end of the cavity opposite the grid and cathode has a number of holes for sampling the beam. Behind the holes is a collector structure which is mounted by a removable ConFlat vacuum flange. The collector structure presently has two coaxial connectors, one to sample current at the beam edge and one on the beam axis.

Construction of the experimental device has been completed; however, it has not been possible to test the device because of lack of time and funds in the existing contract. The construction of the large thermionic cathode proved much more difficult than was anticipated. The cathode problems have been the major factor in delaying the experiment.

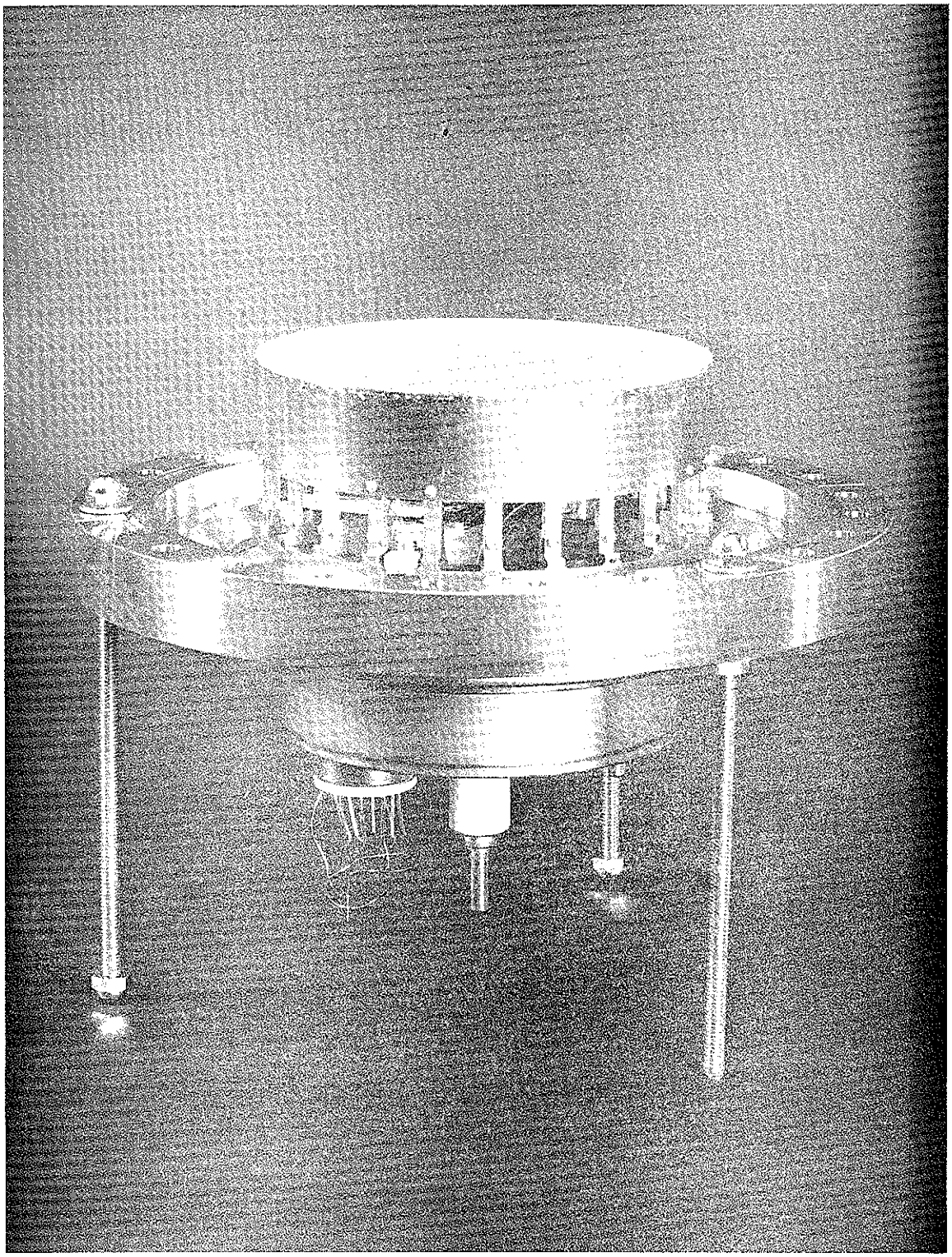

Figure 79. Cathode Structure

V. CONCLUSIONS

The electron flow calculations reported here lend further support to the conclusion that the cathodes in megavolt diodes of the type considered act like space charge limited cathodes. In the high current diode configurations studies, the electric fields at the cathode in the absence of space-charge are generally high enough that field emission can occur over the entire cathode and sometimes on the cathode support structure as well. In that case, a plasma is presumably formed over the entire cathode surface during the early part of the pulse. During the main part of the pulse, the plasma apparently acts like an essentially unlimited source of electrons.

In very high current guns of this type, electrons emitted from the front of the cathode reach the anode but those emitted from back portions of the cathode do not. The current arising from electrons emitted from the front of the cathode generates such a strong magnetic field that the back electrons are forced to return to the cathode or to move parallel to the cathode surface to form a sheath. To predict the electron flow in diodes of this kind, one must properly account for the space charge of these sheath electrons even though they may never reach the anode. To account for the sheath electrons numerically presents considerable difficulty because they are moving very close to the cathode surface where numerical errors are large, and they are generally moving with a highly cycloidal motion which contributes further to numerical errors.

Two methods of accounting for the back electrons were investigated. One method used an extra electrode called a sheath electrode at cathode potential to simulate the space-charge of the sheath electrons. This method gave reasonably good results. However, it required that the total anode current be known (or guessed) before starting the calculation. Another method made use of magnetron theory to determine the cathode emission. It was possible to incorporate this second method directly into the calculation. With this method a cutoff factor is calculated for each point on the cathode based on the electric field normal to the cathode and the self-magnetic field tangential to the cathode. If the cutoff factor is above a particular

value, no emission is allowed. As the cutoff factor becomes smaller than the critical value, emission is gradually allowed to increase in accordance with the magnetron theory. This model was reasonably successful. However, it probably allows too much current to be emitted at the edge of the emitting area, particularly when the cathode radius of curvature is quite small in that region.

The numerical calculations of electron flow using these cathode models show fairly good agreement with measured results. For a diode with a spherical cathode operated at 2.7 MV, the measured current was 60 kA and the calculated current was 63 kA. The overall beam size at the anode was in good agreement, but the current density at the anode was open to some question. The calculated current density at the anode had a peak near the beam edge which can be traced to a peak in cathode emission. The peak in cathode emission is very likely a result of the cathode models used and not a true representation. However, one would not expect exact agreement between calculated current density at the anode and measured x-ray dose, because both time-averaging effects and scattering in the anode will tend to smooth the x-ray dose compared to the current density.

For a diode with a toroidal cathode operated at 4.5 MV, the measured beam current was 98 kA and the calculated current using the crossed field cathode model was 125 kA. For this case also, the current density in the edge of the beam is probably excessive. There was qualitative agreement between current density at the anode and the measured x-ray dose. The agreement between calculated and measured beam size at the anode was good.

Some calculations were made for planar diodes immersed in a confining axial magnetic field. These calculations demonstrated that quasi-planar flow can be achieved even up to current levels of 1 to 2 MA with diode voltages of 15 MV by the use of axial magnetic fields comparable in value to the self-magnetic field of the beam.

A number of calculations were made for 15 MV diodes with no confining axial field. In general, the convergence of the iteration procedures for these calculations was not good. Presumably the lack of convergence is caused by numerical effects. However, there exists the remote possibility that such a flow could in fact be unstable. The convergence of the calculations appears to be good enough to make some estimates with regard to the effects of diode dimensions on electron flow and total current. A good geometry to obtain a 400 kA beam appears to be a toroidal cathode with 21-inch major diameter and 2-inch minor diameter, and an 18-inch cathode-to-anode spacing.

With regard to the use of rf energy storage to generate short-pulse high-power electron beams, calculations continue to indicate feasibility in the use of this approach. However, it was not possible to carry the experiment far enough to conclusively demonstrate feasibility.

With regard to future work, the numerical analysis of megavolt diodes has been brought to a point where fairly good predictions can be made of the electron flow in high impedance diodes. Considerable progress has been made in the method of modeling the cathode, but some additional work could be done, particularly with regard to the edge of the emitting region. Several possibilities exist for improving the convergence of the iteration procedures. These should be investigated. It is likely that the improved models and convergence procedures developed during the past year would make the analysis of lower impedance diodes more practical. This possibility should be investigated.

VI. REFERENCES

1. F. Friedlander, R. Hechtel, H, Jory, C. Mosher, "Megavolt-Megampere Electron Gun Study," DASA 2173, Contract No. DASA-01-68-C-0025, pp 39 - 40, September 1968.

2. E. W. V. Acton, "The Space Charge Limited Flow of Charged Particles in Planar, Cylindrical and Spherical Diodes at Relativistic Velocities," J. Elect. and Control, 3, pp 203 - 210, 1957.

3. J. C. Slater, Microwave Electronics, D. Van Nostrand, pp 336 - 345, 1959.

4. J. C. Slater, Microwave Electronics, D. Van Nostrand, p 352, 1959.

5. S. Ramo and J. R. Whinnery, Fields and Waves in Modern Radio, Wiley and Sons, 1953.

6. H. Jory, "Nanosecond Pulse Generator Study," Technical Report No. RADC-TR-65-193, Contract No. AF30(602)-3353, July 1965.

7. D. Alpert, D. A. Lee, E. M. Lyman, and H. E. Tomaschke, "Initiation of Electrical Breakdown in Ultrahigh Vacuum," Jour. Vac. Sci. and Tech. 1, No. 2, pp 35 - 50, 1964.

8. F. Paschke, "Note on the Mechanism of the Multipactor Effect," J. A. P., 32, p 747, 1961.

9. B. Y. Mills, "A Million Volt Resonant Cavity X-Ray Tube," Inst. of Elec. Engrs., 97, III, p 425, 1950.

10. G. M. Branch, "Electron Beam Coupling in Interaction Gaps of Cylindrical Symmetry," IRE Trans., ED-8, No. 3, pp 193 - 206, May 1961.

DISTRIBUTION LIST

No. of Copies	Address
1	Director Advanced Research Projects Agency Architect Building 1400 Wilson Blvd. Arlington, Virginia 22209 Attn: Strategic Technology Office, Mr. Robert A. Moore
12	Defense Documentation Center Cameron Station Alexandria, Virginia 22314 Atten: TC
	Director Defense Nuclear Agency Washington, D. C. 20305
2	Attn: APTL (Technical Library)
1	APSI (Archives)
1	DDST, Mr. Peter H. Haas
1	DDST, Dr. John A. Northrop
1	STRA
1	RAEV
	Director of Defense Research and Engineering Washington, D.C. 20301
1	Attn: ASST. Dir. (Strategic Weapons), Mr. Ben T. Plymal
1	ASST. Dir. (Research), Dr. Edward M. Reilley
1	Asst. Dir. (Defensive Systems), Mr. C. Robert Wieser
1	Dep. Dir. (Strategic and Space Sys.), Dr. Roland F. Herbst
1	Commander Field Command Defense Nuclear Agency Kirtland AFB, New Mexico 87115 Attn: Technical Library, FCWS-SC
1	Chairman Joint Chiefs of Staff Washington, D. C. 20301 Attn: J-5, Plans and Policy (R and D Division)
1	Chief Livermore Division, Field Command DNA Lawrence Livermore Laboratory P.O. Box 808 Livermore, California 94550 Attn: Document Control
1	Office of The Secretary of Defense Salt Support Group 3E120 The Pentagon Washington, D. C. 20305 Attn: Dr. James P. Wade, Jr.
1	Director Weapons Systems Evaluation Group, ODDR and E Office, Secretary of Defense 400 Army-Navy Drive Washington, D. C. 20305 Attn: Capt Donald E. Mc Coy, USN
	Director Advanced Ballistic Missile Defense Agency Commonwealth Bldg. 1320 Wilson Blvd. Arlington, Virginia 22209
1	Attn: CRDABM-NE, LTC. James H. Sloan
1	Dr. Dr. Jacob B. Gilstein

No. of Copies	Address
1	Commanding Officer Army Electronic Proving Ground Fort Huachuca, Arizona 35613 Attn: STEEP-PA-I
1	Commanding Officer Army Electronics Res. and Dev. Activity White Sands Missile Range, New Mexico 88002
1	Chief Army Nuclear Effects Laboratory Edgewood Arsenal, Maryland 21010 Attn: AMXRD-BNL, Technical Library
1	Commanding Officer Army Nuclear Weapons Surety Group Fort Belvoir, Virginia 22060 Attn: Library
1	Director Ballistic Research Laboratories Aberdeen Proving Ground, Maryland 21005 Attn: Mr. Edward J. Bryant
1	Chief of Research and Development Department of the Army Washington, D. C. 20310 Attn: NCB Division
	Department of the Army Harry Diamond Laboratories Washington, D. C. 20438
1	Attn: AMXDO-NP
1	AMXDO-RBH Mr. Paul A. Caldwell, Jr. R and D Supervisor
1	Mr. Stu Graybill
1	Technical Library
1	Dr. Robert B. Oswald, Jr.
1	Commanding Officer Picatinny Arsenal Dover, New Jersey 07801 Attn: SMUPA-VE, Mr. Louis Avrami, Explosives Laboratory
1	Commanding General Safeguard System Command P.O. Box 1500 Huntsville, Alabama 35807 Attn: Maj. G. T. Ogden
1	Safeguard System Manager Safeguard System Office 1320 Wilson Blvd. Arlington, Virginia 22209 Attn: Plans Division
1	U.S. Army Combat Developments Command Nuclear Agency Fort Bliss, Texas 79916 Attn: CDINS-E
1	Commanding General U.S. Army Electronics Command Fort Monmouth, New Jersey 07703 Attn: AMSEL-RD-P, Mr. Park Richmond
	Commanding General U.S. Army Materiel Command Washington, D. C. 20315
1	Attn: AMCRD-BN-RE
1	AMCRD-BN-RE-2, Mr. John J. F. Corrigan